"Role of Self-assembly for Molecular Devices"

by

J.V. Yakhmi

Bhabha Atomic Research Centre

yakhmi@barc.gov.in

CEA-DAE Workshop on
"Multifunctional Molecular and Hybrid Devices"
October 6-10, 2008, Saclay

collaboration on "Nanoscience: nanomaterials production and characterization, interfaces and self-assembly of monolayers"

Acknowledgements

BARC:

S.K. Gupta, D.K. Aswal, S.P. Koiry, Vibha Saxena, N. Joshi, N. Padma, Anil Chauhan, S. Nayak, A. Singh, Manmeet Kaur, Shilpa Sawant, C.A. Betty, Nitin Bagkar, Sipra Chowdhury, S.Sen, M.D. Sastry, S.M. Yusuf, Purushottam Jha, D.S. Sutar (RA)

S. Gohlen, D. Guerin, D. Vuillaume, Institut d'Electronique, Microelectronique et Nanotechnologie, Lille, France

C. Suergers, Physikalisches Institut, Universitaet Karlsruhe, Germany (Indo-German Project)

S. Palacin, DRECAM, Saclay, (CEA-DAE Collaboration from 2008)

(late) Prof. O. Kahn, ICMCB, CNRS, Bordeaux (France)
Prof. K. Inoue, Inst. Molecular Science, Okazaki (Japan)
Prof. Fritz Scholz, University of Greifswald (Germany)
Prof. W. Haase, Technical University, Darmstadt (Germany)

SINP
Prof. Milan Sanyal
Dr. Satyaban Bhunia

IOP
Prof.S.N.Sahu

IGCAR
Dr. John Philip

TIFR
Dr. Deepa Khushalani
Dr. Roop Mallik

BARC
Dr. Vibha Saxena
Suman Neogy

RRCAT
Dr. Kaustuv Das

Publications of Yakhmi and Colleagues: on Molecular Electronics Devices & related aspects

1. *Small* 1 (2005) 725-729
2. *Nanotechnology* 16 (2005) 3064-3068
3. *Vacuum* 79 (2005) 178-185
4. *J. of Applied Physics* 98 (2005) 026103.
5. *Appl. Surf. Sci.* 243 (2005) 220-227.

6. *Phys. Stat. Solidi (a)* 203 (2006) 1254-1258
7. *Physica Stat. Sol. (a)* 203, (2006) 1464-1469
8. *Analytica Chimica Acta* 568 (2006) 84–108

9. *Appl. Phys. Lett.* 90, (2007) 113118
10. *Proc. of Physics, Chemistry and Applications of Nanostructures,* pp. 541-8, (July 2007), *Belarus*, World Scientific, Sinagpore.
11. *Solid State Comm.* 142 (2007) 200-205
12. *J. of Colloid & Interf. Sci.* 313 (2007)353
13. *J. of Coll. and Interf. Sci.* 313 (2007) 353

14. *Chem. Phys. Lett.* 453 (2008) 68-72
15. *Appl. Phys. A* 90 (2008) 581-589
16. *Physica Stat. Solidi (a)* 205 (2008) 373-373
17. *Org. Electronics 9 (2008) 602-608*
18. *J. Appl. Phys.* 104 (2008) 073717:1-6
19. *Org Electronics (submitted Sep 2008)*
20. *Phyica E (Review Article submitted)*
21. *"Materials Science Research trends" (2008) pp. 293-320. Ed. Mario B. Olivante, Nova Science Publishers, Inc. (in press)*
22. *"New Research on Thin Solid Films" Ed.: F. Columbus, Nova Sci. Publ, (in press)*

Publications of Yakhmi and Colleagues: on Sensors, Self-assembly of Functional Materials

1. *Langmuir* 18 (2002) 7409-7414
2. *Synth. Metals* 125 (2002) 401-413
3. *J. of Crystal Growth* 258 (2003) 197-203
4. *Thin Solid Films* 440 (2003) 240-246
5. *Jl of Mater Chem* 14 (2004) 1430
6. *Langmuir 20 (2004) 4874-4880*
7. *Pramana-Journal of Physics*, Vol. 63, No. 2 (2004) 277-283.
8. *Sensors and Actuators B* 97 (2004) 334-343.
9. *Thin Solid films* 493 (2005) 267-272
10. *Phil. Mag Vol* 85 *(2005) 3659-3672*
11. *Asian J. of Physics* 14 (2005) pp. 1-9
12. *Sensors and Actuators B* 107 (2005) 277-282.
13. *J. Phys. Chem. B* 109 *(2005) 5653-56*
14. *J. Phys. Chem. B* 110 (2006) 24530-24540
15. *Thin Solid Films* 497 (2006) 259-266
16. *Sensors and Actuators B* 115 *(2006) 270–275*
17. *Phys. Rev. B* 74 (2006) 224421-8
18. *Phys. Rev. B* 75 *(2007) 224419-11*
19. *Appl. Phys. Lett.* 90 (2007) 43516
20. *J. of Appl. Polymer Sci.* 103 (2007) 595-599
21. *Analytica Chimica Acta* 594 (2007) 17-23
22. *Sensors and Actuators B Chemical*, 128 (2007), p.286-292
23. *Biosensors and Bioelectronics* 22 (2007) pp. 1027-033
24. *Jl. of Pure and Appl. Phys* 45 (2007) 354-357
25. *J. of Colloid and Interface Sci.* 313 *(2007) 353–358*
26. *J. of Phys. Chem., Part B* 112 *(2008) 6467-6472*
27. *J. Appl. Phys. 103 (2008) 123902, 1-6*
28. *Physica E (2008) accepted.*
29. *Phys. Rev. Lett. (submitted)*
30. *Nanotechnology (submitted Sept 2008)*
31. *Synth. Metals* (submitted Sep 2008)

Microactuators (ARTMUS) from Polypyrrole (Ppy) doped with DBS (dodecylbenzene sulfonate, $C_{12}H_{25}C_6H_4SO_3^-$) anions

$$PPy^+(DBS^-) + e^- + Na^+(aq) \longleftrightarrow Ppy^0(DBS^-Na^+)$$

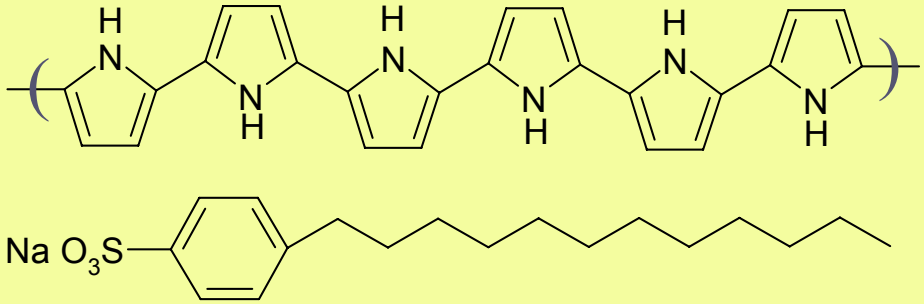

(a) V_{app} = 0V

(b) V_{app} = +2V

(c) V_{app} = -2V

Na^+ diffuses in and out of PPy during electrochemical switching. A reduction in volume occurs when the ion exit (during oxidation) and vice versa

Sutar, Aswal, Gupta and Yakhmi *Jl. of Pure and Appl. Phys* 45 (2007) 354

Using MNP-loaded Polyurethane film Membrane in Artificial Heart

BARC &

Ramachandra Med. college, Porur, Chennai (Dr.K R Balakrishnan)

adhesion of blood platelets to the arterial surface

Cell surface modified with phosphatidylcholine adsorbs albumin preferentially, helping in reducing cell adhesion.

Goal: deposition of LB films of

phospholipid L-α- Phosphatidylcholine (PTC), i.e. egg yolk, glycolipid Galactocerebroside (gal) and cholesterol (Chol) in the ratio (1: 0.7: 0.125, the cell mimetic composition) on polycarbonate (PC) membrane surfaces;

study their blood compatibility and adhesion on the surface.

Sree Chithra Tirunal Institute for Medical Science and Technology (SCTIMST).,Thiruvanmanthapuram and
Bhabha Atomic Research Centre (BARC) [Dr. Sipra Choudhury]

Goal: to obtain Highly ordered 2D - Polymers thin films

(Electro)polymerization from solution yields three-dimensional amorphous polymer films

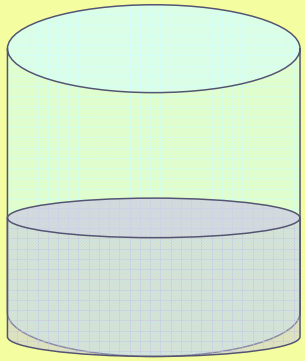

monomer

Solution Polymerisation

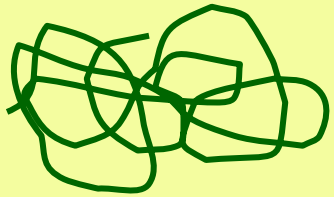

Coiled polymer

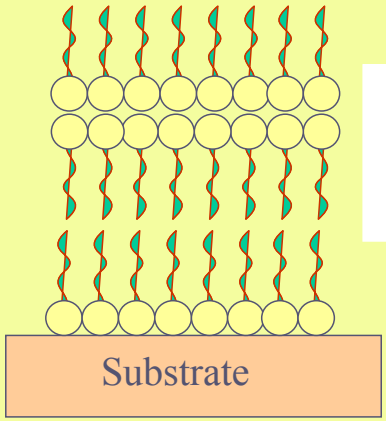

Electrochemical Polymerization

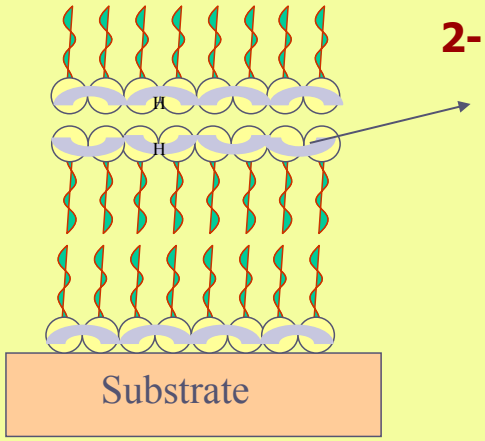

2-D polymer

Arrange the monomer in the form of an Ordered LB film, then electropolymerize

Sawant, Dhoble, Yakhmi, Kulshreshtha, Miyazaki and Enoki, *J. Phys. Chem. B* 110 (2006) 24530

Materials used forming LB film of phenosafranine dye:

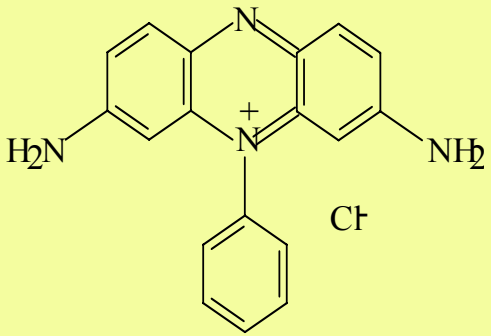

Phenosafranine dye

1 mg/ml of AA in chloroform used as spreading solution.
pH adjusted using dil. NaOH or dil. HCl

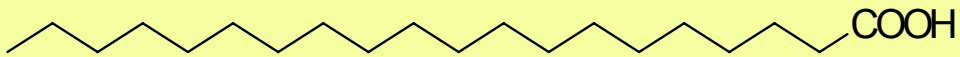

Archidic Acid

2D Films of Poly-phenosafranine prepared by Electropolymerisation

Uses of Poly-phenosafranine modified electrodes:

1. **Possess electrolytic activity for oxidation of NADH (β-nicotinamide adenine dinucleotide) to enzymatically active NAD^+. The NADH/NAD^+ redox couple (coenzyme) is used by many dehydrogenase enzymes.**
2. **Can detect the neurotransmitter dopamine in the presence of interfering ascorbic acid.**

Langmuir-Blodgett Films

LB technique enables preparation of ultrathin films with controlled thickness, (multilayers), and well defined molecular orientation.

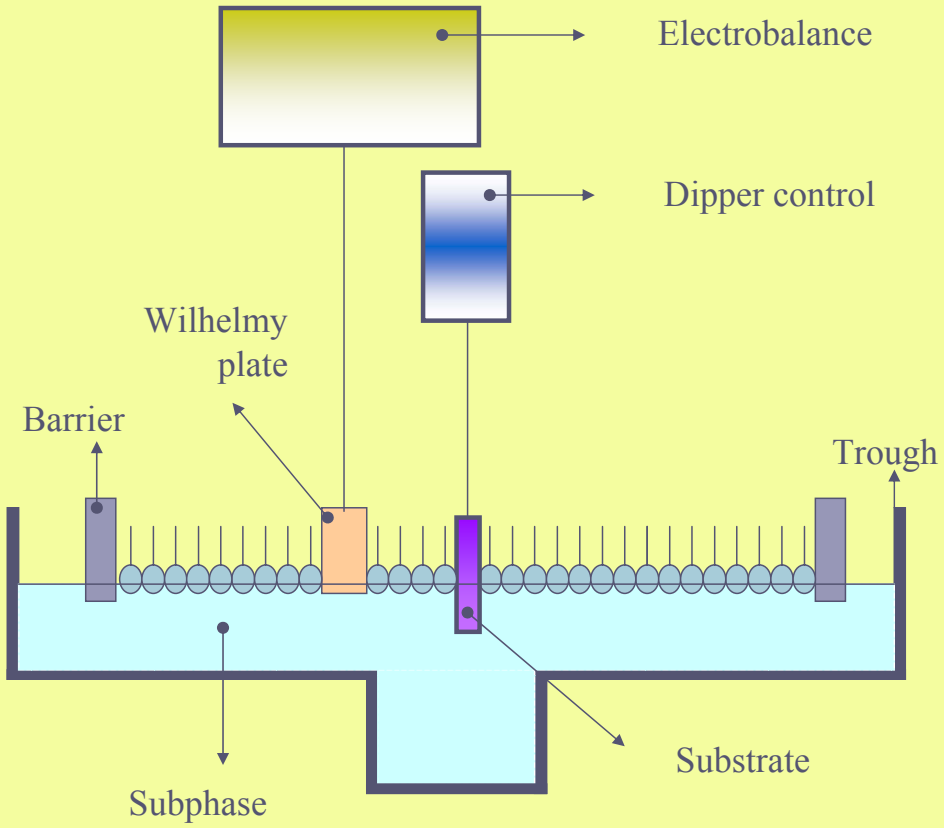

Schematic Diagram of Langmuir- Blodgett trough KSV 5000

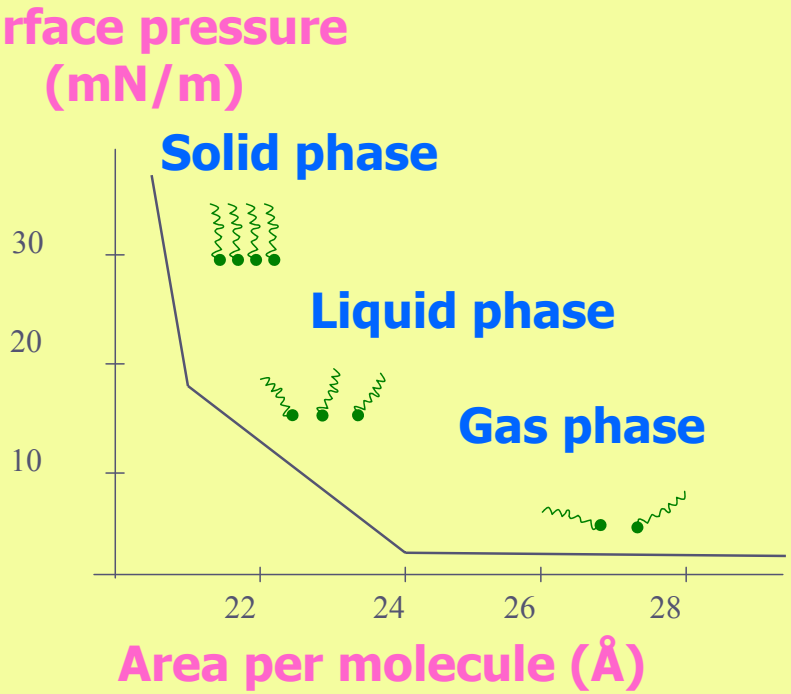

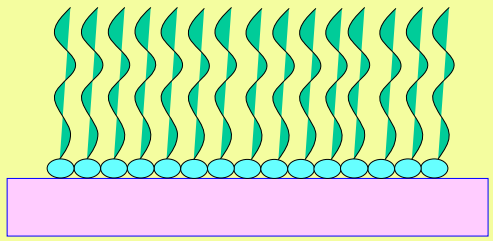

No restriction on type of substrate

In this talk we discuss our efforts at BARC on:

Self-assembly (general)

Polyaniline: growth of Crystals using a SAM template, NH3 sensing, conduction across (MIS)

Polyindole: fibres using self-assembly

Silanes: dielectric on Si-substrate, Al/OTS/Si(n^{++}) device

Cathode electrografting of OTS, TPP-C11 (for resistive memory)

APTMS: lbl self-assembly of 3-aminopropyltrimethoxysilane on Si-substrates, and memory effect in Hg/APTMS-multilayer/Si(p^{++})

Metal Phthalocyanines: FePc nanoweb/nanobrush formation, NO2 Sensor, Hysterisis in I-V

P3HT: NO_2 sensing, FET device on APTMS monolayer (Dr. V. Saxena)

Polycarbazole: LB film NH3 sensor

NiHCF: LB films for K-ion sensor

Polypyrrole: electromechanical actuator

Self-assembly by Nature:

energy economy – non-covalent interactions;
– ambient regime

Structural materials (*wood, bioceramics, bone, spider silk, magnetite*),
DNA, Viruses, Bacteria, Proteins… : coded self-assembly

Ambitious yet to compete in the lab!

(self-organization, self-repair, self-replication)

Nature's assembly-line doesn't make a mistake!

Simple Self-assembly

* Float glass (surface tension of molten metal);
* Growth of single crystal from seed.

Self-assembly in the lab (BARC)

Bulk: *Self-assemble functionalized molecules into a lattice*

Films:
* Self-assembled monolayers (SAMs);
* Amphiphilicity at air-water interface (LB films);
* Electrochemically grown films

Polyaniline-Prussian Blue Molecular Hybrid,
Sawant, Bagkar, Subramanian and Yakhmi
Philosphical Magazine 84 (2004) 2127-2138

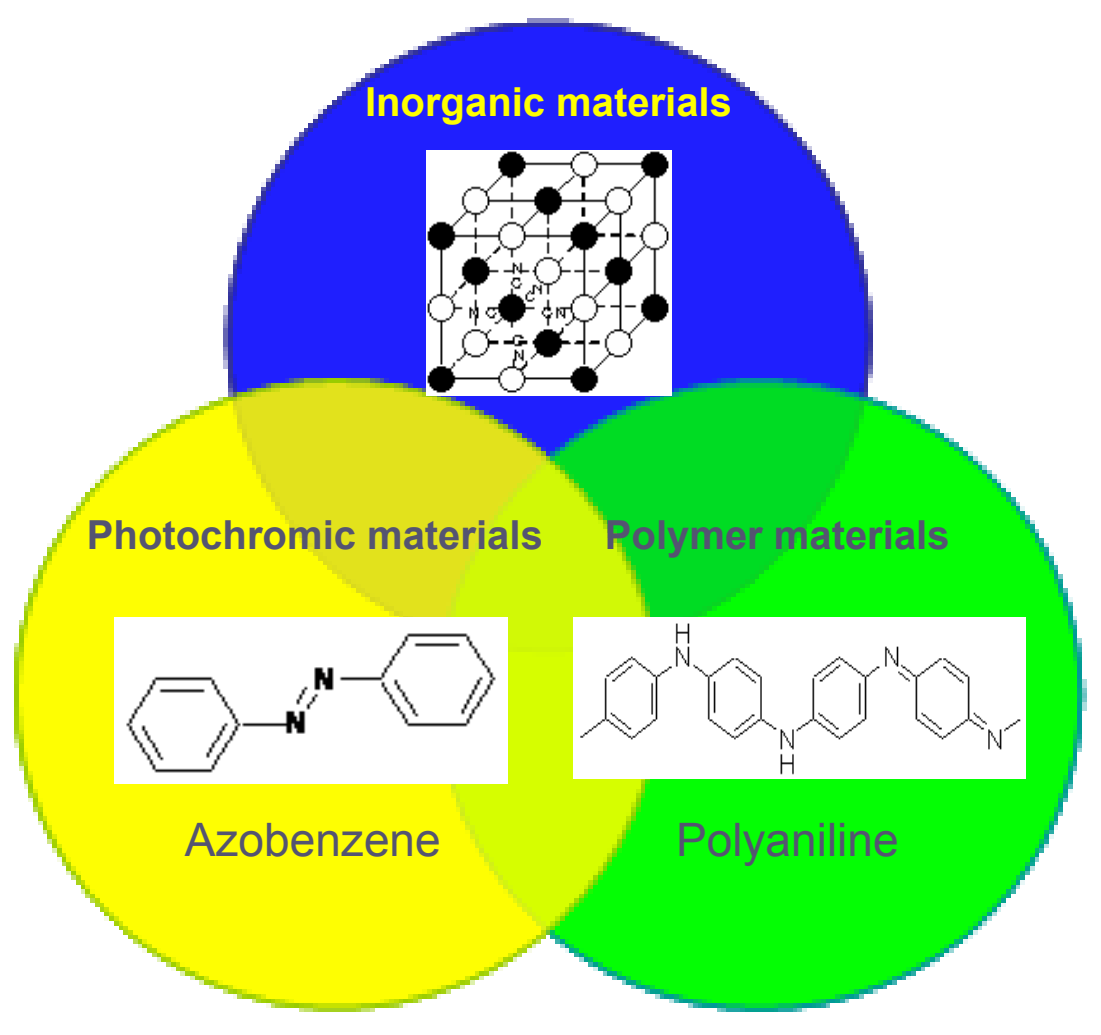

Multifunctional materials
Photocontrol of the electronic states
Prof. Y. Einaga, Keio University, Japan

Molecular Engineering: Constructing functional molecular lattices, *whose properties are derivable from molecules used*

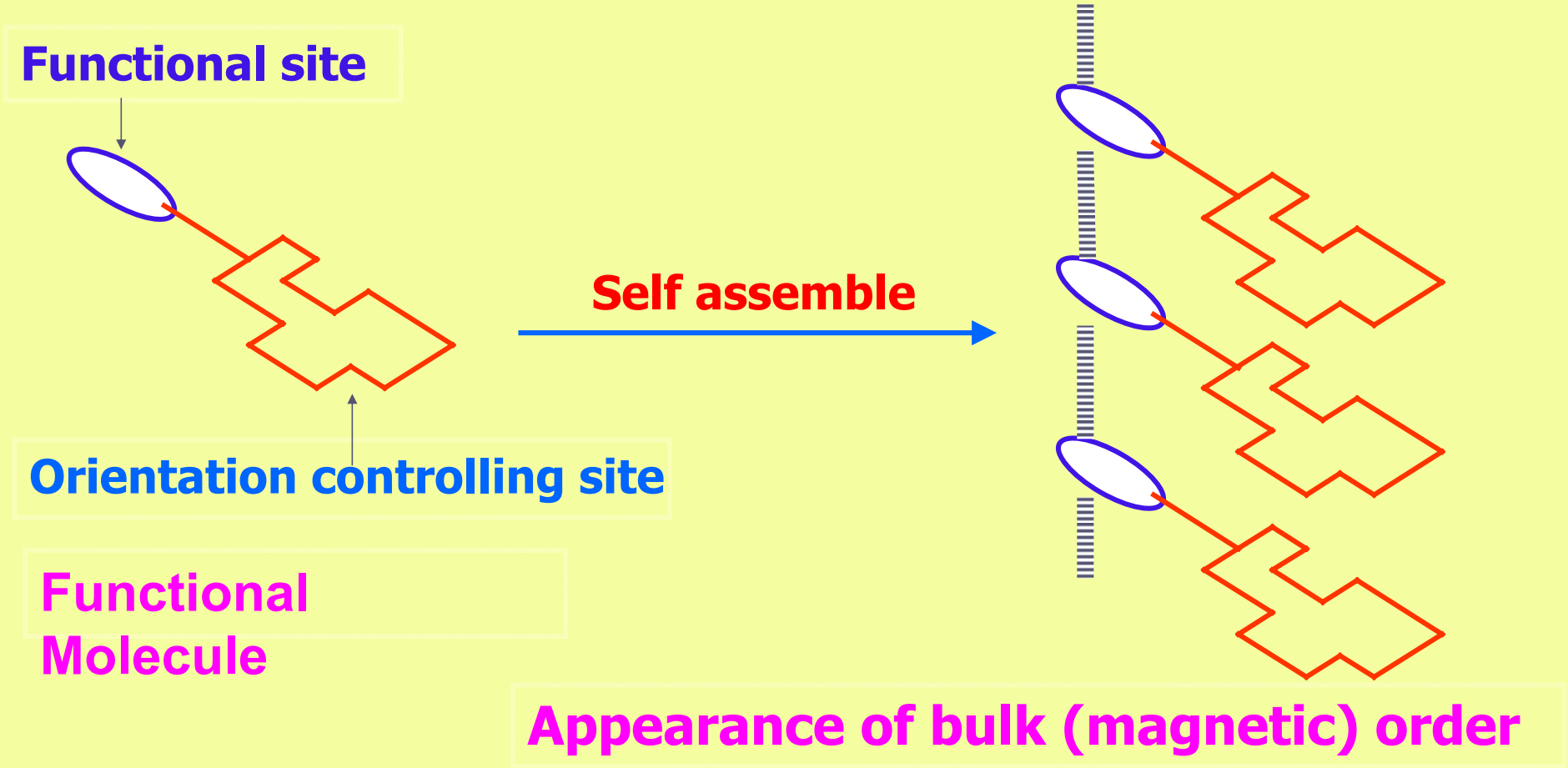

Orientation controlling site helps in arranging functional molecules, using non-covalent forces to bring about long-range magnetic order.

Mn(III) tetra(*ortho*-fluorophenyl)porphyrin-tetracyanoethylene anisotropic Heisenberg chain compound with slow magnetic relaxations

Bałanda, Rams, Nayak, Tomkowicz, Haase, Tomala and Yakhmi, Phys. Rev. B 74 (2006) 224421

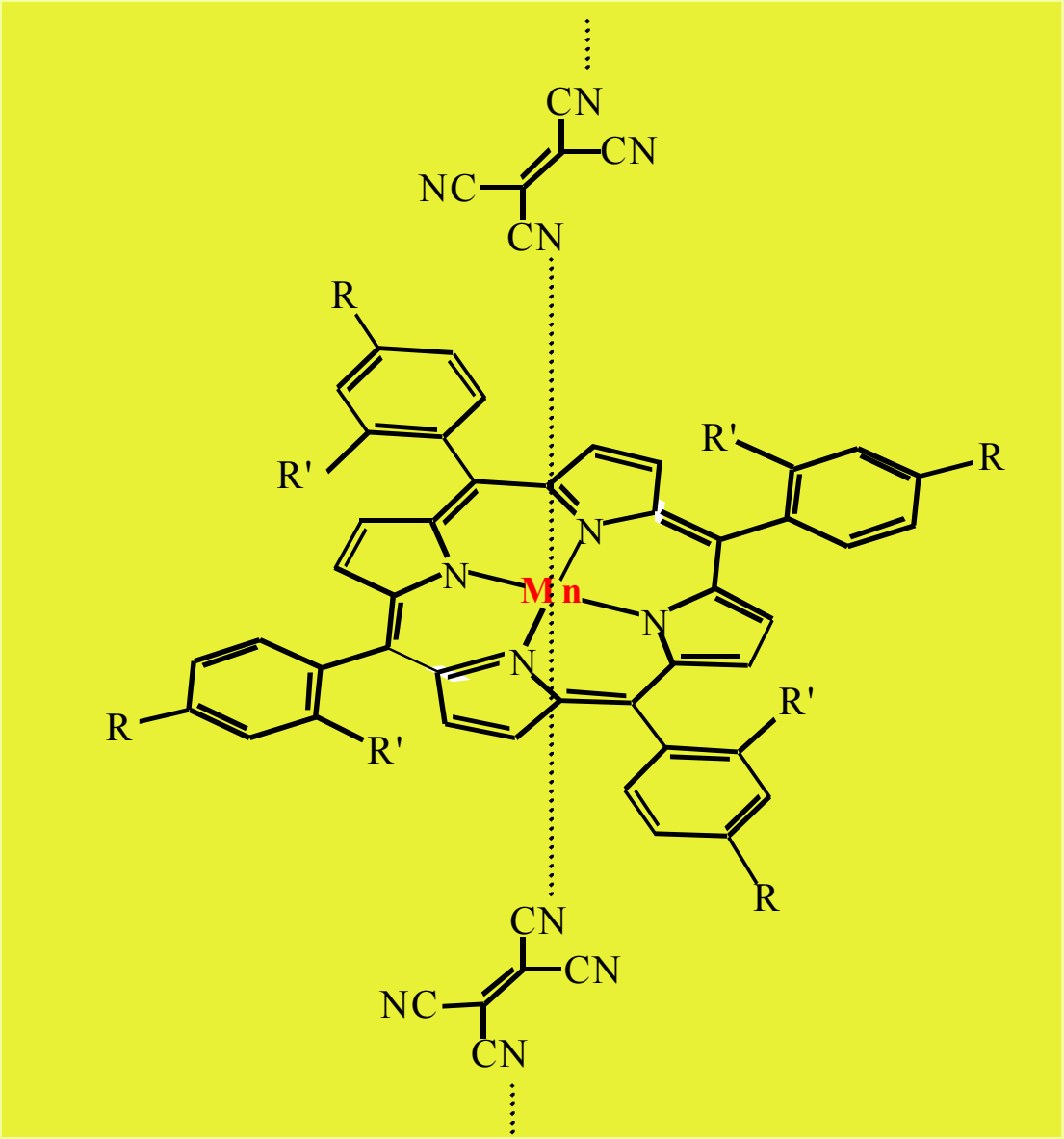

ferrimagnetic chains between magnetic moments of Mn ion $S=2$ and TCNE radical, $S=1/2$

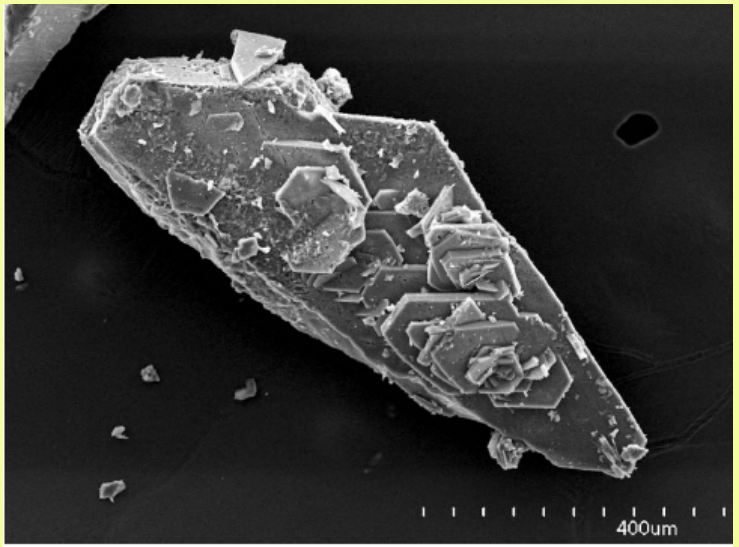

A Three-Dimensional Ferrimagnet with a High T_c of 53 K Based on a Chiral Molecule

Inoue, Imai, Ghalsasi, Kikuchi, Ohba, Okawa and Yakhmi

Angew. Chem. 40 (2001) 4242

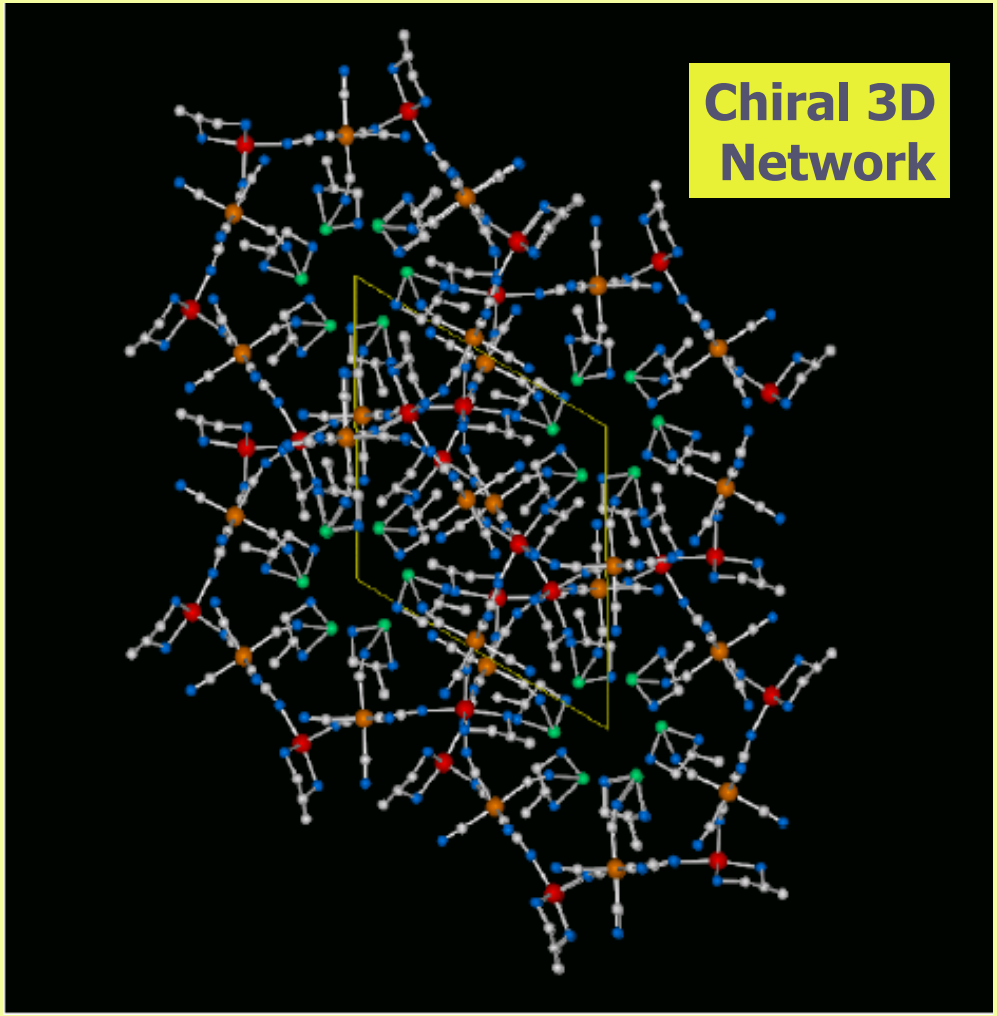

Strategy: Use π-conjugated high-spin oligonitroxide radicals as bridging ligands for paramagnetic TM ions to assemble and align electron spins.

A single unit possesses two chiral ligands (*S*)-pn; one coordinated to an Mn^{2+} ion and the other located in the cavity of the helical loop

Crystal structure of $K_{0.4}[Cr(CN)_6][Mn(S)\text{-pn}](S)\text{-pnH}_{0.6}$. View along *c* axis. K atoms are shown in green, Cr in brown, Mn in red, C in gray and N blue.

Photo-induced magnetic switch

$(NBu_4)_2Mn_2[Cu(opba)]_3.6DMSO.1H_2O$

Sastry, Bhide, Kadam, Chavan, Yakhmi & Kahn
Chem. Phys. Lett. 301 (1999) 385;
J. Mater. Chem., 7 (1997) 1263

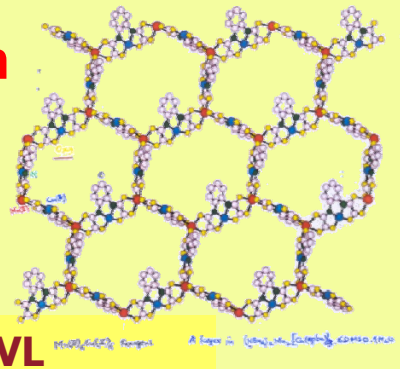

Effect of CVL illumination 510.5 and 578.2 nm on EPR (X-band) low (3381 G) & high field (3423G, 40% change) components at 14K

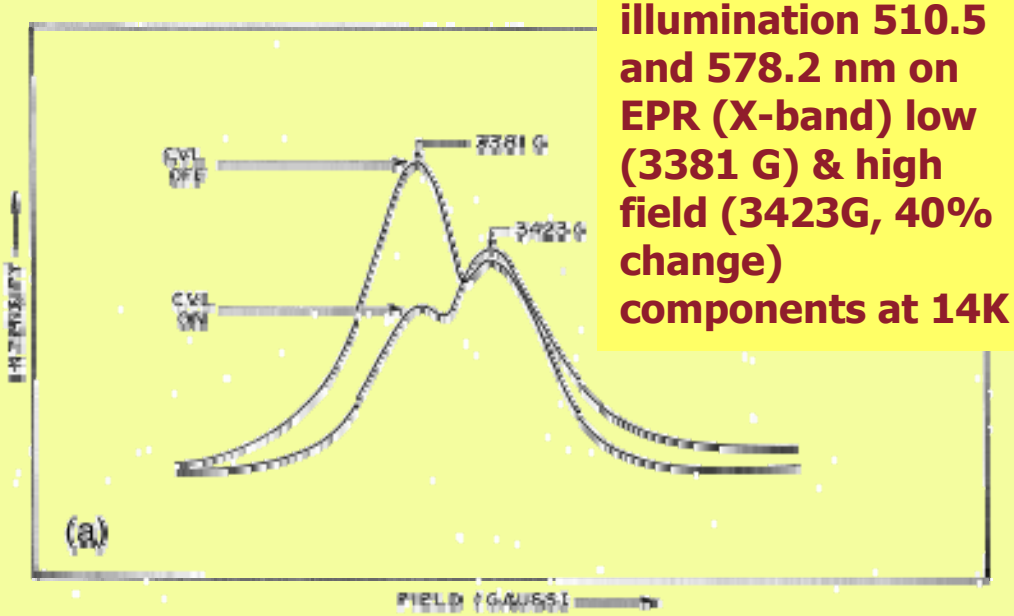

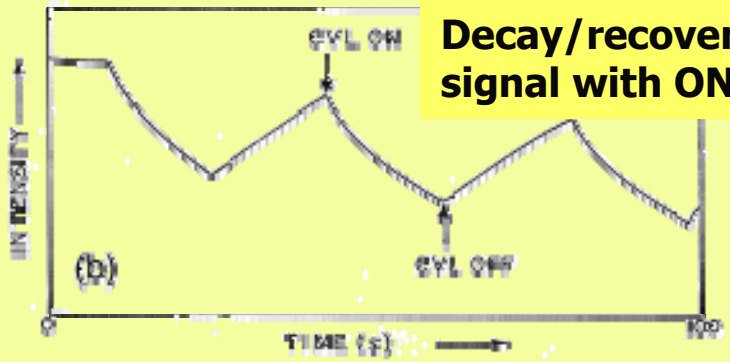

Decay/recovery of low field signal with ON/OFF of CVL

Electronic excitation follows decoupling of spins

Bistability

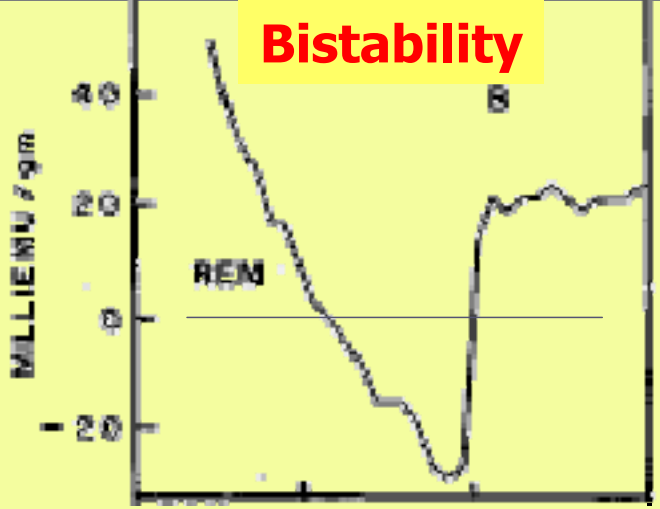

A: $(NBu_4)_2Mn_2[Cu(opba)]_3.6DMSO.1H_2O$
B: $(NBu_4)_2Mn_2[Cu(opba)]_3$
Chavan, Ganguly, Jain and Yakhmi,
J. Appl. Phys. 79 (1996) 5260

Magnetic Bistability first seen in ferrites.

M(T) passes thru zero when two sub-lattice magnetizations have different M vs. T

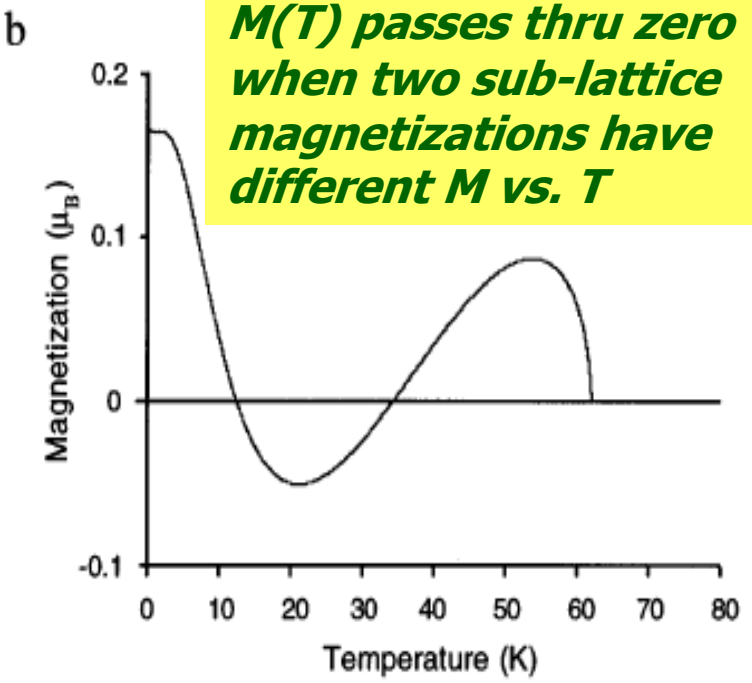

As transistor size ≤20 nm, "Moore's law" will not hold, because

1. transistors would have unacceptable heat dissipation;

2. lithography to fabricate Si-devices of smaller size doesn't exist.

That would herald "molecular electronics" –

***information processing at the molecular-scale*.**

Monolayers/organic molecules (0.5 to 2.5 nm, mechanically flexible/chemically tunable).

tunnel junctions (Metal/(molecule or monolayer)/Metal, wires, rectifying diodes, switches, memories…) all MOLECULAR/Organic/Polymer

We discuss SAMs (self-assembled monolayers) of alkyl chains on Si-substrates ["HYBRID electronics"]

Alkyl chains consisting of:

σ bonds can act as dielectric,

σ–π molecules as rectifier and/or transistor, and

σ–π–σ molecules as resonant tunnel diodes.

Organic Semiconductors

Polymer Semiconductors

Poly(3-hexylthiophene)

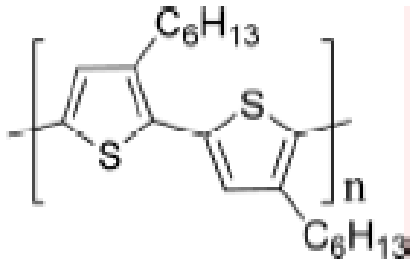

MEH-PPV

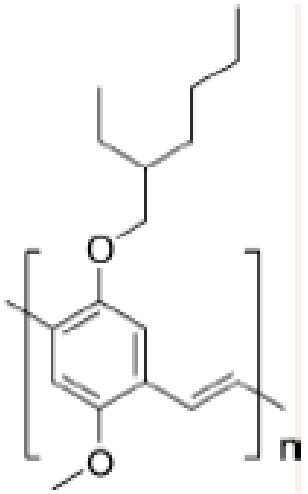

Polyaniline

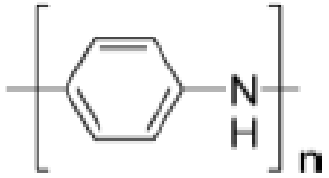

Small Molecule Semiconductors

Sexithiophene

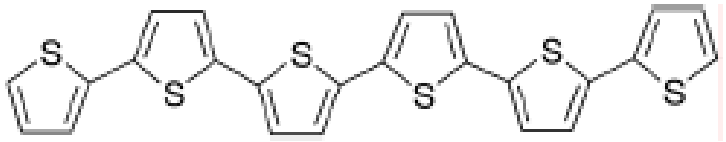

Alq_3

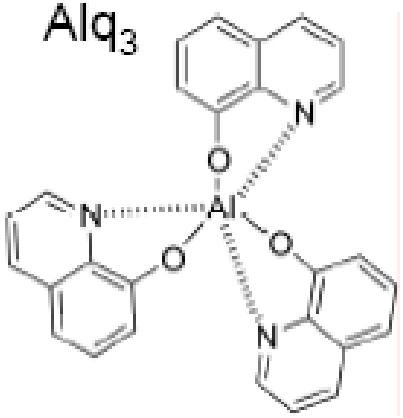

Pentacene

Phthalocyanine

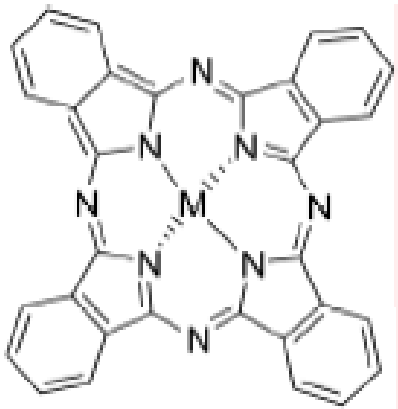

Perylene

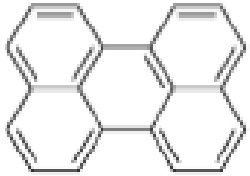

Relative Charge Mobilities

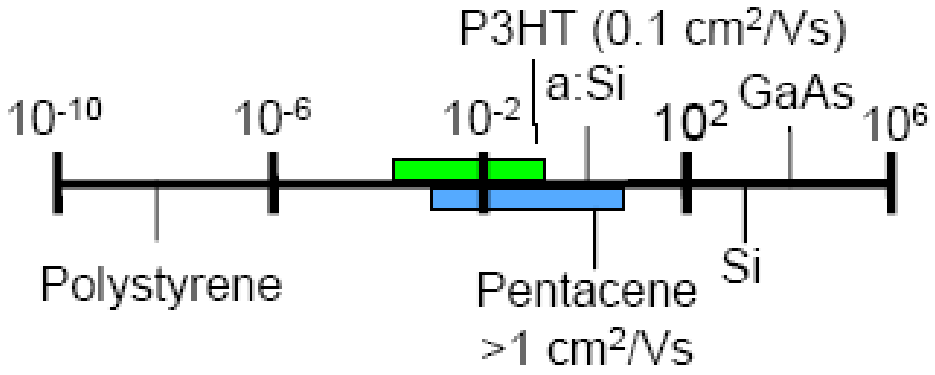

molecular electronic devices using Self-Assembled Monolayers

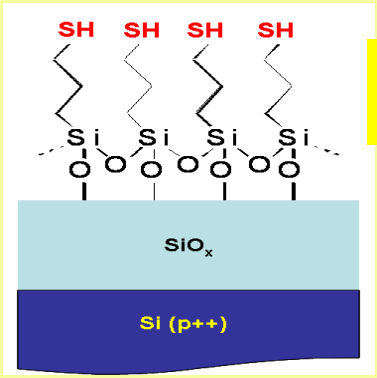

(a) σ–monolayer as dielectric

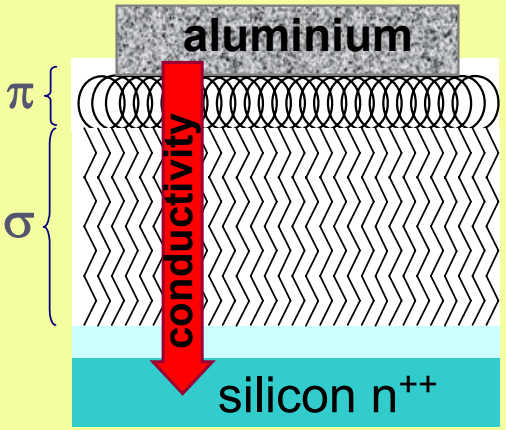

(b) Rectifying diode (σ–π SAM on Si)

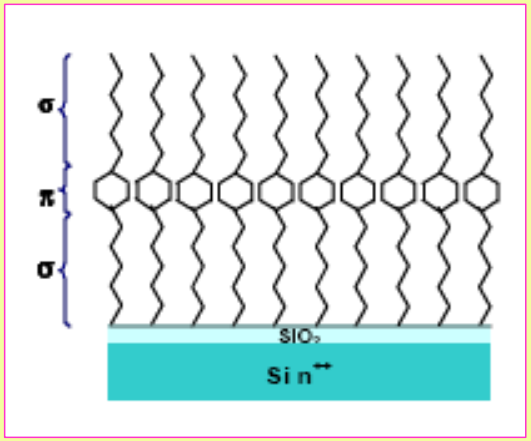

(c) Resonant tunnel diodes (RTD) using σ–π–σ SAM on Si

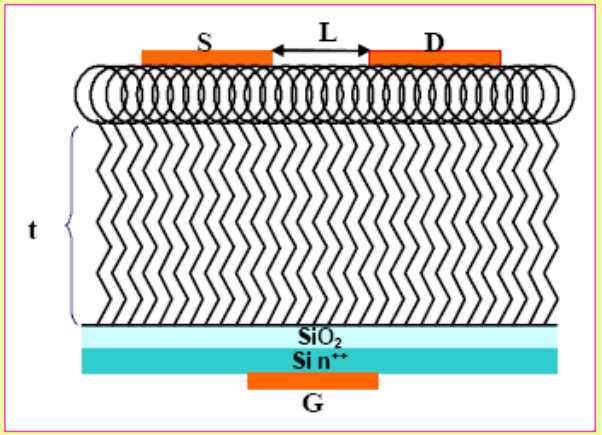

(d) Molecular transistors based on σ–π SAM on Si

Heterostructure, σ/π/σ, SAM. RTD effect occurs when the LUMO or HOMO of the π group is in resonance with the conduction or valence band of the silicon electrode.

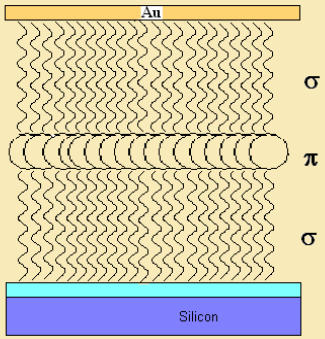

(a)

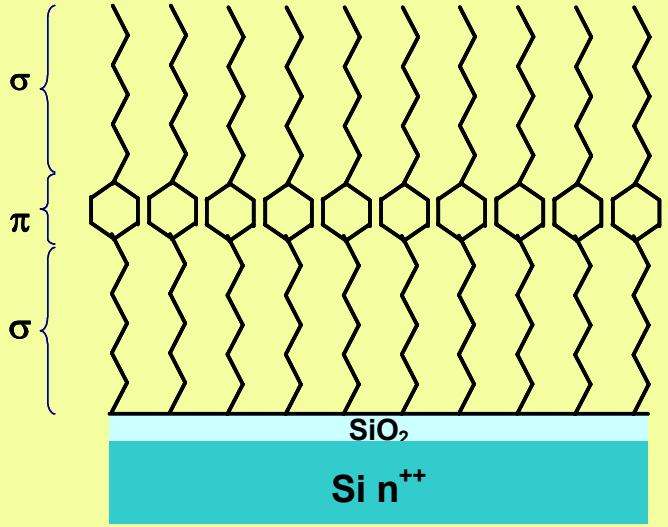

(b)

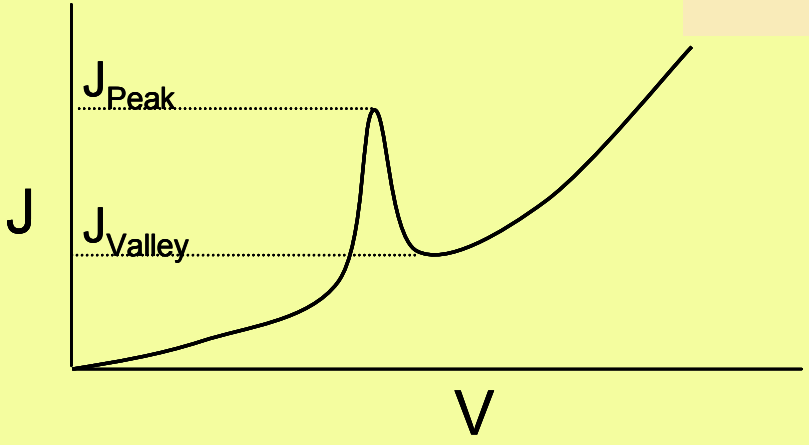

(c)

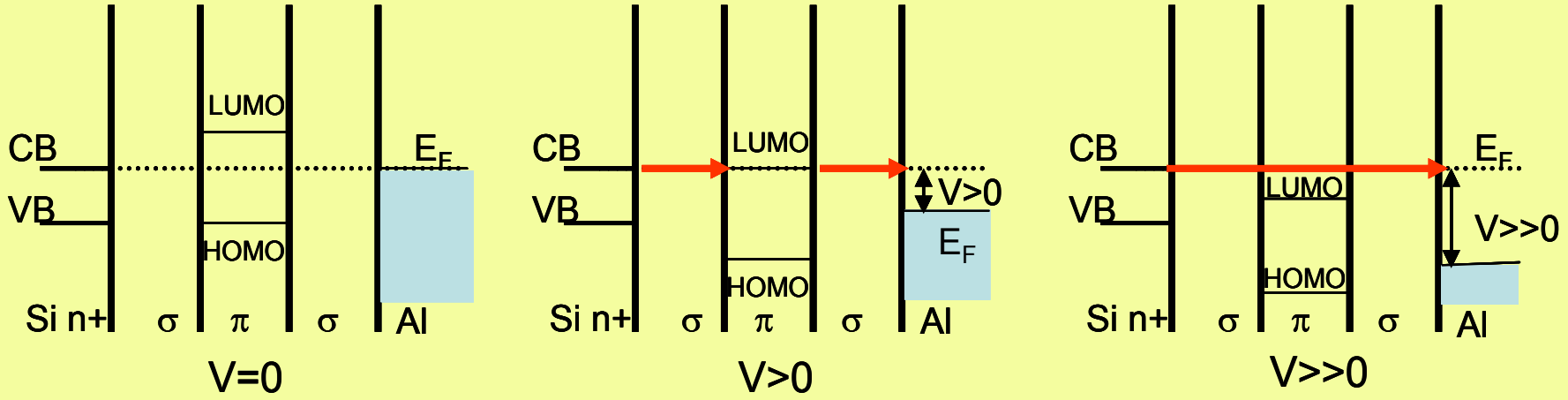

(a) concept, (b) characteristic J-V and (c) the mechanism of a σ-π-σ SAM based Molecular Resonating Tunneling Diode (MRTD).

Design of new functional materials (even single crystals) for devices using:

SAM as a template;
DNA as a tempate;
Air-water interface (Langmuir trough);
Liquid-liquid interface

DNA as a template to prepare nanocrystals

Denaturation: upon heating DNA base pairs open up, causing damage to DNA structure.

Beautiful fractal structures are formed during denaturation, due to diffusion limited aggregation – which act as templates!

DNA template used to prepare nanocrystals of NiHCF, which got arranged in different morphologies.

Templating comes from electrostatic interactions with the polyphosphate backbone etc. and covalent attachment to nanoparticles

Bagkar, Choudhury, Bhattacharya and Yakhmi, *J. of Phys. Chem., Part B* 112 (2008) 6467-6472

Room Temp. synthesis of NiHCF nanocrystals using calf thymus (CT)-DNA as a template. Electrostatic interaction between the negatively charged DNA and NiHCF nanocrystals arranges the nanocrystals along the chain of base pairs.

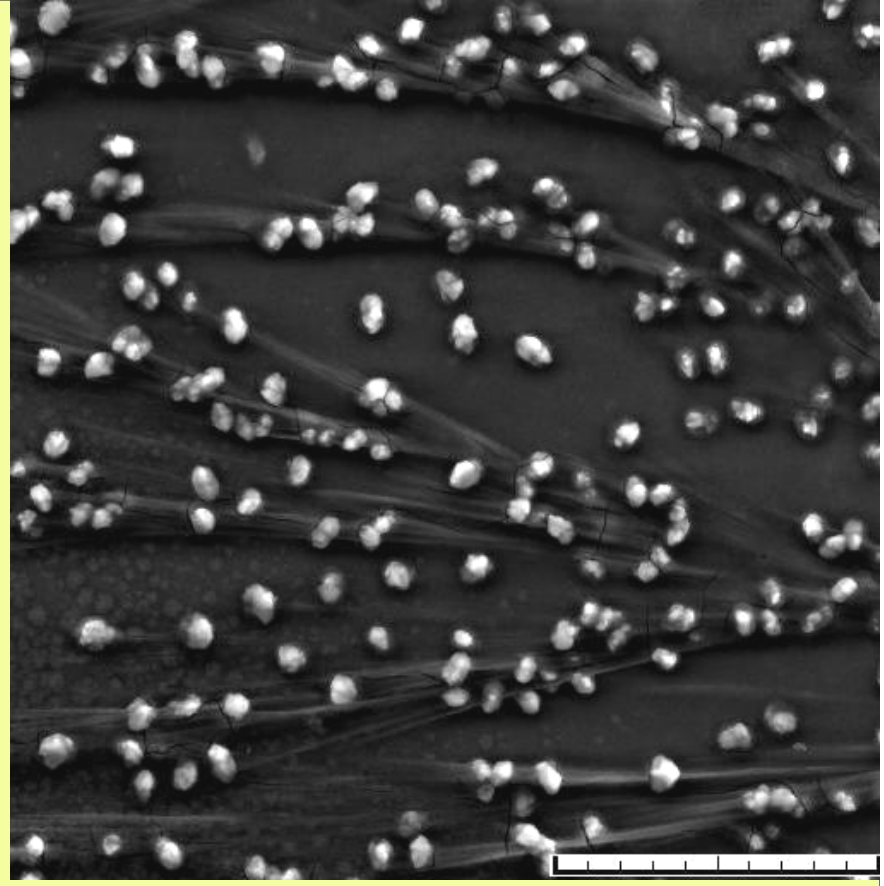

SEM image of DNA-NiHCF at room temp. (scale bar – 100 μm). Cubic nanocrystals of NiHCF (average dia of 400 nm) are arranged along the DNA chain.
These long rods extending upto few micrometers at R.T.

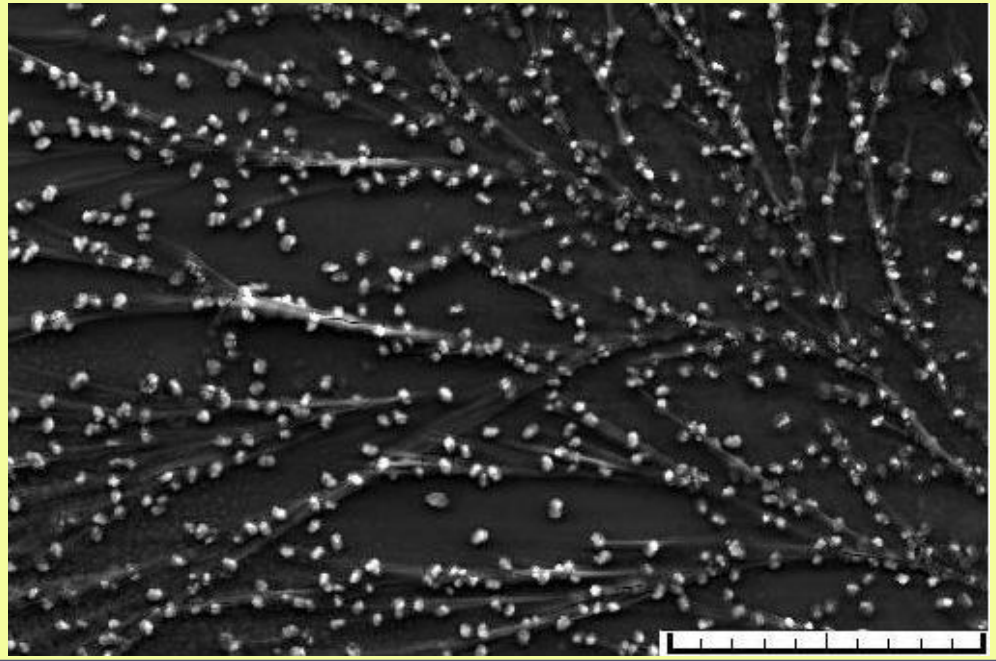

Enlarged view to depict uniform distribution of crystals of NiHCF over a large area (scale bar - 200 μm)

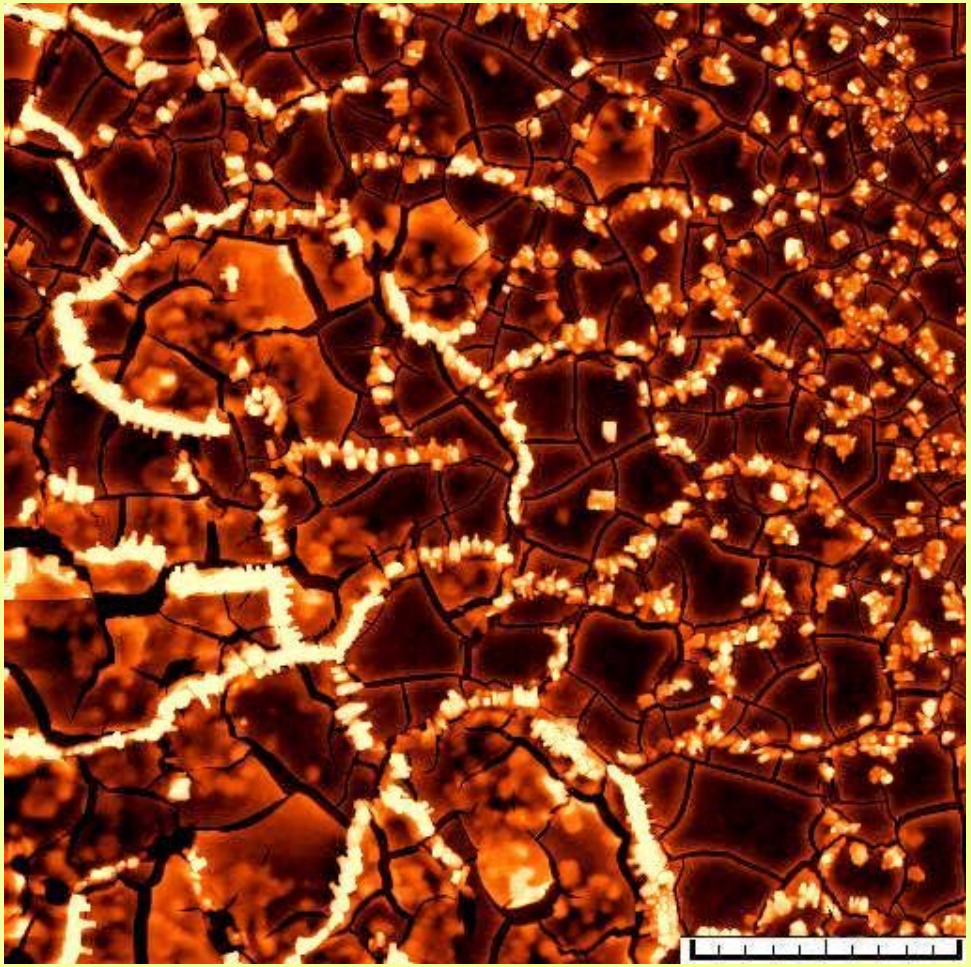

DNA-NiHCF conjugate at 50° C (scale bar: 50 mm).

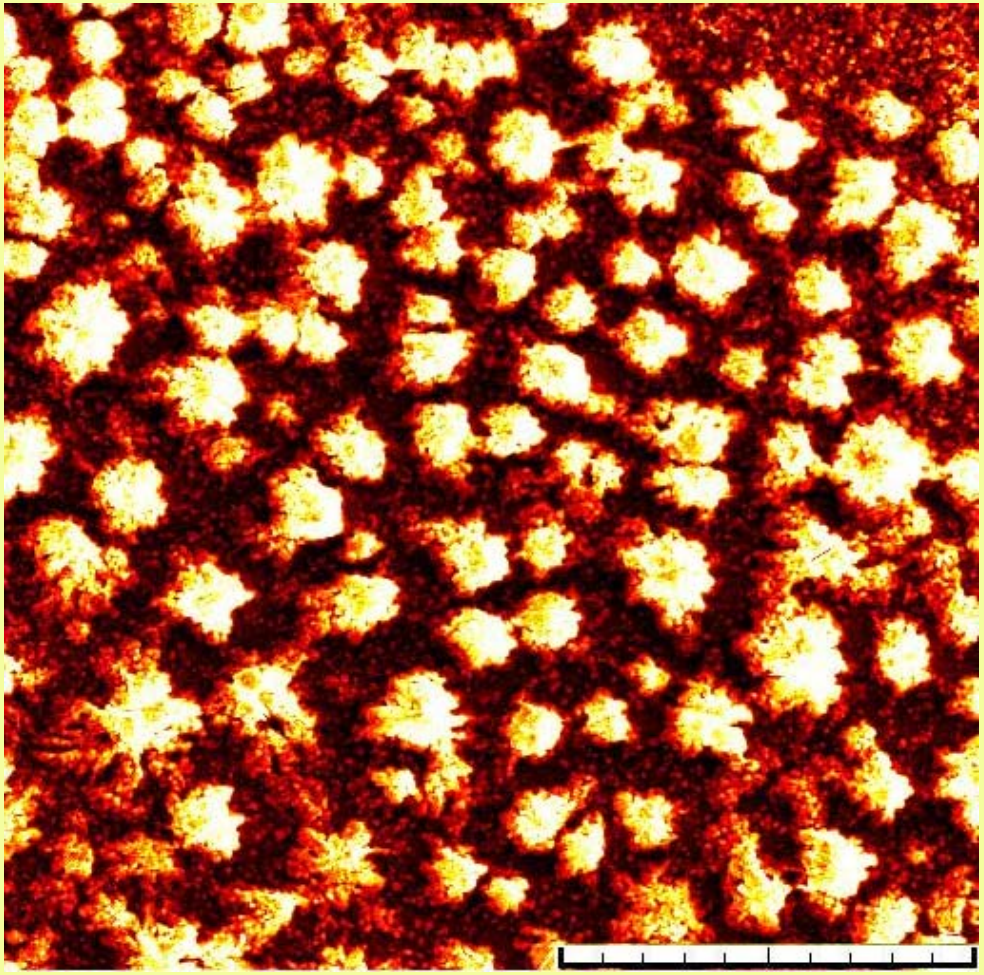

spherical globules of DNA-NiHCF at 60° C (scale bar: 200 mm)

Bagkar, Choudhury, Bhattacharya and Yakhmi, *J. of Phys. Chem., Part B* 112 (2008) 6467-6472

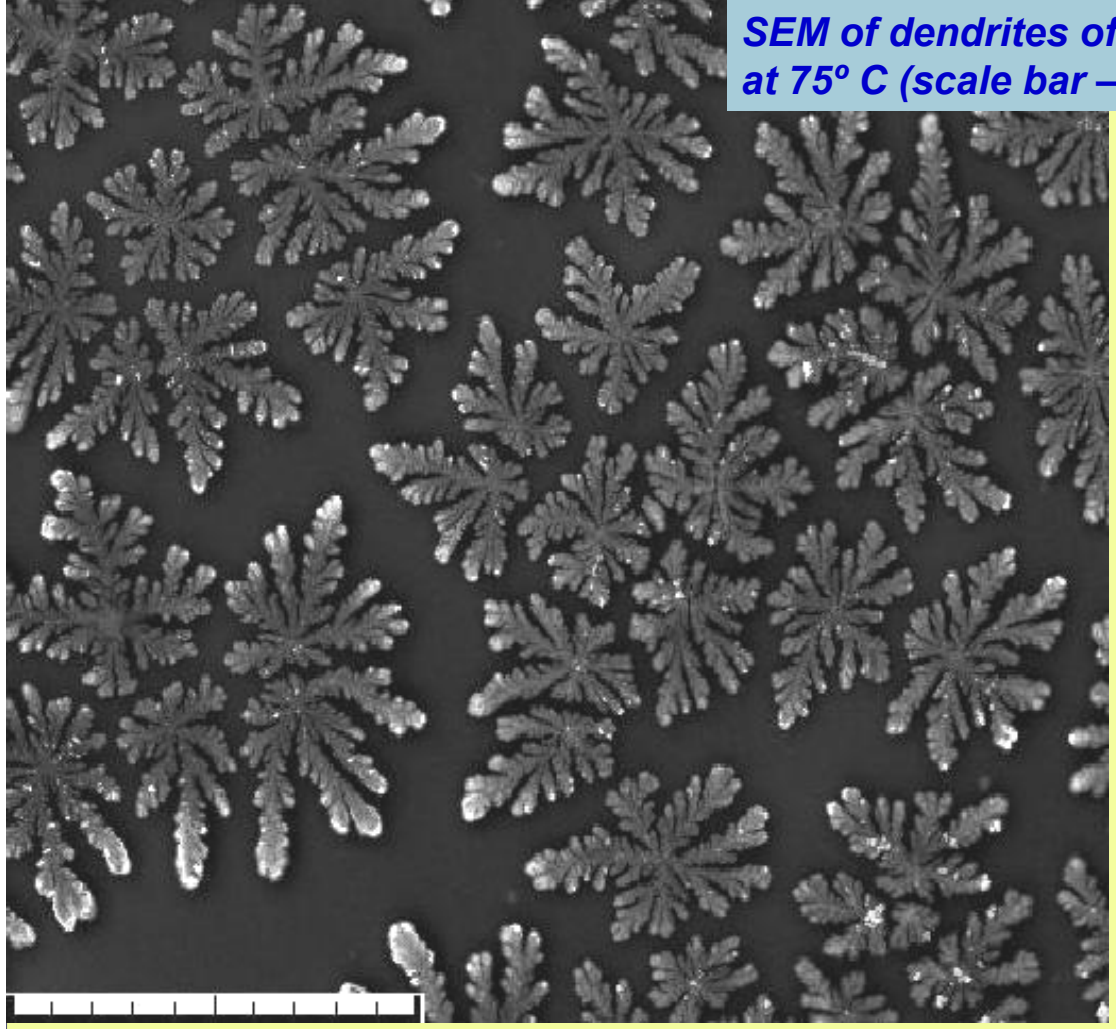

SEM of dendrites of DNA-NiHCF conjugates at 75° C (scale bar – 100 µm).

Dendritic fractals appear at 75° C Each lobe is about 10 micrometer in size. NiHCF particles within these aggregates retain their physical shape and size.

Surface of dendrimer curls with numerous chain-ends, acting as a template directing the self-assembly of nanocrystal aggregates of NiHCF along the tip of a branching unit.

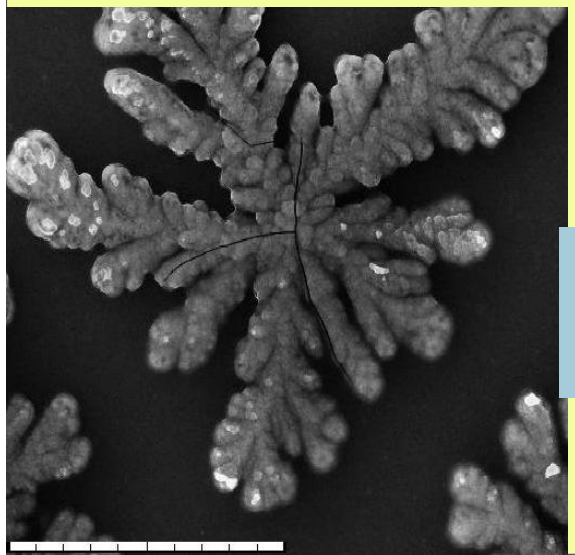

a single dendrite of DNA-NiHCF conjugate. Scale bar- 20 µm

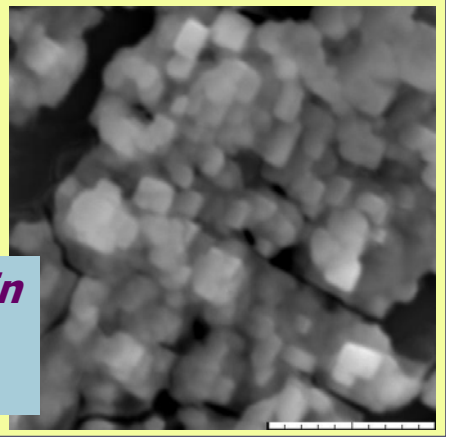

cubic crystals within dendrites (scale bar – 5 µm)

Interfacial synthesis of long *1000 μm, ~25μm dia* polyindole fibers

Self-assembly

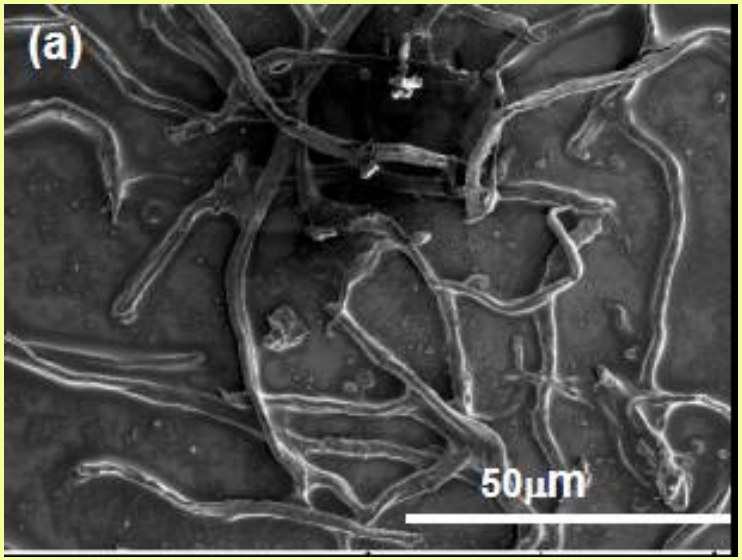

SEM of polyindole Synthesized by (a) interfacial and (b) bulk polymerization

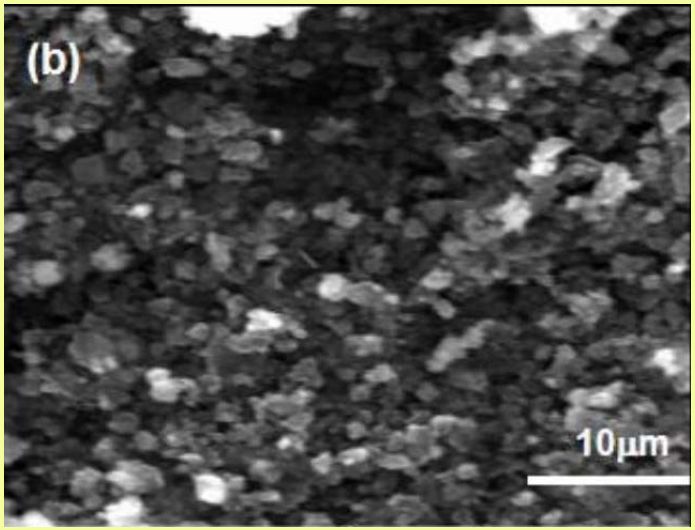

Polymerization conducted at a stationary interface of aqueous ($FeCl_3$ solution)/organic (indole in dichloromethane) biphasic system.

But, disturbing the aqueous/organic interface by constant stirring (viz. bulk polymerization) gives globules (av. size ~2 μm) of polyindole.

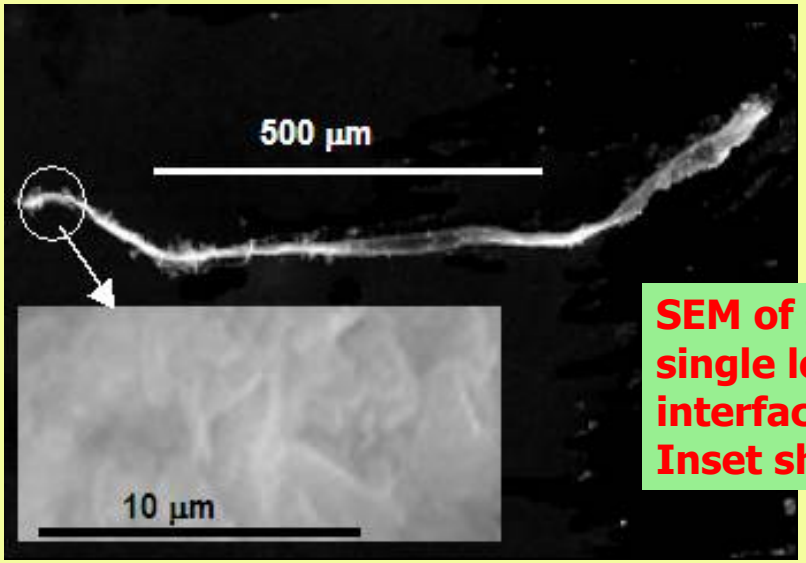

SEM of a mechanically separated single long fiber obtained by interfacial polymerization. Inset shows a magnified section.

Koiry, Saxena, Sutar, Bhattacharya, Aswal, Gupta, Yakhmi, *J Appl. Polymer Sci.* 103 (2007) 595

Chemical structure of indole – consists of a benzene and a pyrrole ring.
Core level C1s and N1s XPS spectra: nitrogen not involved in polymerization.

FTIR: polymerization takes place at C-atoms located at positions 2 and 3 in indole monomer.

The CV data indicated a high electroactivity of polyindole fibers

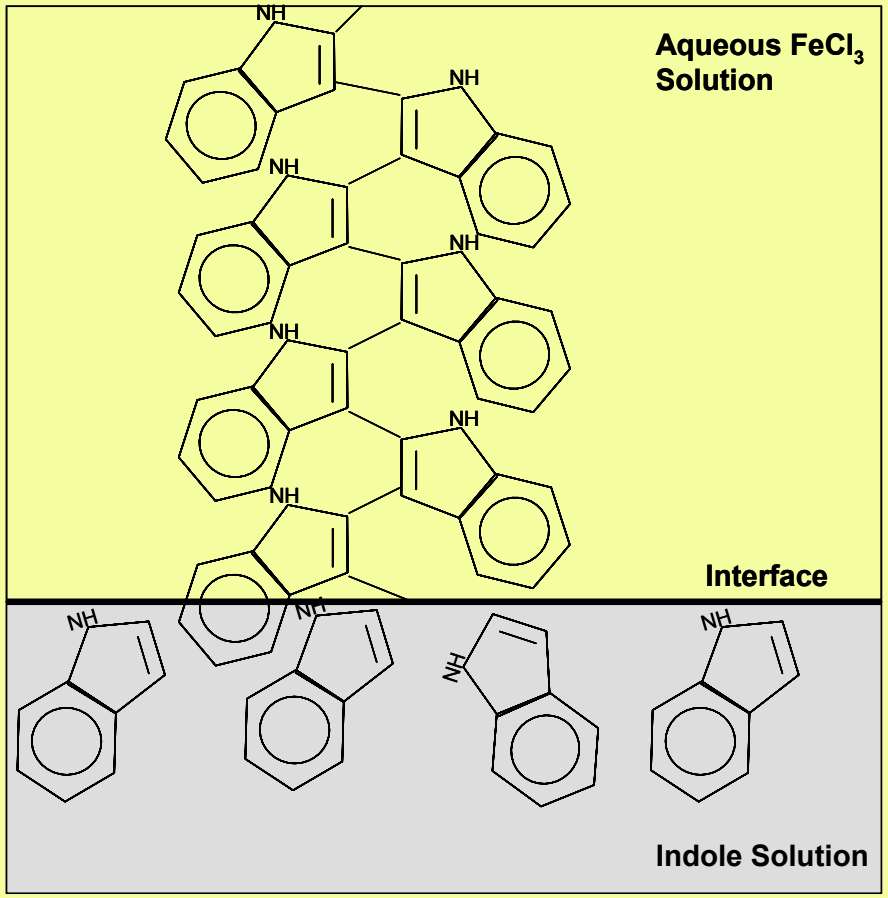

why long fibers are synthesized During interfacial polymerization?

At the immiscible aqueous/organic interface, indole monomer gets protonated in the presence of oxidant $FeCl_3$. This preferentially aligns them at the interface.

Polymerization sites in indole being 2 and 3 carbon positions, preferentially aligned monomers undergo a directional polymerization via self-assembly, leading to long fibers of polyindole.

Stirring destroys preferential alignment!

using SAM as a template to grow Single crystals of PANI

SAM of aminosilane [$((CH_3O)_3$-Si-$(CH_2)_3NH(CH_2)_2$-$NH_2)$]

N-[3-Trimethoxy silyl propyl]-ethylene diamine

deposited on hydroxylated silicon

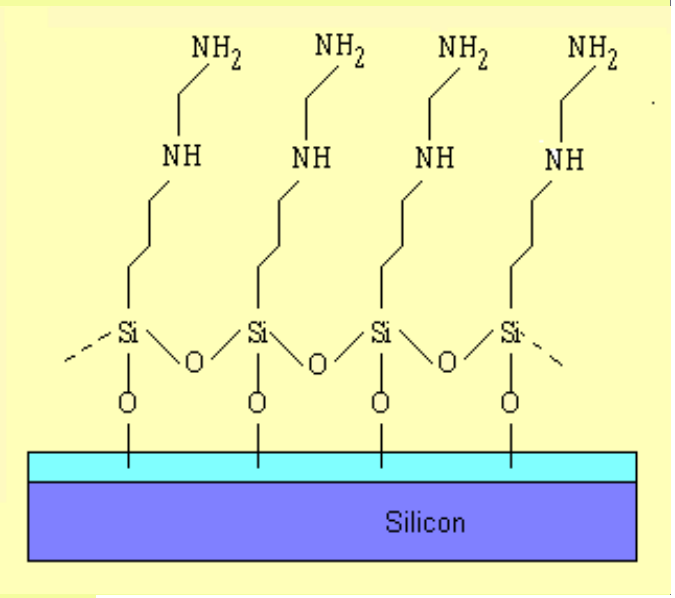

amino groups (NH_2) on SAM-modified surface act as seeds for self-organization of PANI, during chemical polymerization of aniline. Polyaniline (Emeraldine hydrochloride**) thus grafted on silanized substrate**

Sutar, Padma, Aswal, Deshpande, Gupta and Yakhmi,
J. Coll. And Interf. Sci. 313 (2007) 353-8

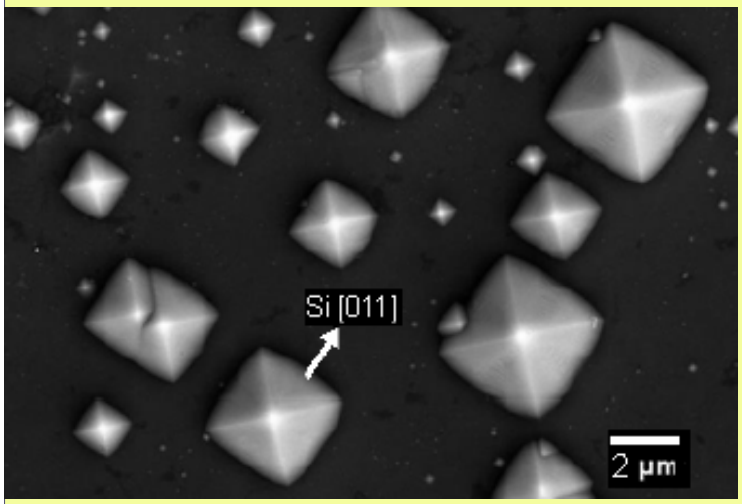

SEM

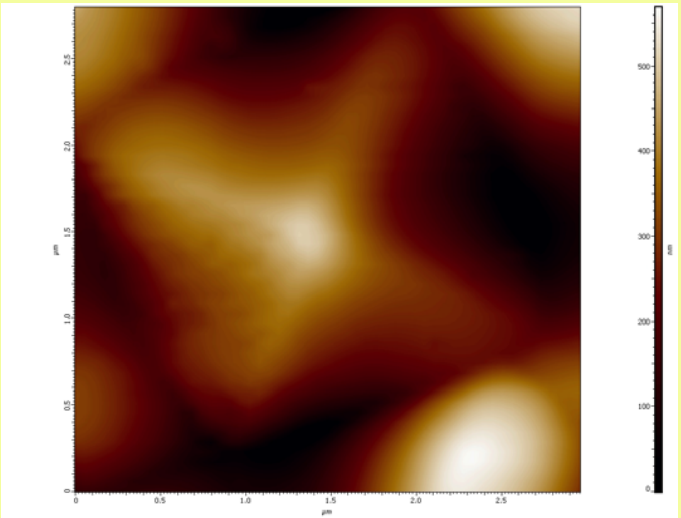

AFM

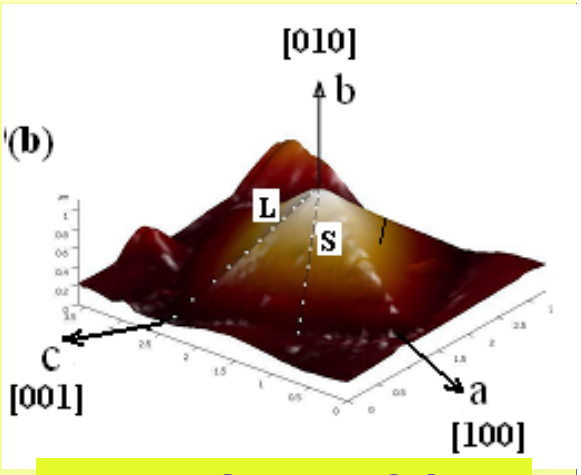

3D-AFM image of the single crystal pyramid, L and S denote lateral and slant heights.

surface amino (NH_2) groups on aminosilane SAM are converted to radicals ($NH_2^{+\cdot}$) on which the aniline monomers are immobilized. These monomers get self-organized into polymer chains

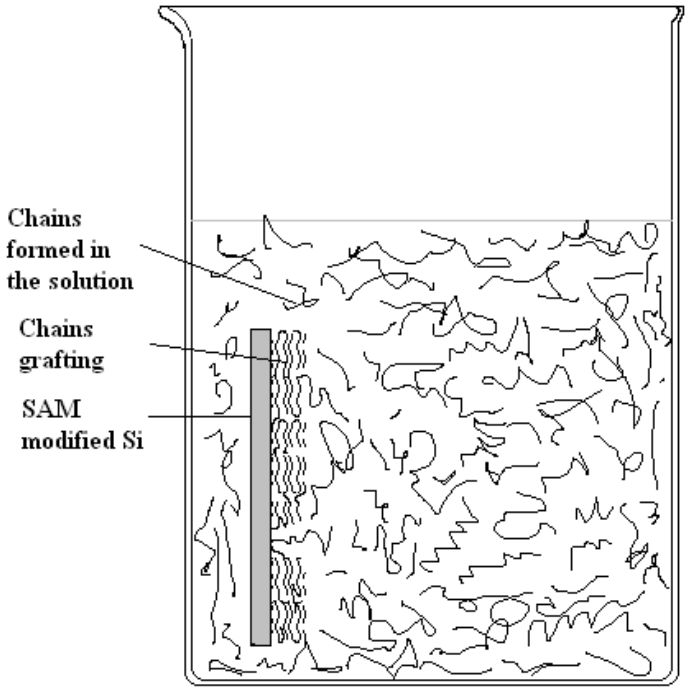

(a)

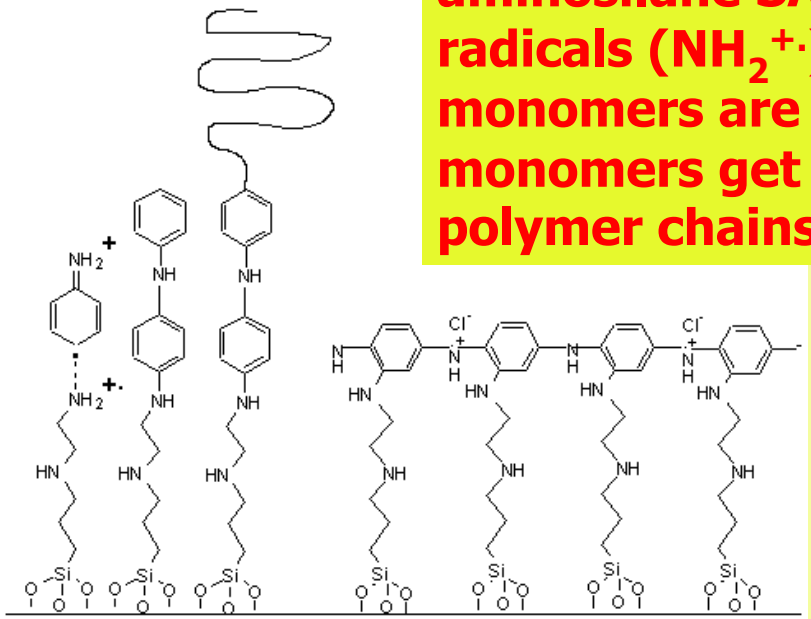

(b)

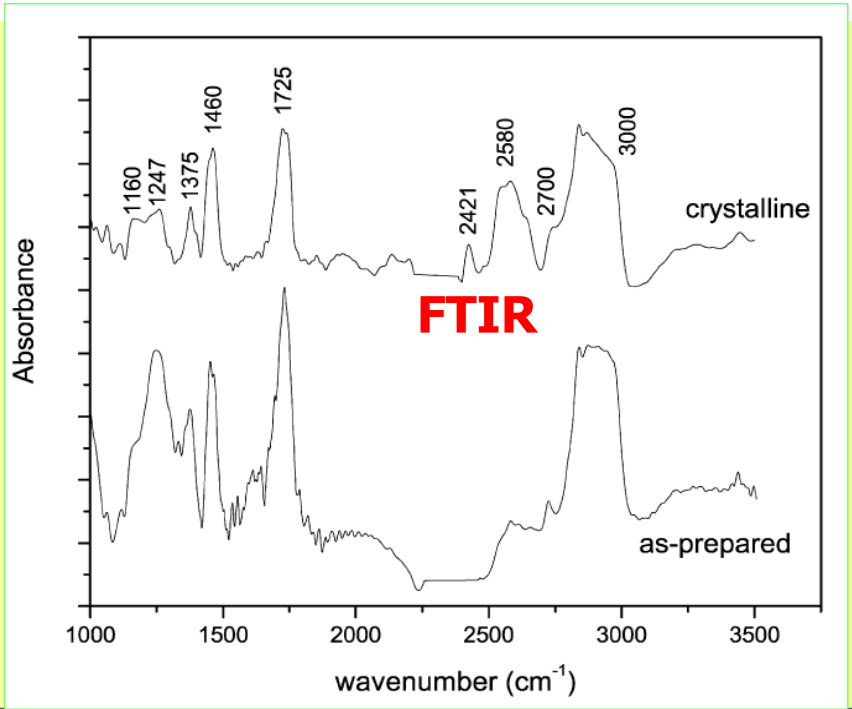

FTIR

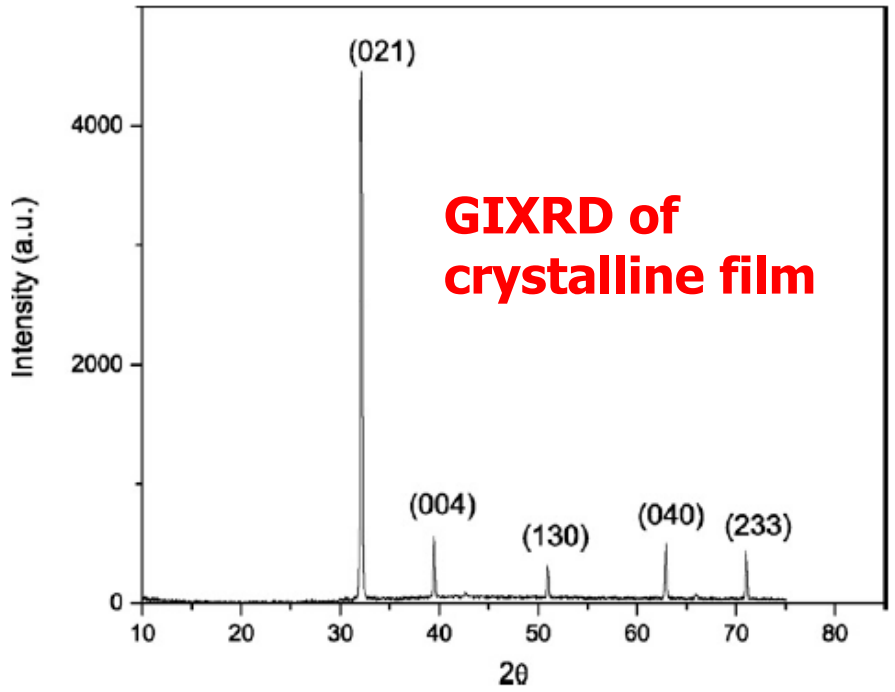

GIXRD of crystalline film

tapping mode AFM of PANI film: for Surface Morphology

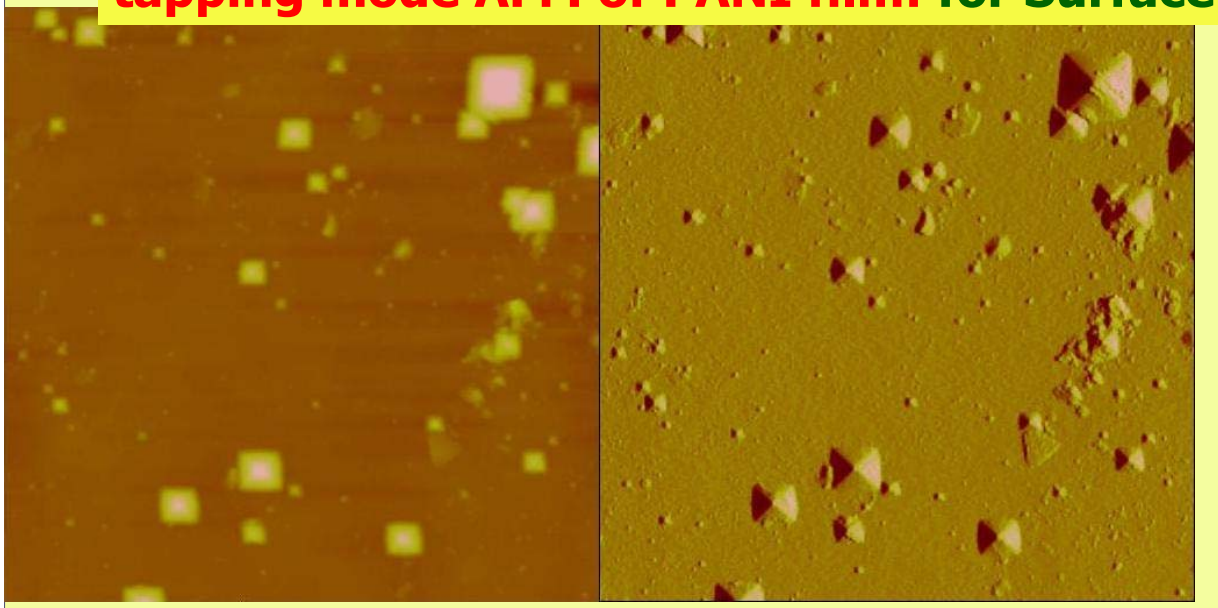

(a) topography image shows crystalline domains scattered all over,
(b) amplitude image shows pyramid shaped crystallites facets more clearly;

scan size is 25 μm and Z scale is 2 μm.

C-AFM Scans of the PANI film :

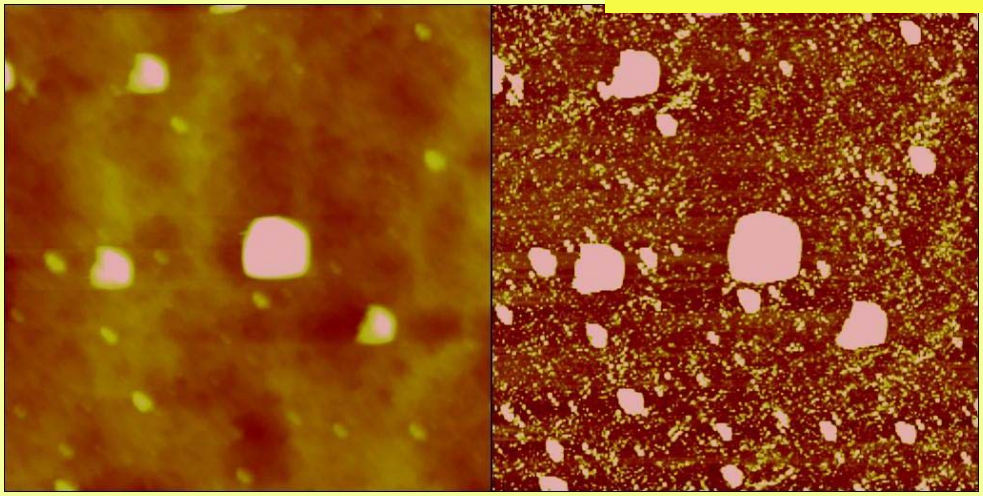

(a) Topography and (b) current image. Both taken concurrently under 0.8 V bias; *10 μm scan size.*

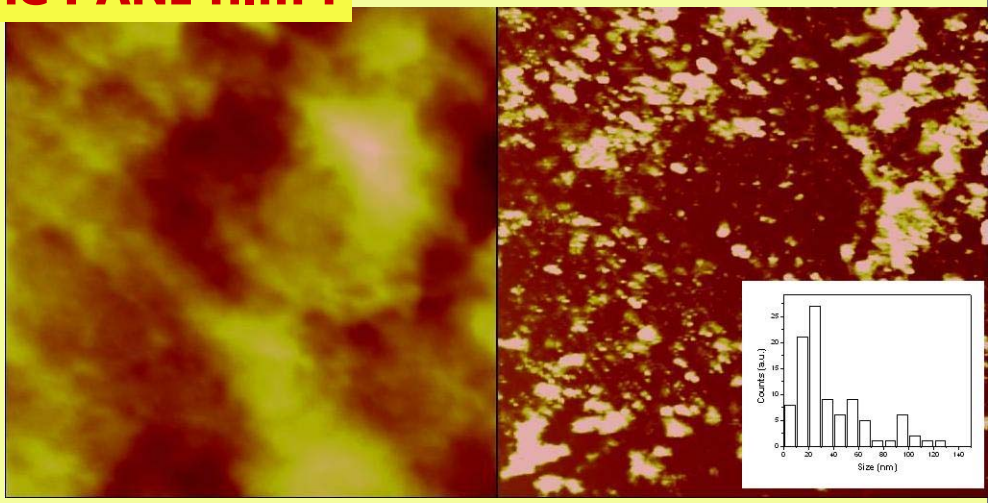

(c) Topography and (d) current images taken at higher magnification and 1 V bias. *scan size is 2 μm.* Nanocrystallites are 20-55nm (inset)

(a) Bright field, and
(b) Dark field image of single crystal lamellae

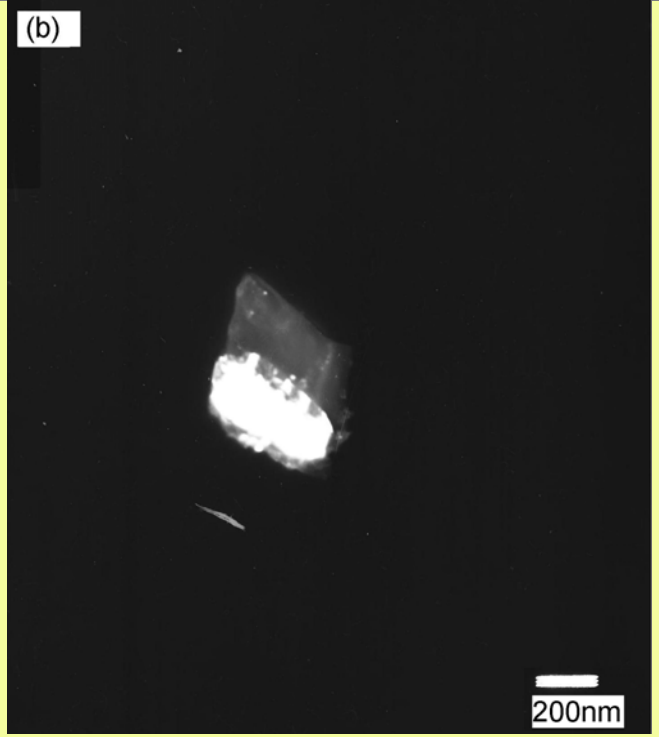

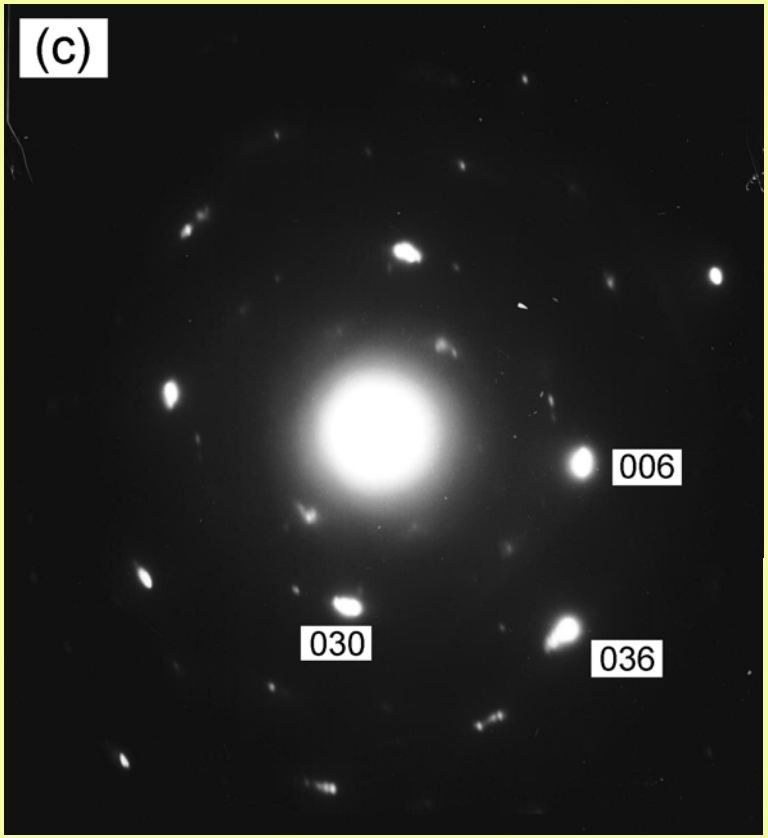

Sutar, Tewari, Dey, Gupta and Yakhmi
Synth. Metals (submitted Sep. 2008)

(c) Selected area electron diffraction (SAED) pattern for the single crystal lamellae

rectangular symmetry **observed for the first time for PANI single crystal.**
{100} plane is the easy cleavage plane.
Unit cell parameters are *b*=5.8 Å, *c* =9.8 Å.

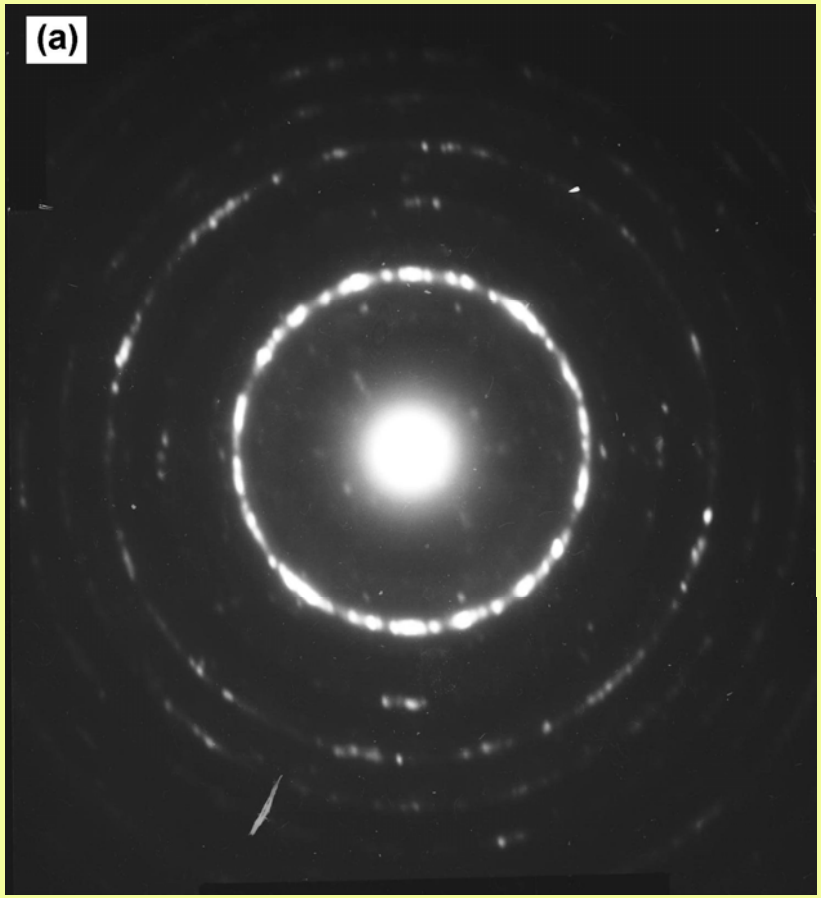

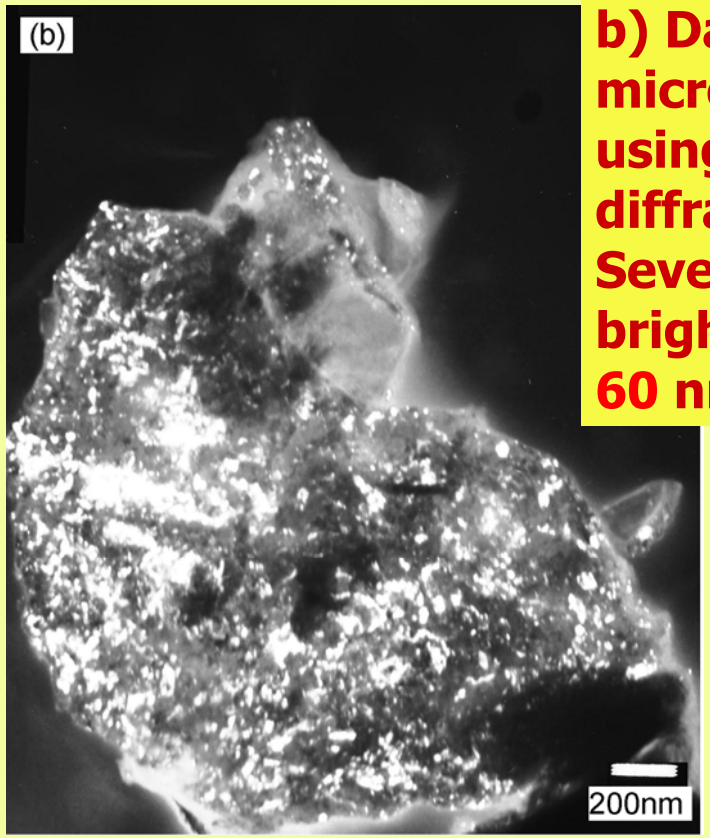

b) Dark field electron micrograph obtained using an arc of diffraction pattern. Several diffracting bright particles (10 – 60 nm) seen

a) Electron diff. pattern shows bulk of film is polycrystalline.
(Several sharp concentric rings)

orthorhombic structure unit cell parameters are *a* =4.2 Å, *b*= 5.9 Å and *c* = 9.8 Å.

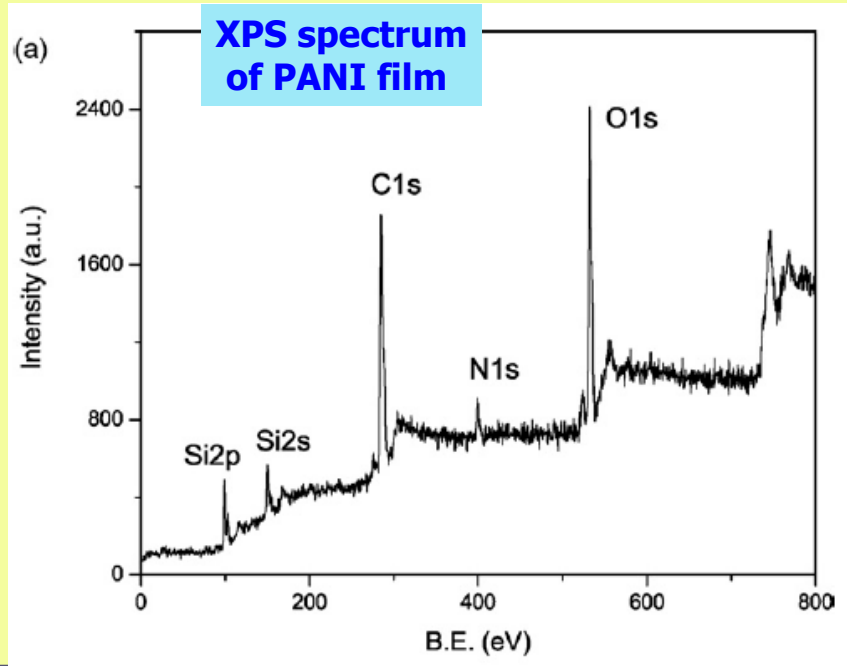

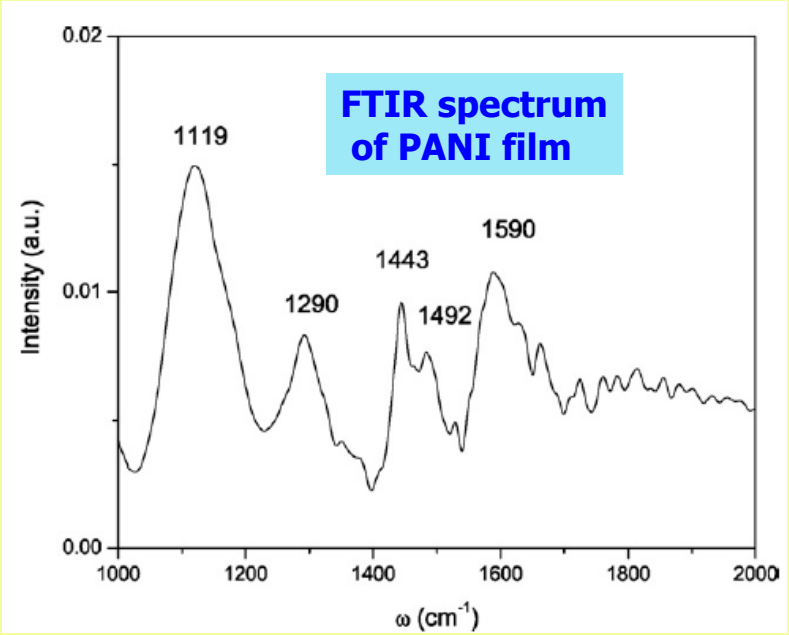

NH3 Sensing by these PANI films

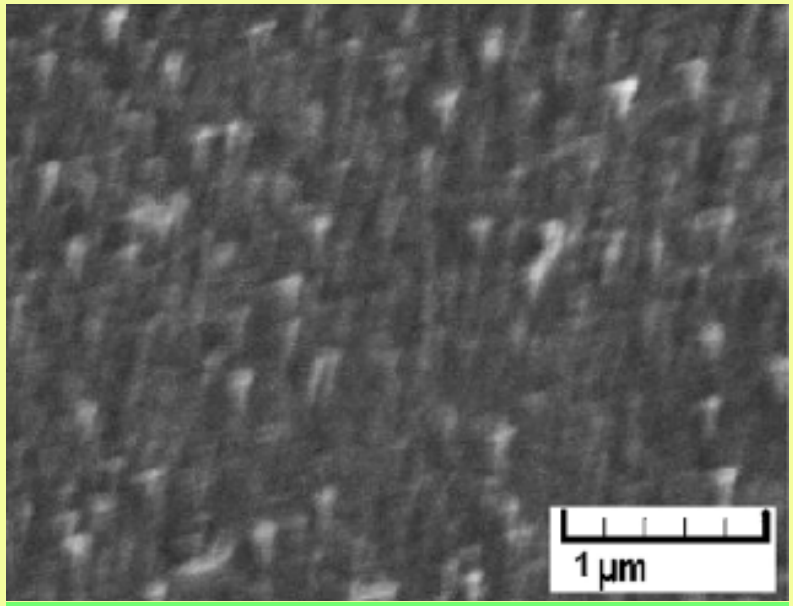

nanofibrous morphology. Most fibers oriented normal to the substrate

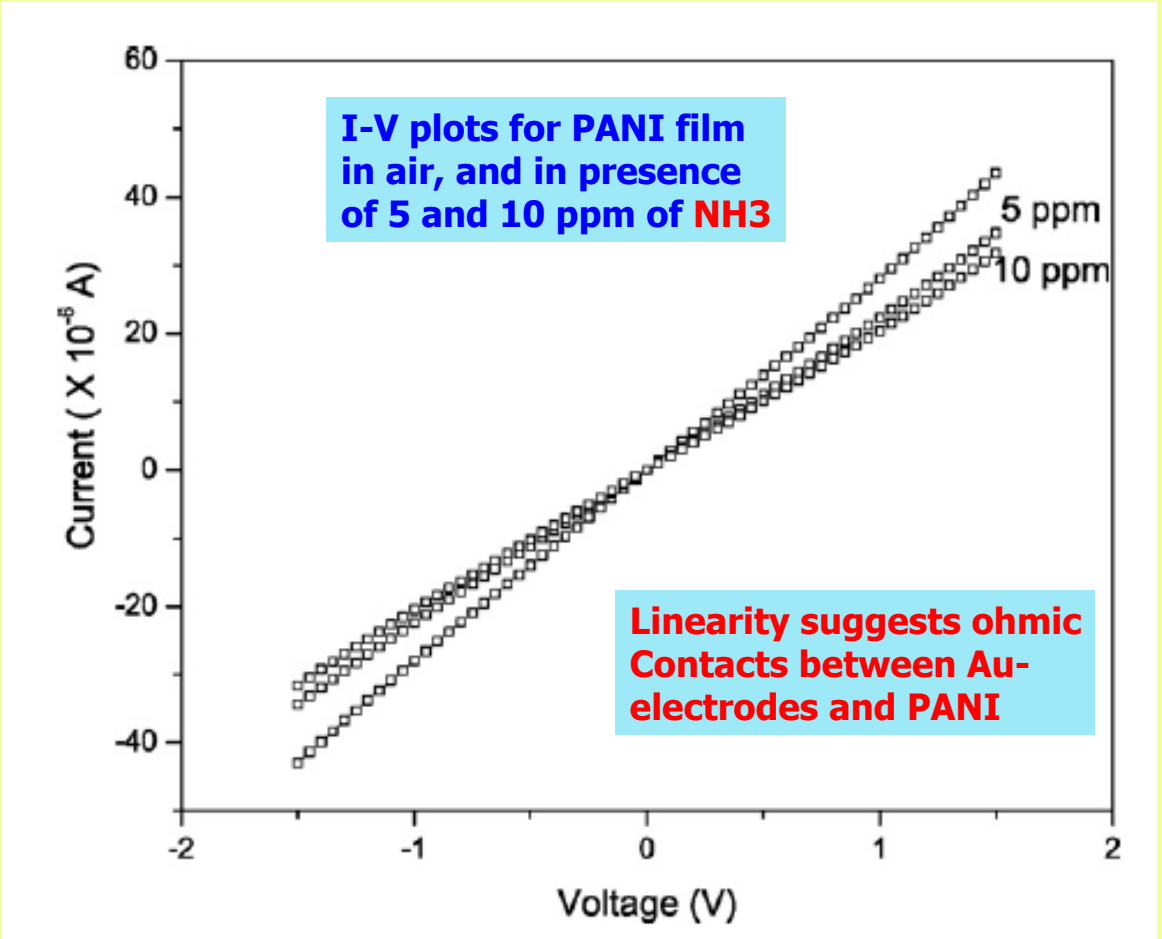

PANI sensor for very low concentrations (0.5ppm) of NH3

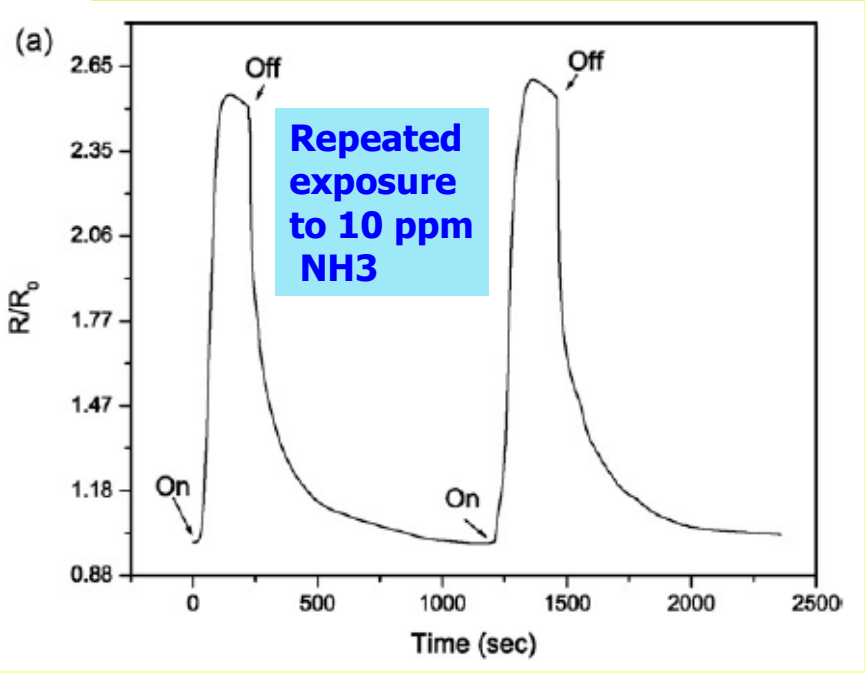

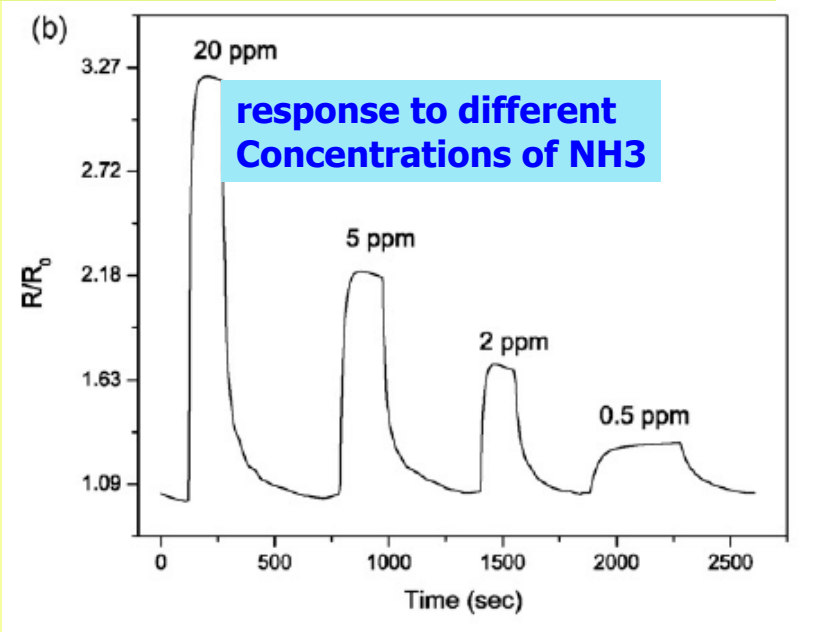

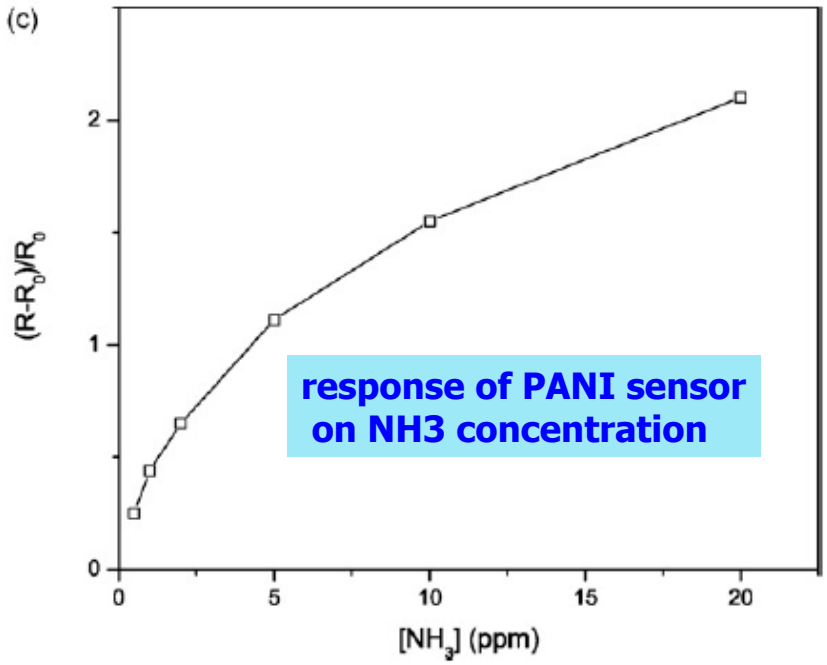

Emeraldine (PANI) is efficient sensor for NH3 because *N-atoms in both can bond with protons on the polymer chain.*

Sensitivity and reversibility of PANI to NH3 comes through deprotonation–reprotonation mechanism

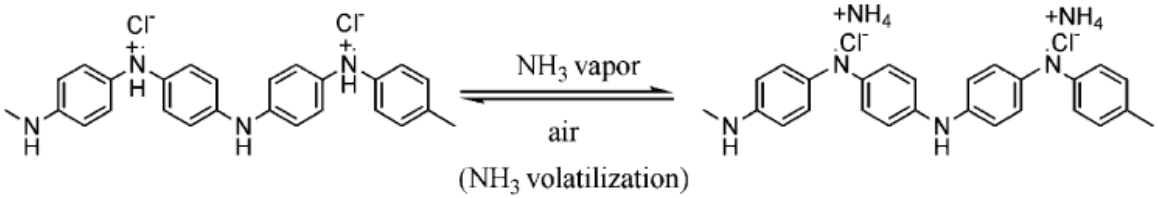

Sutar, Padma, Aswal, Deshpande, Gupta and Yakhmi, *Sensors and Actuators B* 128 (2007) 286

Study of Tunneling Conduction across n^+-Si/SAM/PANI (MIS) heterostructure from *I-V* measurements using C-AFM probe

Insulating aminosilane SAM can act as a tunneling barrier between metal-like substrate and PANI, forming an ideal MIS structure

Crystalline PANI films deposited on (100) oriented n+-Si substrate, surface modified with SAM of amino-silane.

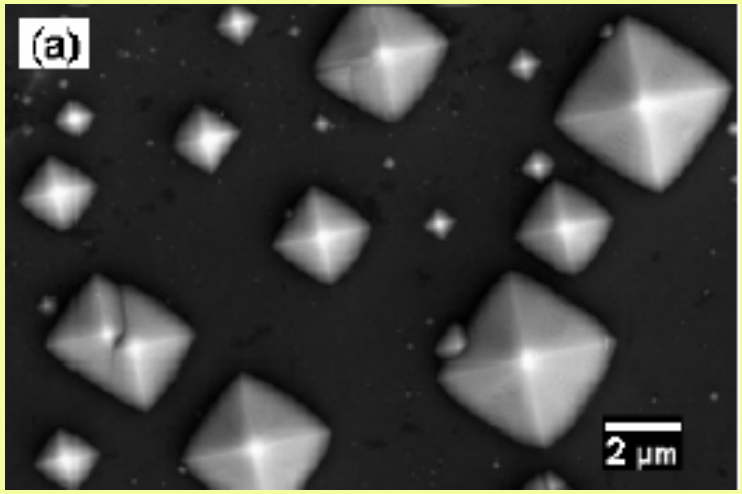

SEM: pyramid shaped crystallites (largest 3-4 microns) distributed on a textured polycrystalline base layer!

Orientation of all pyramids is same, hence they are in registry with the underlying SAM, & with the Si- substrate

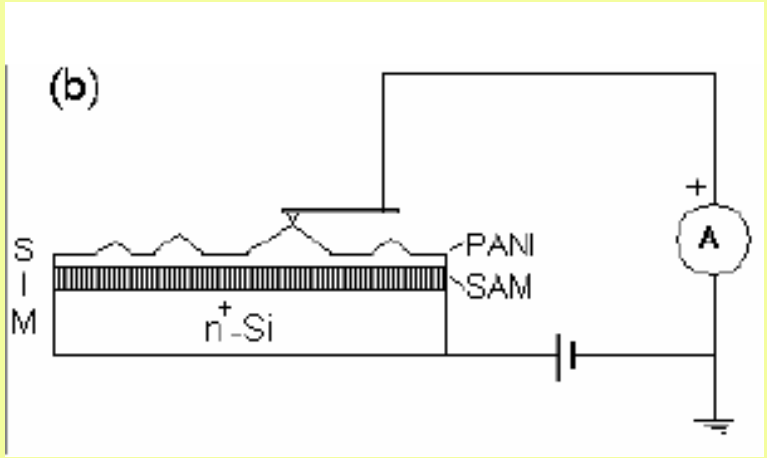

C-AFM measurement, on the MIS structure:
Si substrate (metal) and PANI (semi conductor) separated by thin alkyl SAM (insulating).
Transport through alkyl silane monolayer separating the electrodes, is through tunneling conduction.

I-V characteristics measured at different points on film surface

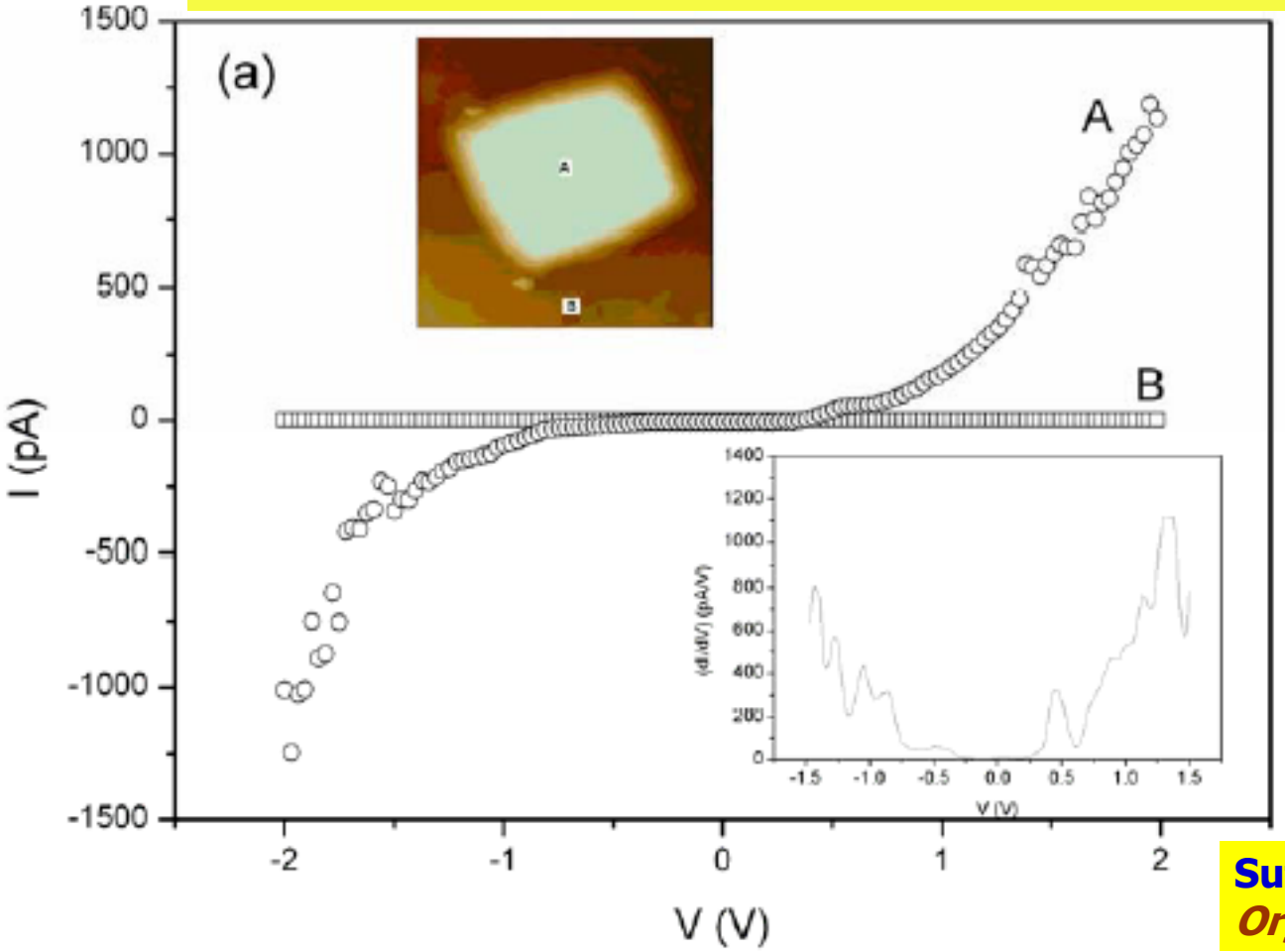

contact is ohmic, since Pt/Ir and doped PANI have same work-function (~5.0 eV)

Upper Inset shows points where the tip was placed for *I-V* measurement

Sutar, Lenfant, Vuillaume, and Yakhmi
Org. Electronics 9 (2008) 602-608

Crystallites are conducting, whereas bulk of the film is Insulating.

Curve A (measured at point A on the crystallite): tunneling conduction through insulating alkyl SAM. Small shoulder in range +0.3 to +0.8 V, manifesting as a peak in the tunneling conductance spectra obtained from this curve, (lower inset-plot).

Plot B (measured at point B) shows no current flow, implying insulating nature of this area of the film.

SAMs on Si-substrates for molecular electronics: of long alkyl-chains (C > 18) for gate dielectric in FETs; of short alkyl-chains σ–π–σ (C=3–6) for RTDs

OH-terminated Si-substrate

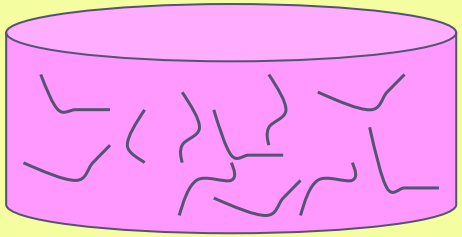

Silane-solution

Chemisorption

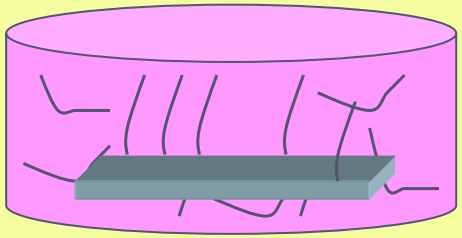

Organization

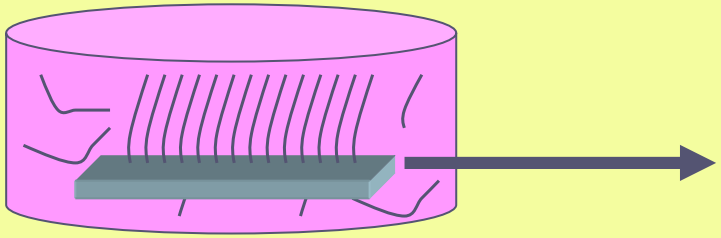

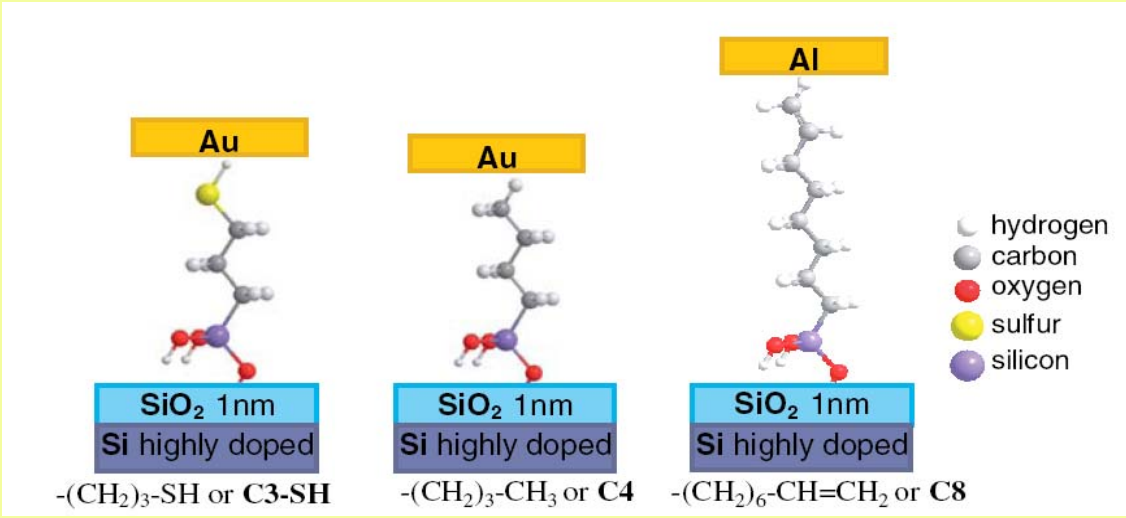

Silanes: $R(CH_2)_nSiX_3$ (X = Cl, OCH_3 or OC_2H_5) dissolved in alkane/CCl4

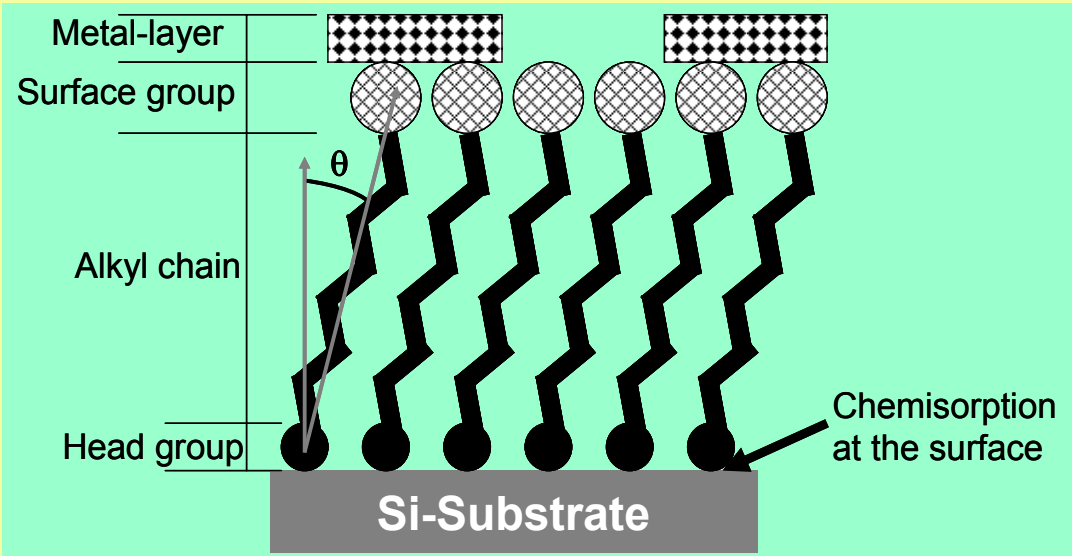

(oxygen and humidity <1 ppm)

Growth kinetics of C-18 monolayer

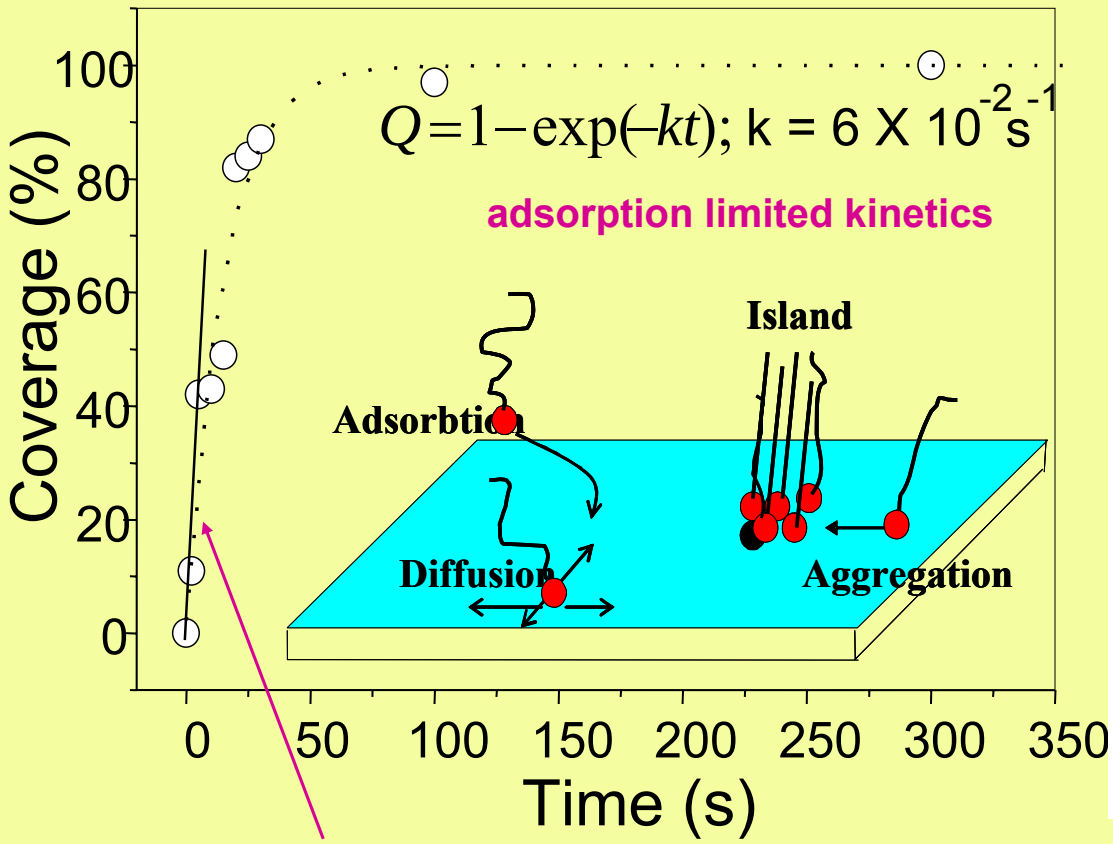

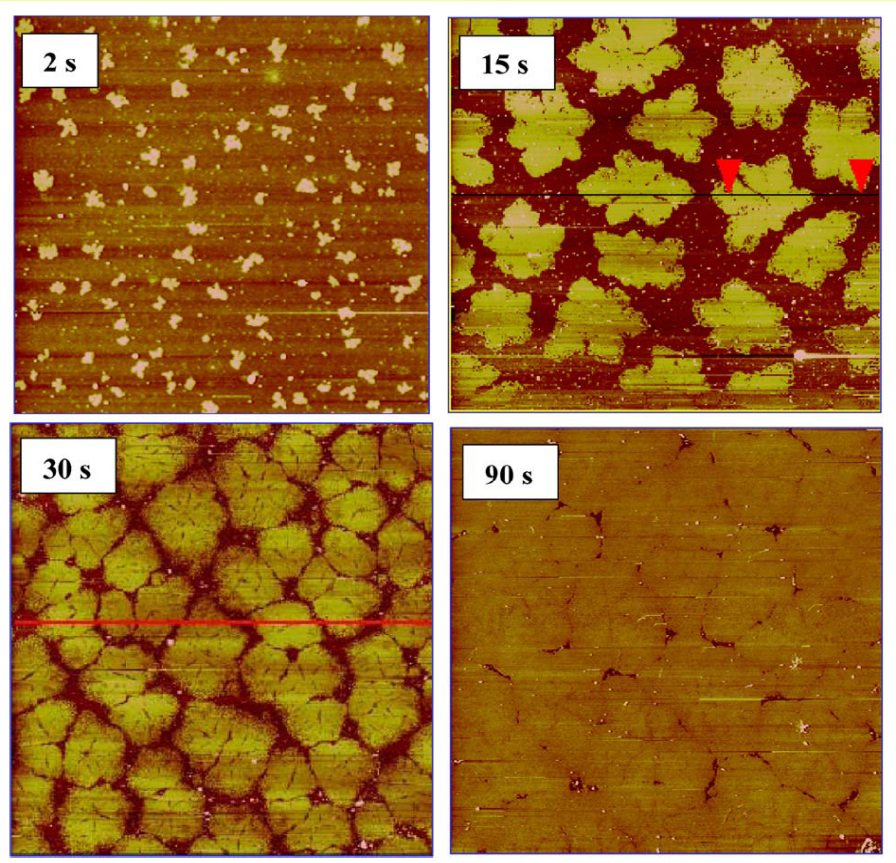

10μm×10μm images of partial C18 monolayer on Si immersed in octadecyltricholorosilane (OTS) solution for varying amounts of time.

L. Breuil, Ph.D. Thesis, 2000. University of Science and Technology, Lille, France.

Why HYBRID? - a molecular/organic layer device on Si

Leakage current thru SiO_2 layer at <1 V increases from $<10^{-12}$ to 10 A cm^{-2} (12 orders of magnitude!) as it is thinned from 3.5 to 1.5 nm

leakage current decreased to $<10^{-8}$ A cm^{-2} when *n*-alkyltrichlorosilane ($CH_3(CH_2)_{n-1}SiCl_3$; n >8) molecules (length <2 nm) were grafted, on native SiO_x surface.
Rectification ratio of 37 observed at 1V when a conjugated (π) group was attached to the alkyl-chain (σ), making a σ–π SAM.

Bright future of hybrid electronics: organic molecules on Si !

We showed that SAM of 3-mercaptopropyltrimethoxysilane (MPTMS) , i.e. 3-C chains, SH–(CH2)3–Si–(OCH3)3, on the oxide layer of highly doped Si is an excellent tunnel dielectric and *We are well below the limits of Si-based dielectrics, Since the SAM has a short length (0.8 nm)!*

Why deposit SAMs from small (only 3-C) alkyl-chain? viz 3-mercaptopropyltrimethoxysilane $SH-(CH_2)_3-Si-(OCH_3)_3$

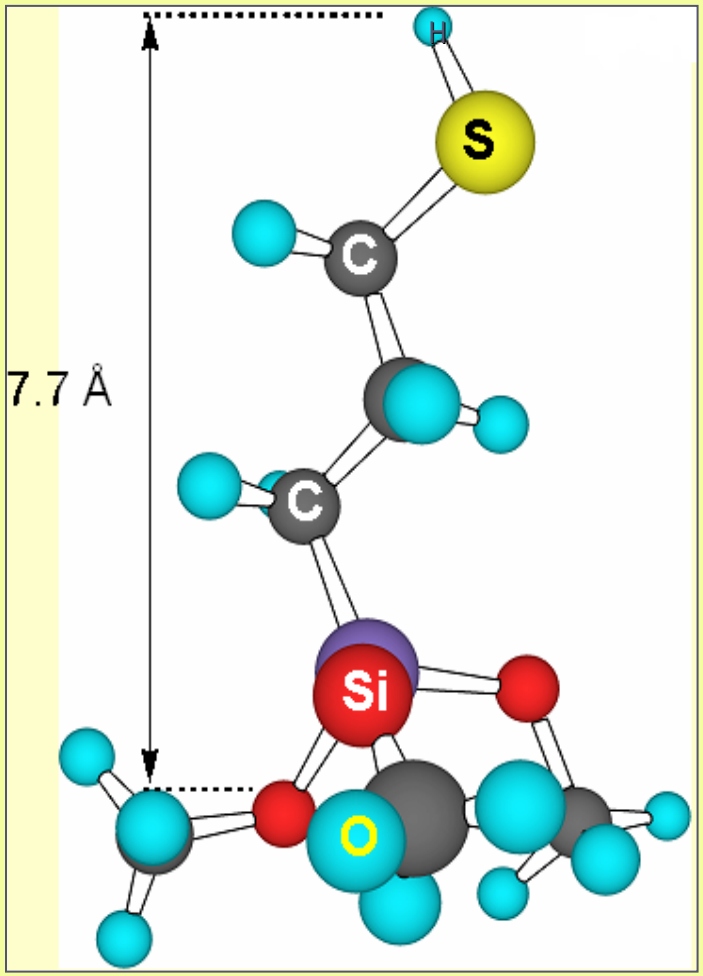

1. Low BP = 92°C at 40 mm Hg
   Suits Vapor-phase technique for SAM

2. the aliphatic chain of only 3-C
   has a very short length (0.8 nm),
   Earlier lowest studied was 8C

3. It has siloxane group:
   SAM can be grown on SiO_x/Si

4. the molecule is thiol (-SH) terminated,
   prevents diffusion of counter electrode
   Au, owing to strong S-Au chemical bond,
   facilitates further attachment of π and/or π - σ moieties

Ellipsometry:

Thickness = ~8 Å

Pin-holes & Defects ? thru Electrochemical characterization

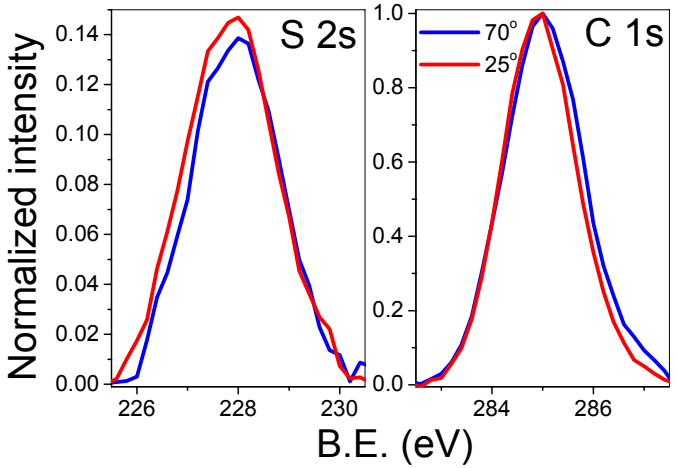

XPS : -SH terminated

Molecular order and density from FTIR data

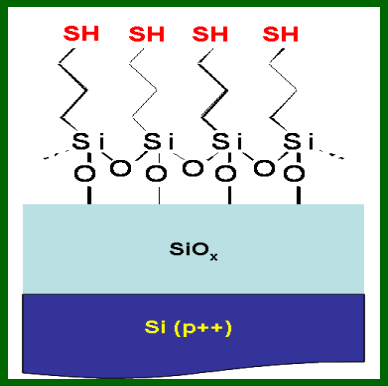

Characterization

AFM : uniform SAM

Water contact angle:

65±3°

typical of –SH group

AFM

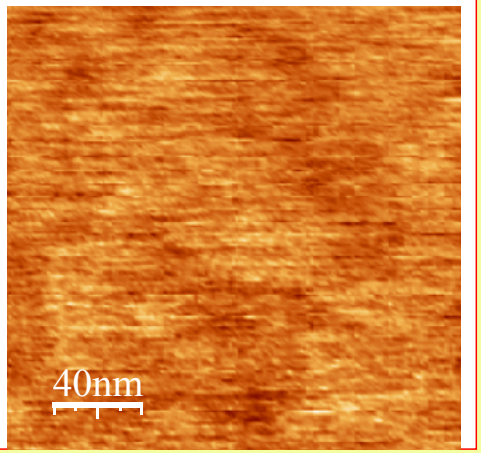

Electrical measurements

Au- counterelectrodes deposited by thermal evaporation

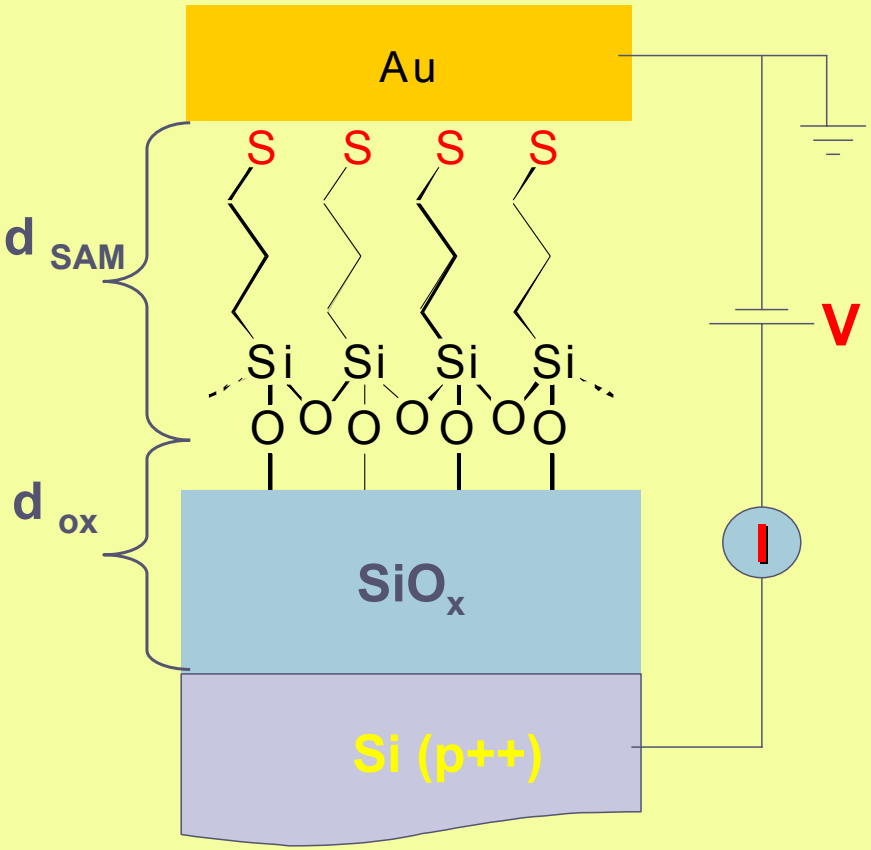

Schematic of device

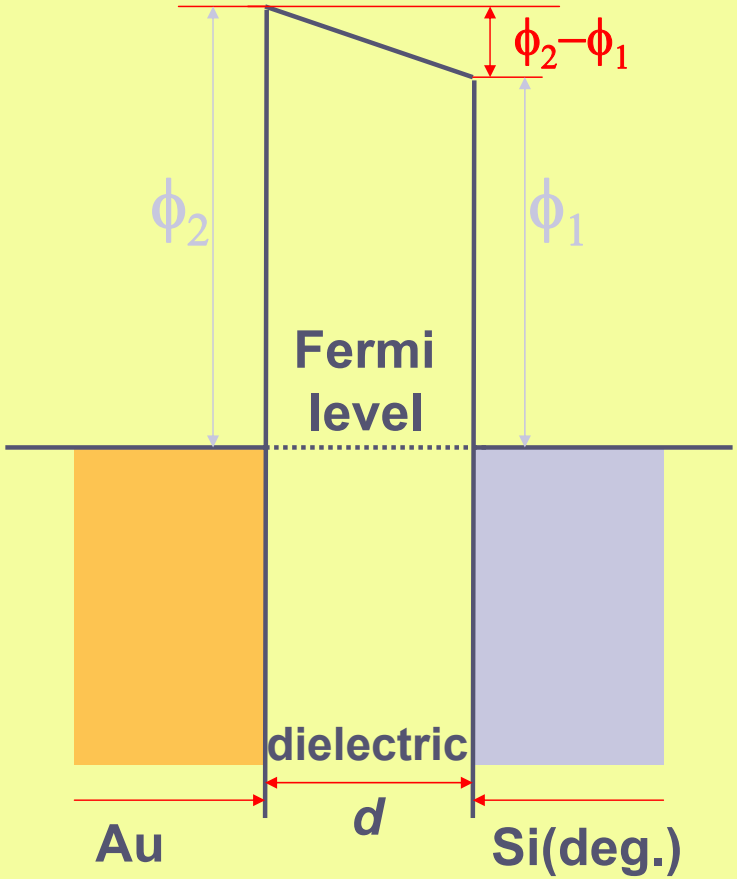

Energy band diagram

(metal-insulator-metal junction)

Tunnel barrier heights are ϕ_1 = 2.14 eV and ϕ_2 = 2.56 eV at Au and Si interfaces

Aswal, Lenfant, Guerin, Yakhmi and Vuillaume, *Small* 1 (2005) 725.

C-3 monolayer (thickness ~0.7 nm)

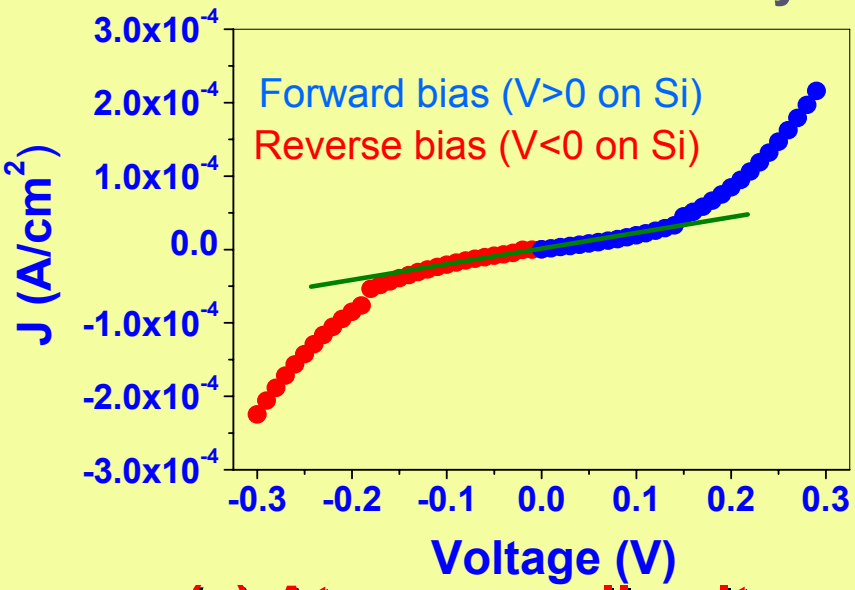

(a) At very small voltages

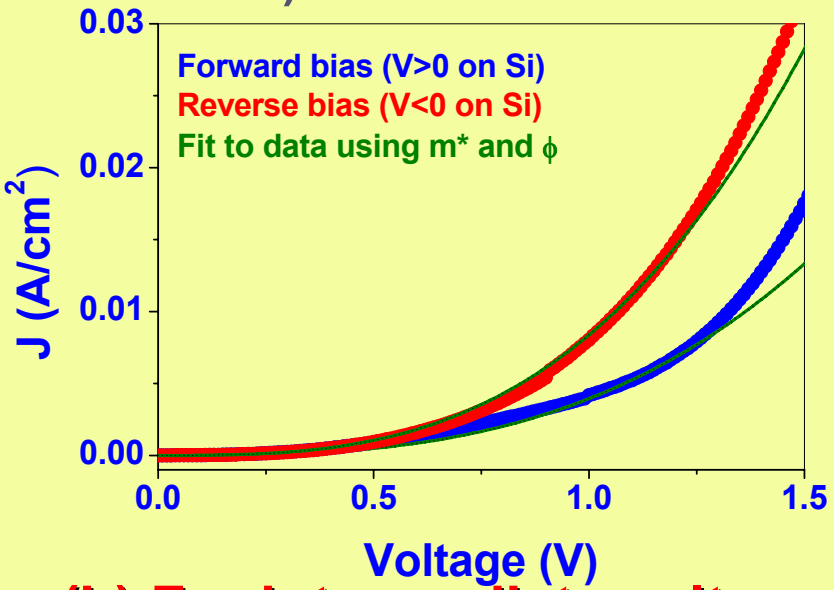

(b) For intermediate voltages

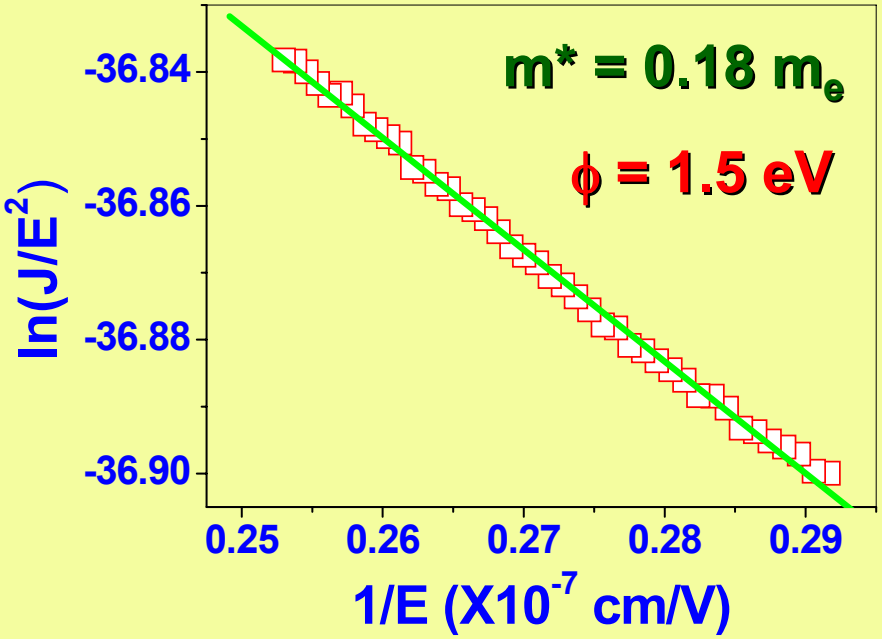

(c) *High voltage range*
(Fowler-Nordheim)

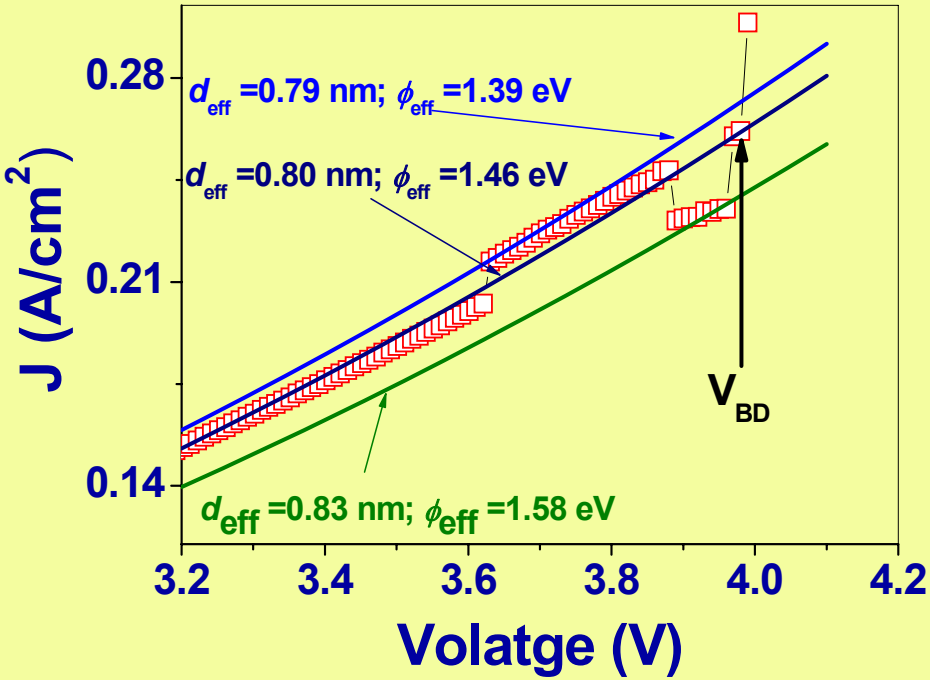

(d) Dielectric breakdown

$$E_{BD} = 50MV/cm$$

Inelastic Electron Tunneling spectra at 4.2 K

1. The CH2 rocking mode appears at 95.8 mV (773 cm^{-1}) for the C3-SH and 95.2 mV (768 cm^{-1}) in C8.
2. the (C–C) vibration appears at 136.6 mV (1102 cm^{-1}) in C3-SH and 134.3 mV (1083 cm^{-1}) in C8.
3. the scissor mode of CH2 vibration appears at 181.9 mV (1467 cm^{-1}) in C3-SH and 187.9 mV (1515 cm^{-1}) in C8.

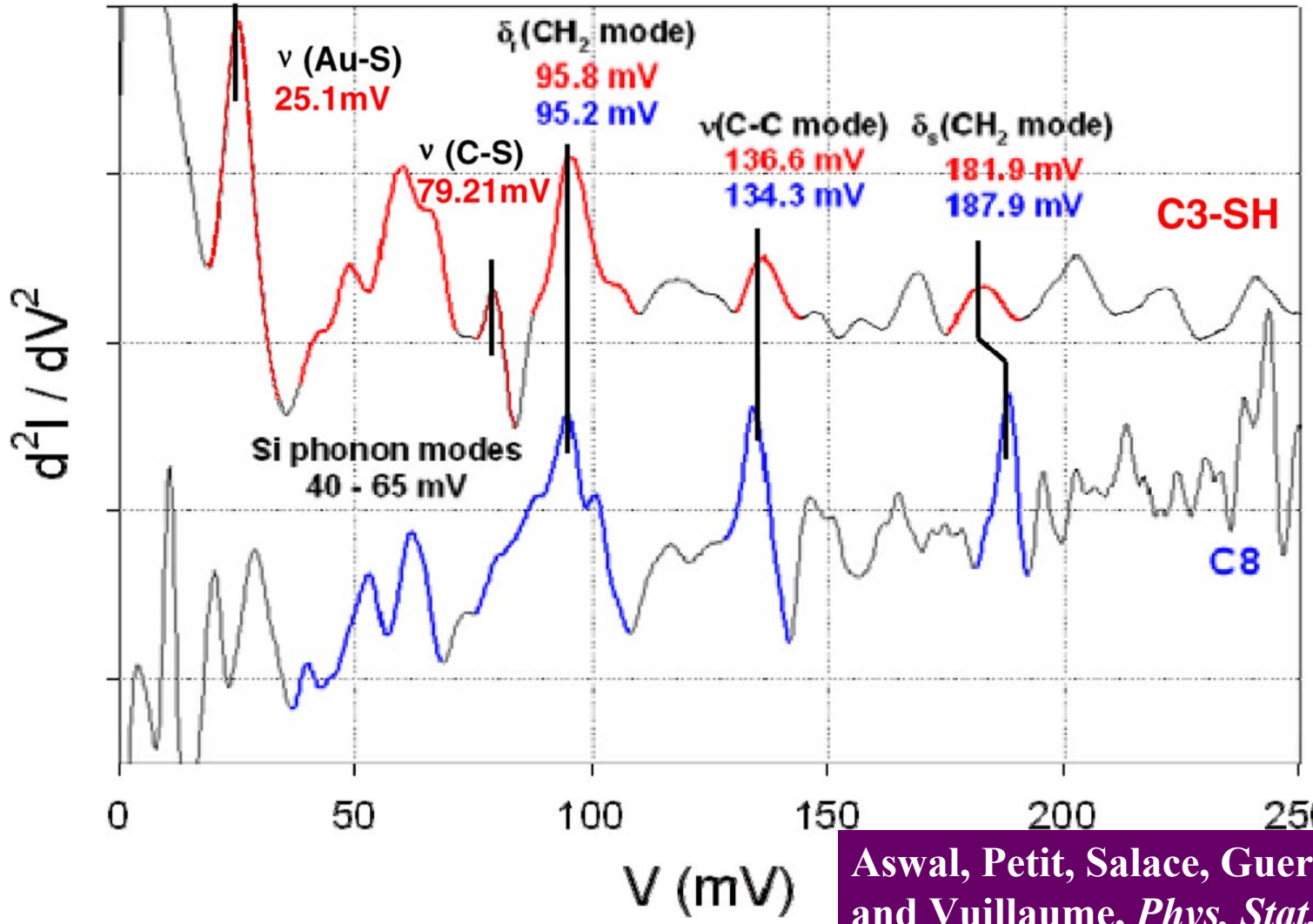

C3-SH SAM showed the (Au–S) molecular vibration at 25.1 mV (202 cm–1), which **involves the formation of a Au–S bond at the interface.**

The (C–S) stretch mode is at 79.2 mV (639 cm–1).
This peak confirms the presence of sulfur and provides information about C–C bonds adjacent to the C–S bond.

Aswal, Petit, Salace, Guerin, Lenfant, Yakhmi and Vuillaume, *Phys. Stat. Sol. (a)* 203, (2006) 1464

Self-assembly Lab

Characterization Lab

Chemistry section

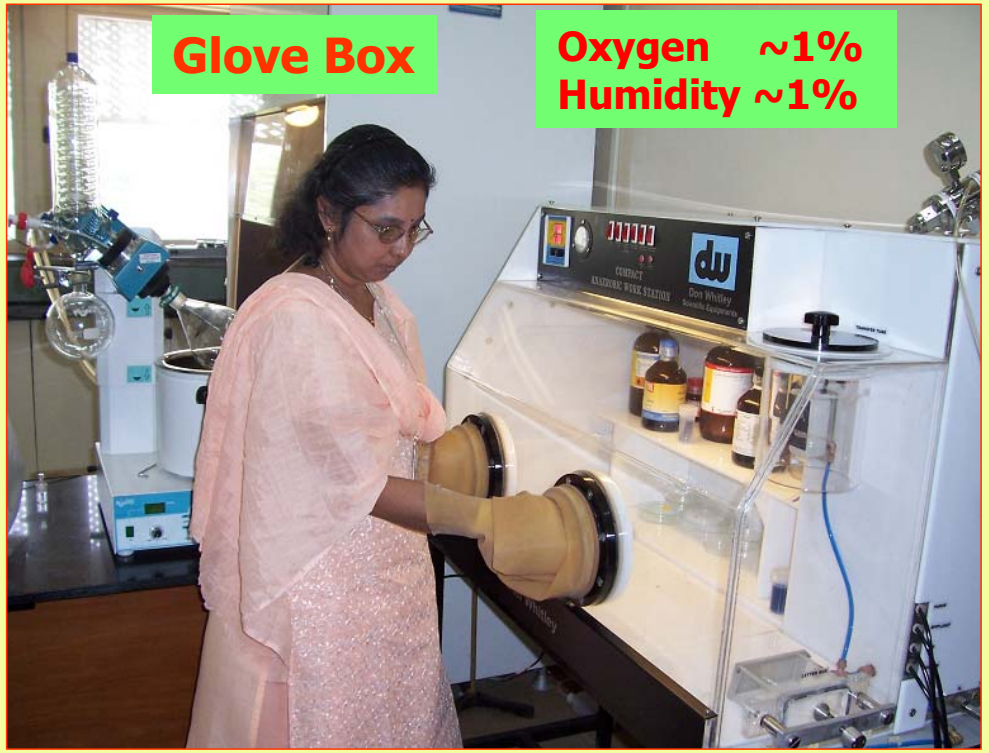

Glove Box

Oxygen ~1%
Humidity ~1%

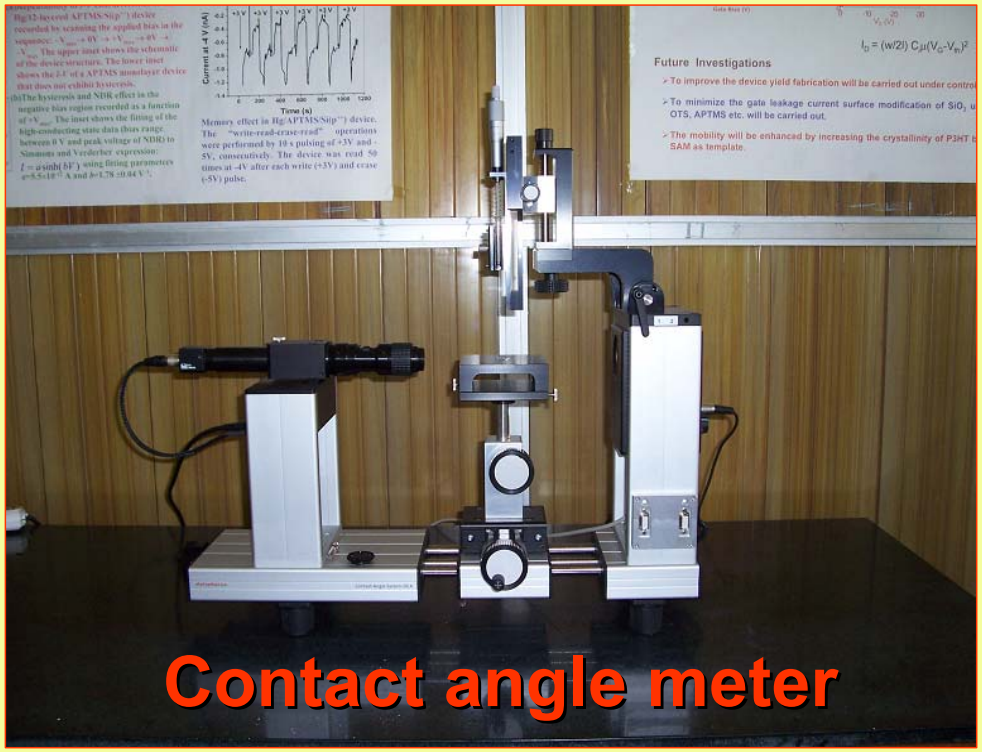
Future Investigations
Contact angle meter


Electrochemical setup

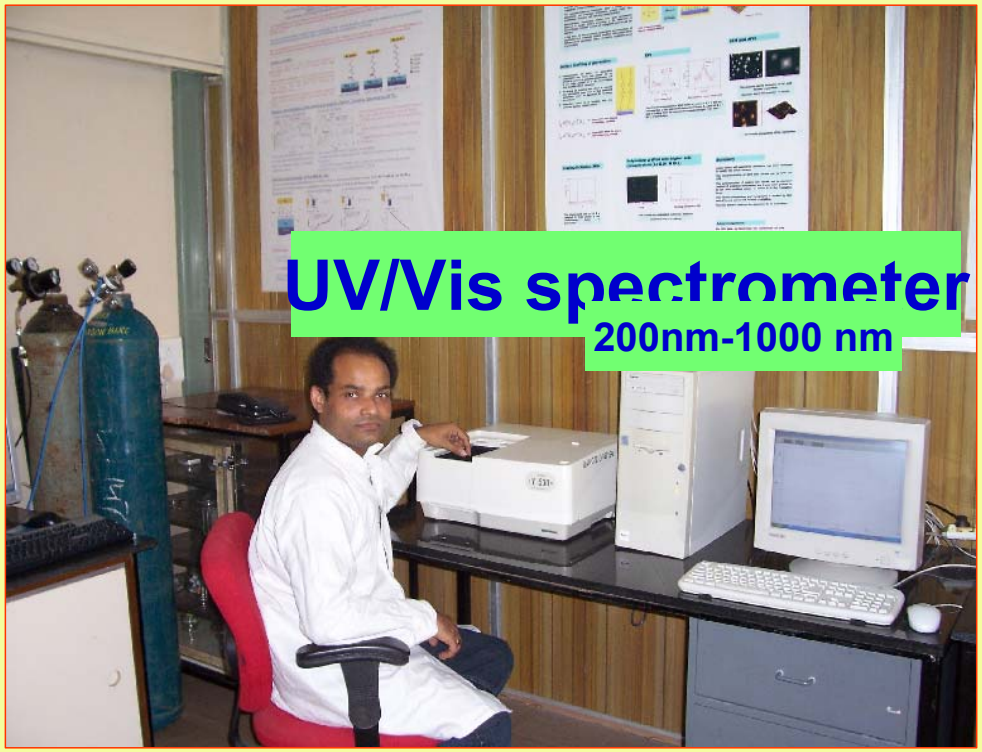
UV/Vis spectrometer
200nm-1000 nm


FTIR spectrometer
VERTEX-80V
400-7000 cm-1
Transmission
Diffuse reflectance
Attenuated Total Reflectance

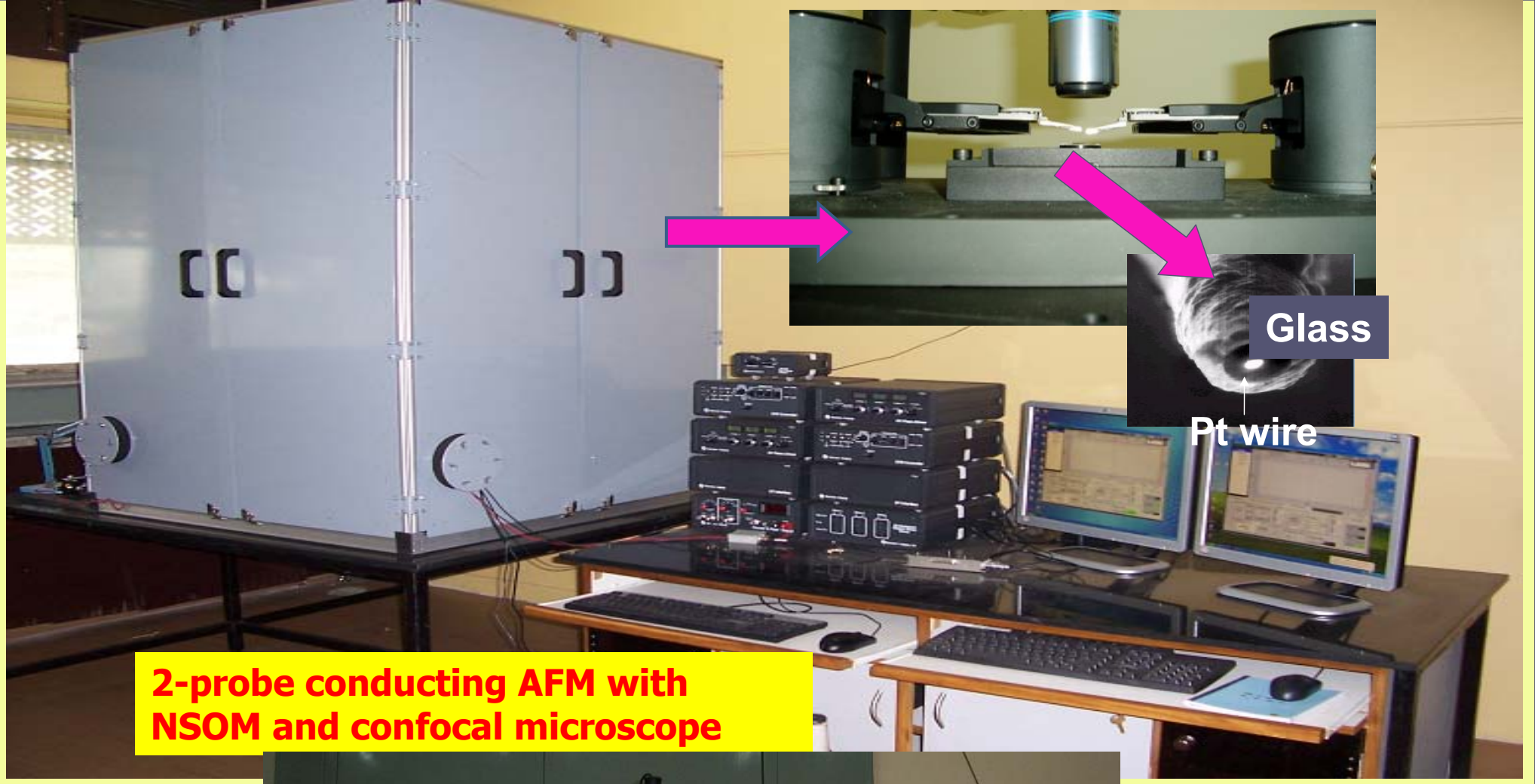

2-probe conducting AFM with NSOM and confocal microscope

Ellipsometer

SAMs by "silanization":

Native SiO_2 removed (high density of traps).
Fresh oxide layer (1-1.5 nm) grown thermally. We Obtain
OH-terminated SiO_x/Si. ~10^{15} groups/cm^2

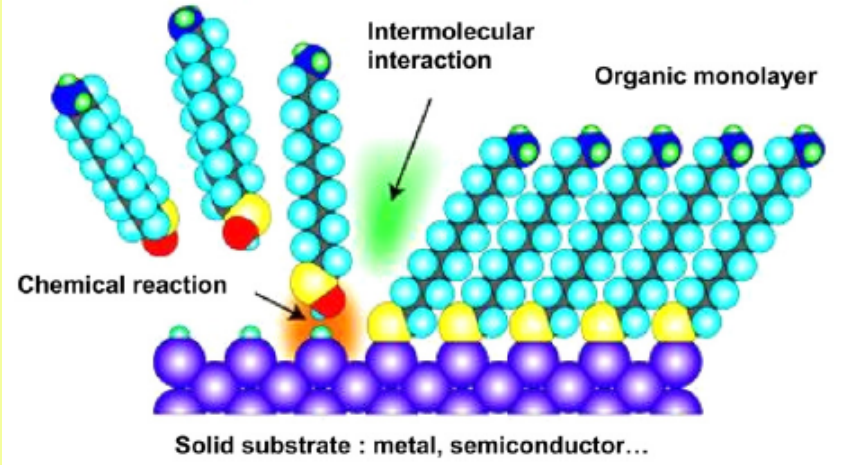

silanes [$R(CH_2)_nSiX_3$ where X = Cl, OCH_3 or OC_2H_5]

Deposition is driven only by 2 forces:
(i) chemisorption of organic molecules on Si-H / Si-OH surfaces;
and *(ii) VdW interactions among alkyl-chains.*

Problems with Silanization: **a) Short alkyl-chains (C ≤ 8) difficult to deposit, due to reduced VdW interactions among chains;**
AND b) adsorption of impurities on Si surface.

Hence, we have developed Cathodic Electrografting …..

Electrografting of organic molecules, using covalent bonds between the Si-atoms and the molecules.

Both cathodic/anodic electrografting possible at room temperature

2 advantages:

1. Applied negative potential acts as a controlling parameter for driving organic molecules to the Si surface, giving a dense monolayer!

2. With a negative potential applied to Si, the oxidation and/or hydrolysis of Si surface is obviated during grafting.

Cathode Electrografting at BARC on hydrated Si (111) surfaces (Si – H):

(i) OTS, i.e. octyltrichlorosilane (CH_3-$(CH_2)_7$-$SiCl_3$;
a σ-molecule of short chain length on Si *via* Si – Si bond formation

(ii) *5-(4-undecenyloxyphenyl)-10,15,20-triphenylporphyrin* (TPP-C11),
a new σ–π molecular rectifier, *via* Si-C bonds

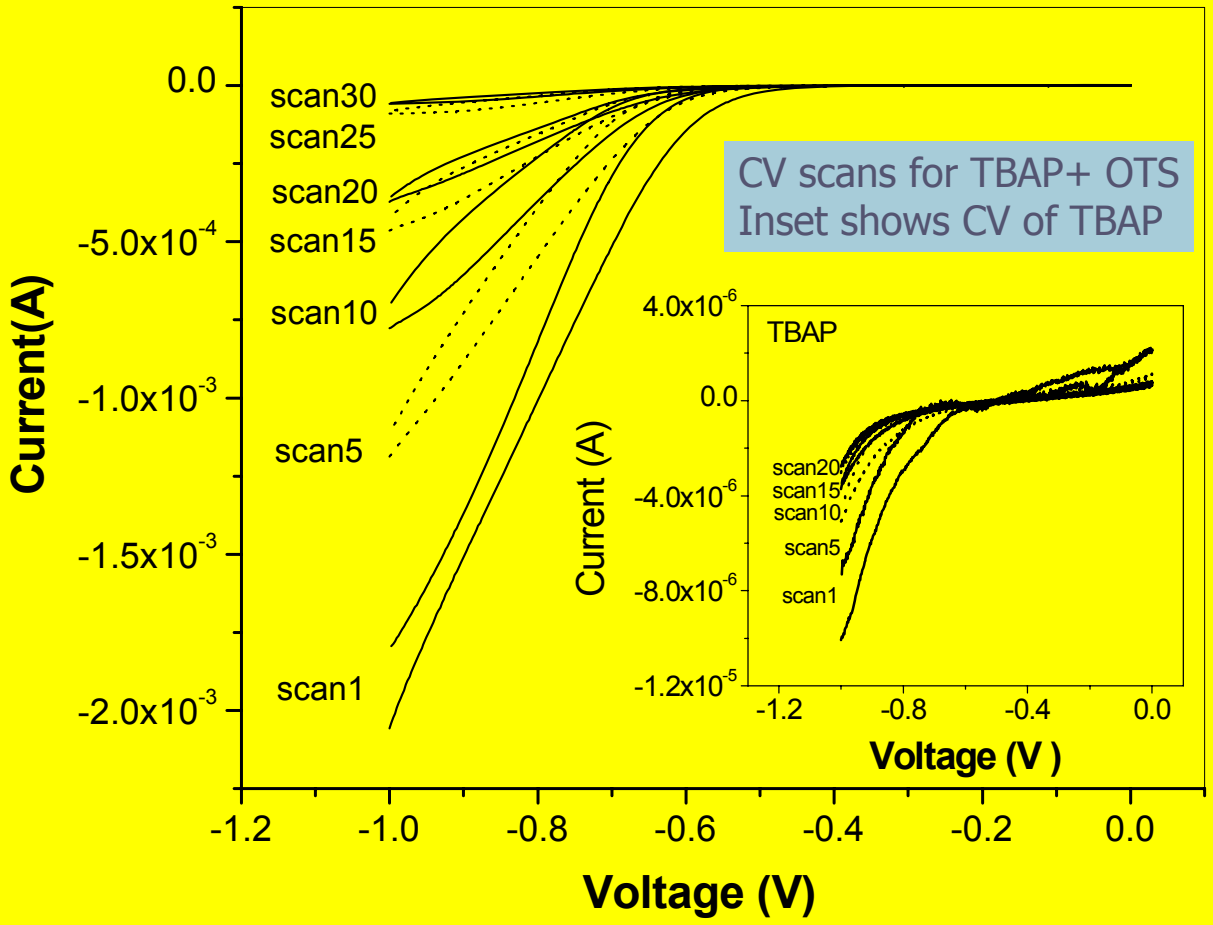

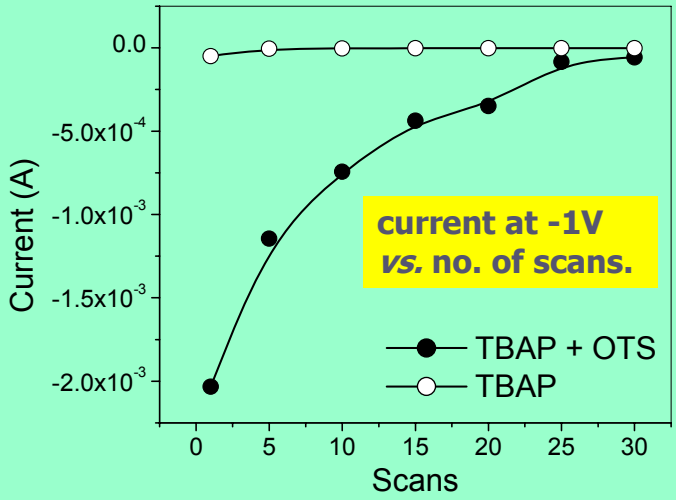

Current falls exponentially for (OTS + TBAP) with no. of scans. monolayer coverage ~97% after 30th scan.

AFM after each scan confirms coverage of OTS

For supporting electrolyte tetrabutyl ammonium perchlorate (TBAP) alone, current is only ~10^{-6} A, and does not vary much with scans.
No chemical reaction between H-terminated Si Working Electrode and TBAP
i.e. electrochemical (ECH) grafting of TBAP does not take place.

for (OTS + TBAP) the current for Scan 1 is very high (~10^{-3} A), but falls steeply to ~10^{-5}A for Scan30 (2 orders in magnitude).
Suggests *ECH reaction between H-terminated Si Working Electrode and OTS*

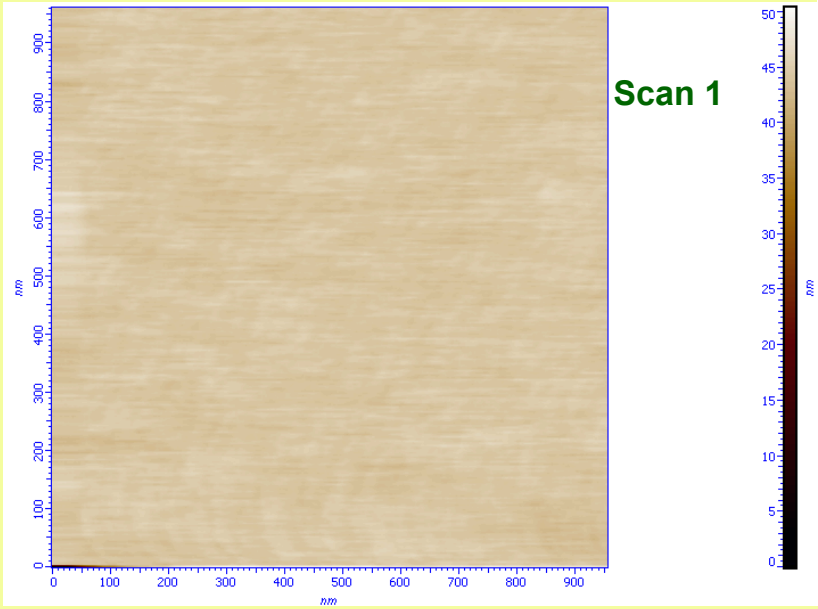

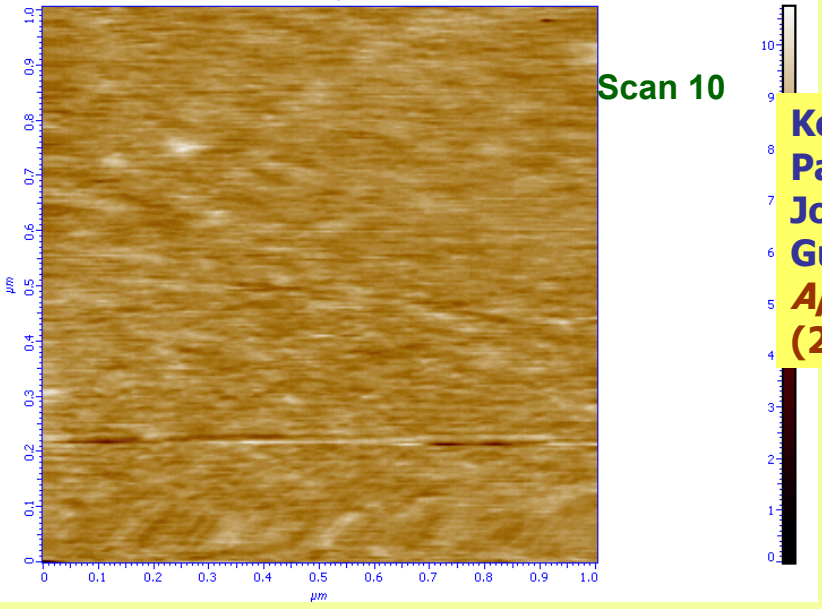

Koiry, Aswal, Saxena, Padma, Chauhan, Joshi, Gupta, Yakhmi, Guerin and Vuillaume, *Appl. Phys. Lett.* 90, (2007) 113118

AFM images of Electrochemically grafted OTS after Each scan

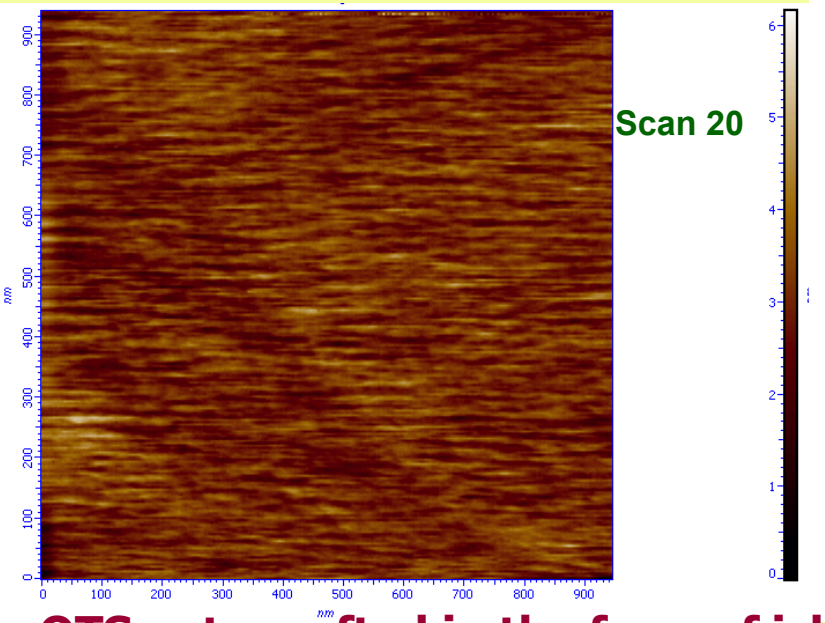

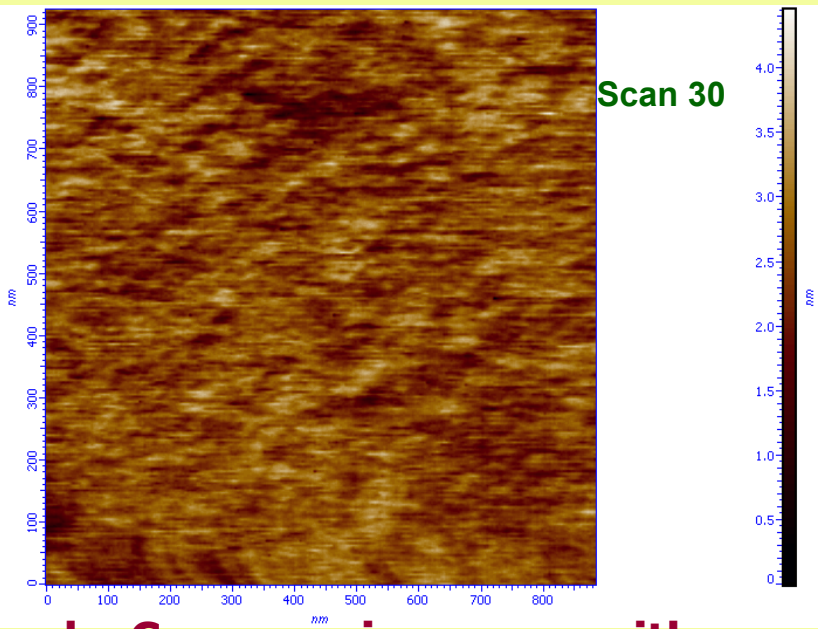

OTS gets grafted in the form of islands. Coverage increases with repeated Scans, to ~100% after Scan-30, confirming CV results.

Average height of monolayer islands, (from line-height profile of AFM images, was ~13 Å. Thickness of fully covered monolayer: (1.32 nm from ellipsometery). Theoretical length of OTS molecule (i.e. 1.36 nm). *Grafted film is not a multilayer.*

How it Happens? negative potential applied to H-terminated working electrode generates "nucleophilic Si" atoms at the surface by librating *hydrogen free radicals*.

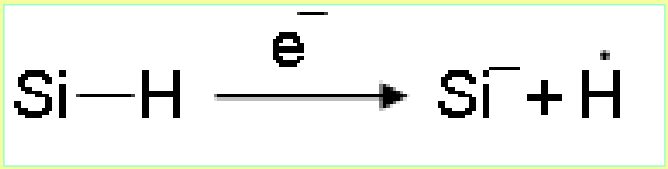

These "nucleophilic Si" atoms react with "electrophilic Si" atoms Of OTS molecule to form Si-Si bond, releasing chlorine ions

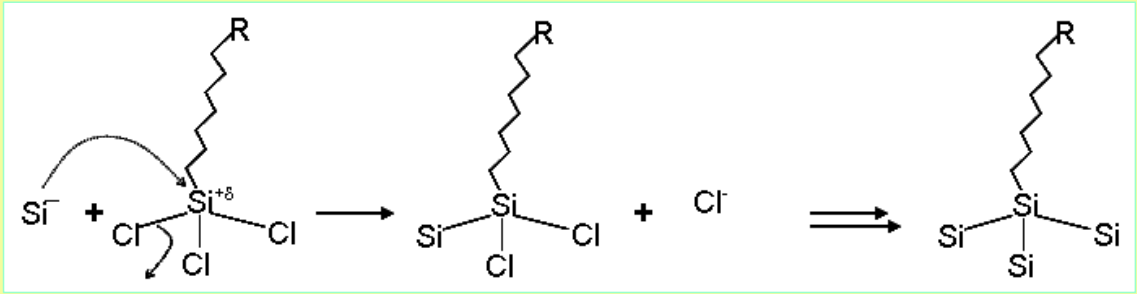

Electrochemical reaction between hydrated-Si and OTS (R represents the CH_3 group)

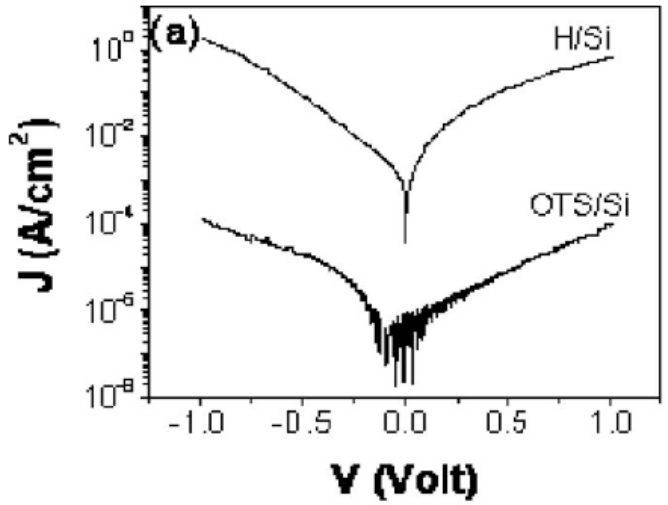

Impedance Spectroscopy on *Al/H/Si(n⁺⁺), and Al/OTS/Si(n⁺⁺) structures* shows reduction in leakage current, thru OTS monolayer, by four orders Of magnitude, AND absence of oxide formation (ensured by –ve potential) **Device yield : >70%**

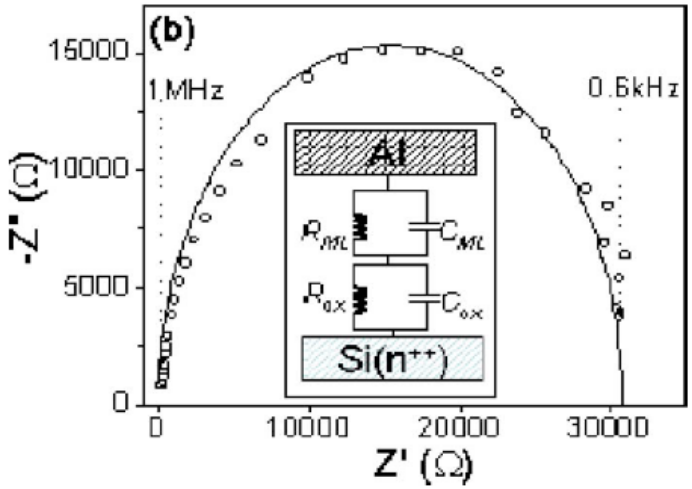

Electrografting a porphyrin derivative on n-Si for hybrid nano-electronics

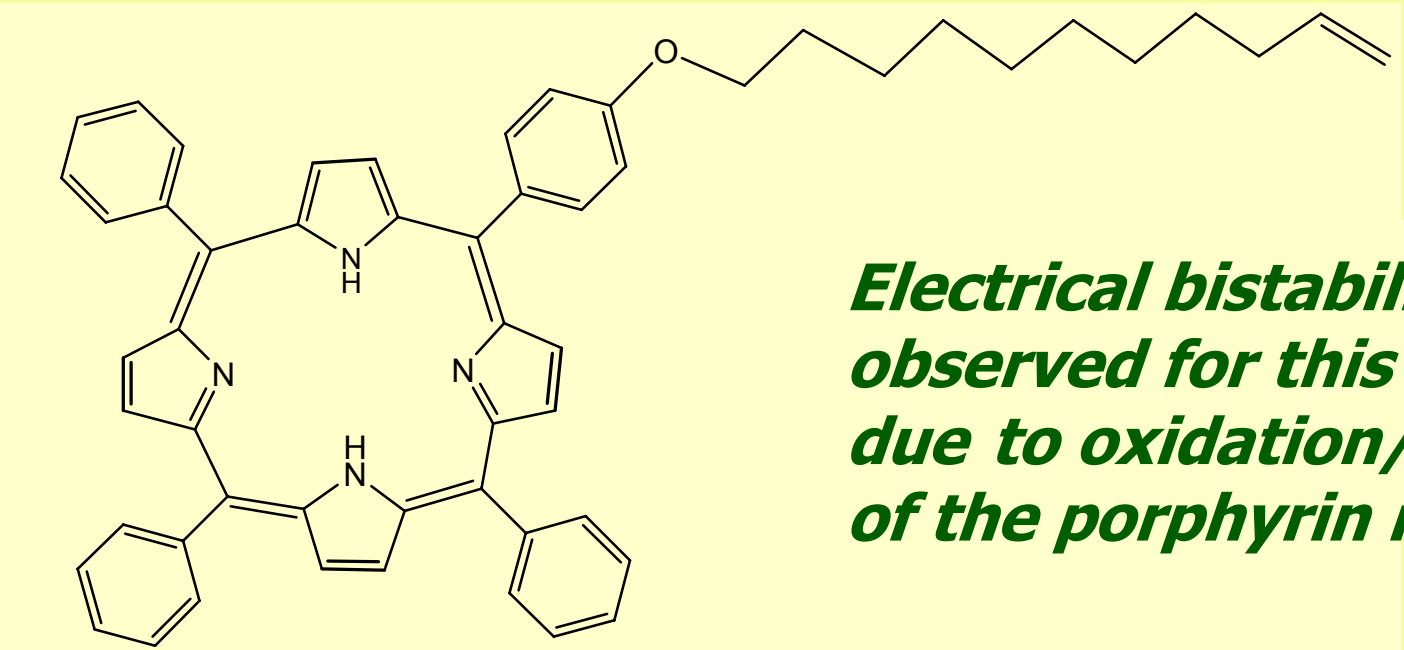

5-(4-Undecyloxyyphenyl)-10,15,20-triphenylporphyrin (2)

Electrical bistability observed for this molecule due to oxidation/reduction of the porphyrin ring!.

Vinyl group (C=C) convenient for electrografting on H-terminated Si surface. A new molecule designed (purple solid, m.p of ~ 95°C): 5-(4-undecenyloxyphenyl)-10,15,20-triphenylporphyrin (TPP-C11). It has a vinyl terminated 11-C alkyl-chain, attached to porphyrin ring. Structure confirmed using NMR.

CV runs using the TPP-C11 + TBAP solution.

Inset is schematic of 2-step electrografting process of TPP-C11 monolayer on Si *via* formation of Si–C bonds.

The irreversible oxidation peak at ~0.3V is associated with the bonding (Si-C bond) of TPP-C11 molecule with the H-terminated surface.

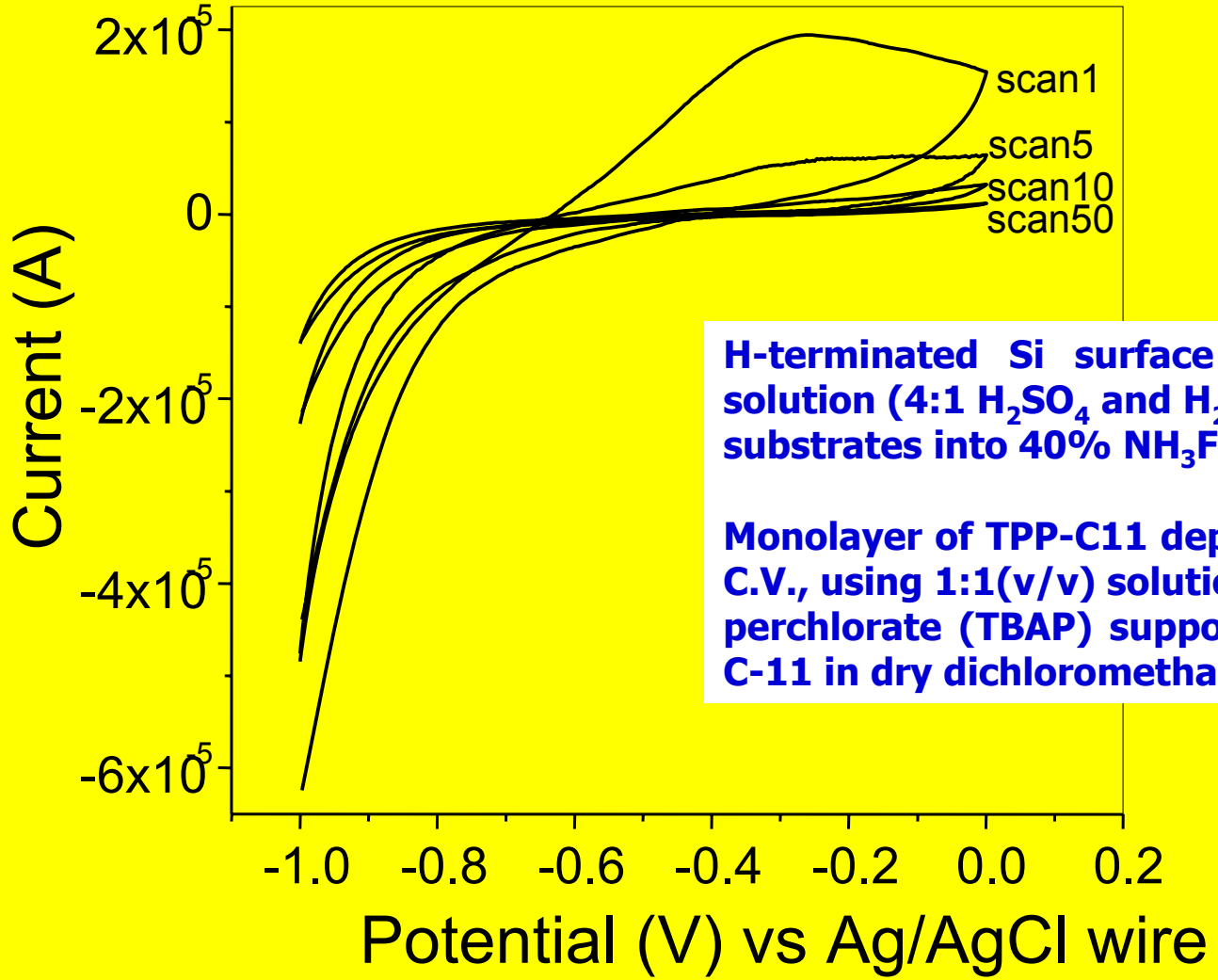

H-terminated Si surface prepared by dipping piranha solution (4:1 H_2SO_4 and H_2O_2 (v/v)) treated n-type Si(111) substrates into 40% NH_3F solution.

Monolayer of TPP-C11 deposited on H-terminated Si using C.V., using 1:1(v/v) solution of 0.1M tetra butylammonium perchlorate (TBAP) supporting electrolyte and 1mM TPP-C-11 in dry dichloromethane.

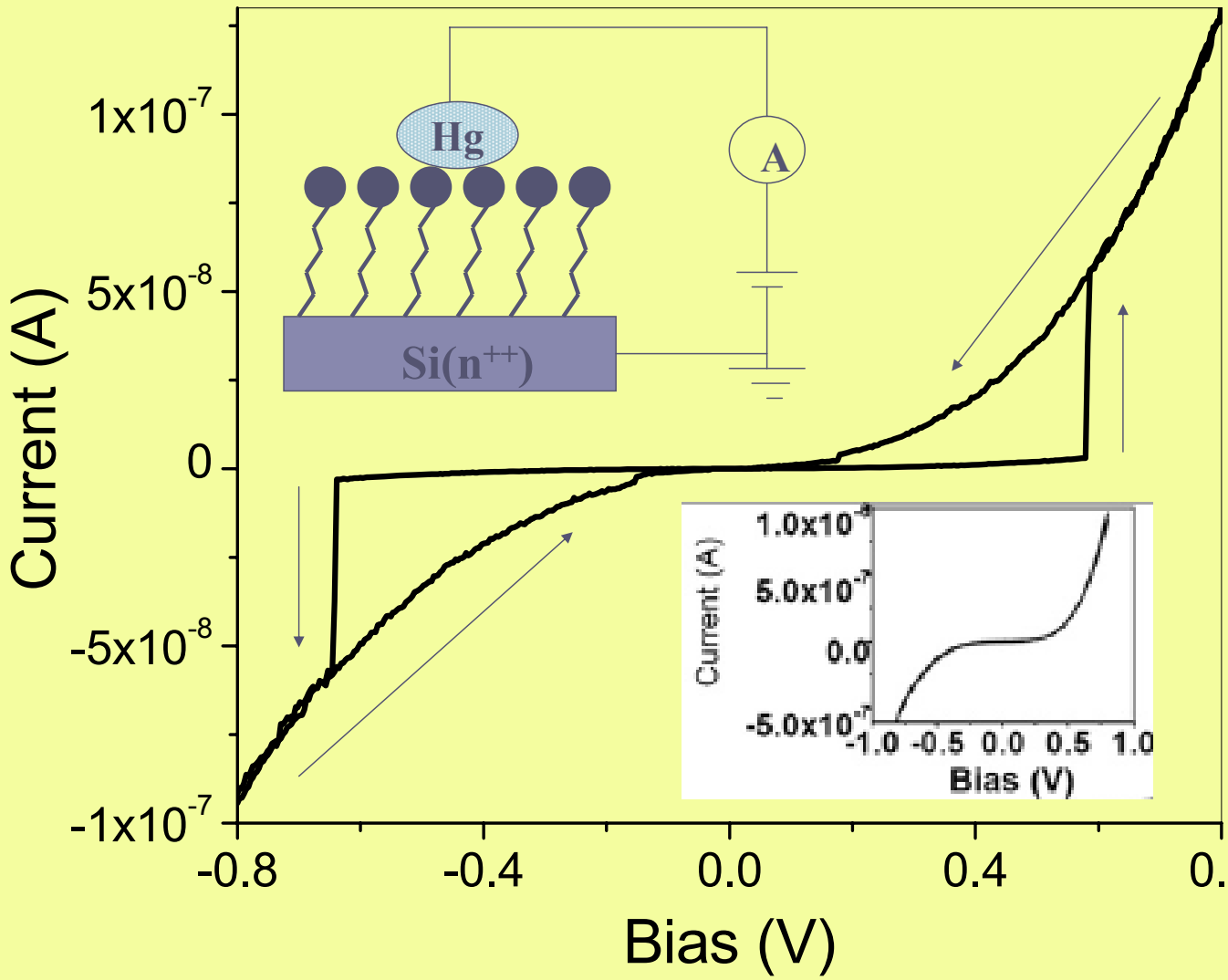

I-V **characteristics of TPP-C11 monolayer, for a metal/TPP-C11 monolayer/Si(n^{++}) structure, using Hg drop counterelectrode , at a scanspeed: 5 mV/s**

Upper Inset: schematic of the device structure
Lower Inset: J–V plot for C11 monolayer.

Plots are slightly asymmetric, due to different work functions of the electrodes i.e. Si (4.1 eV) and hg (4.5 eV). **Pronounced hysteresis seen.**
In the positive bias scan (0 to +0.8 V), current jumps by an order of magnitude at +0.6 V, but does not retrace the curve during the reverse scan (+0.8 to 0V) and remains at higher values. ***Hence, 2 conduction states!***

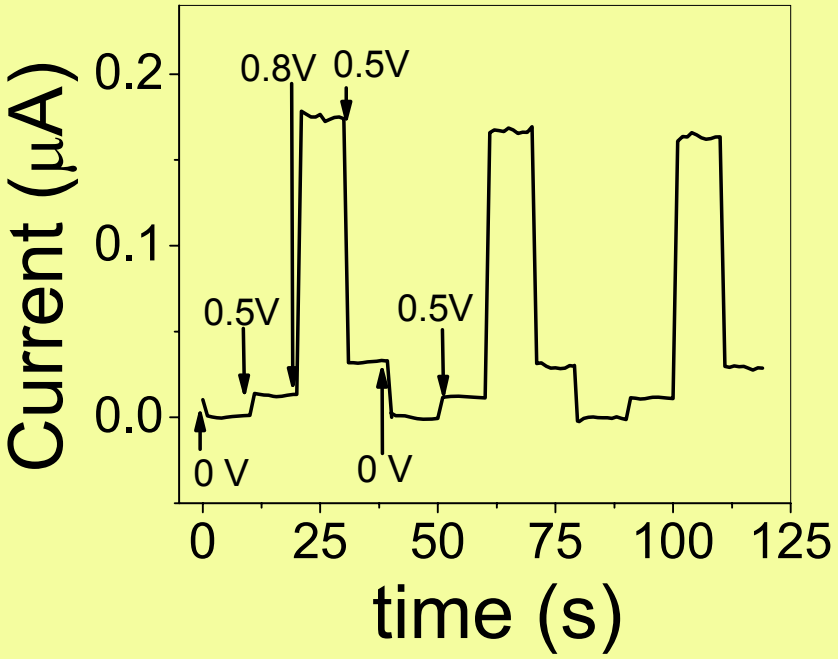

Demonstration of resistive molecular memory effect Koiry, Aswal, Chauhan, Saxena, Nayak, Gupta, Yakhmi, Chem. Phys. Lett. 453 (2008) 68

Two conduction states: one with low current (OFF) and other with higher current state (ON). This electrical bistability is useful for fabricating a molecular memory.

0 V and +0.8 V pulses for 10 s were applied, respectively, to "write" the high-conducting state and "erase" to a low-conducting one. These states were monitored ("read") by measuring the device current at 0.5 V.

Fast scan CV

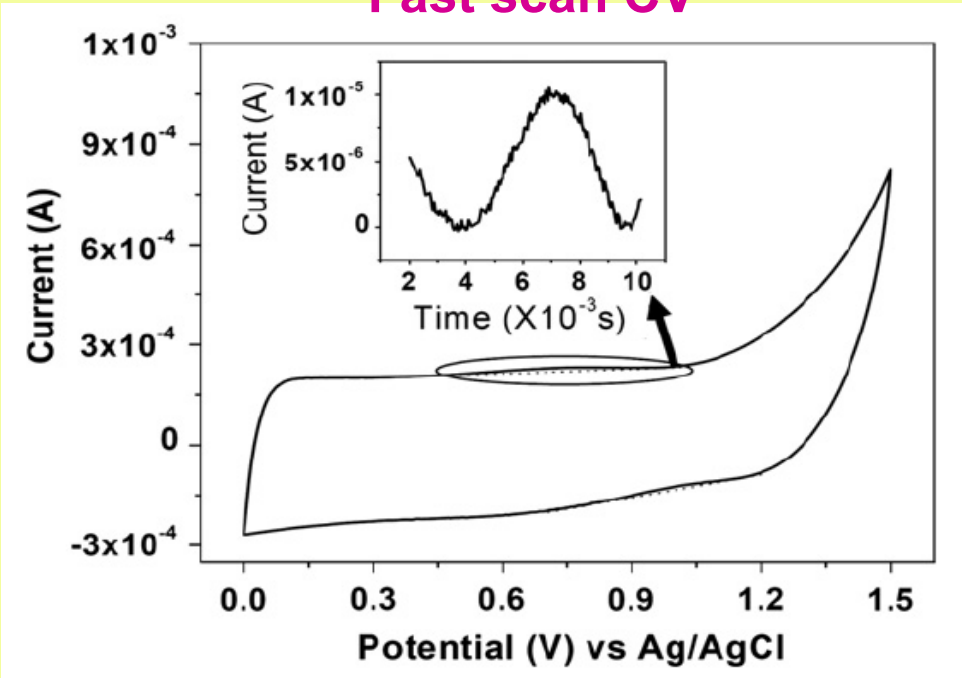

sharp jump in current at a bias of ±0.6 V indicates switching due to resonant tunneling. The onset values of oxidation and reduction potentials (versus Ag/AgCl) were +0.3 and 1.2 V, respectively. The redox couple ferrocene/ferricenium ion (Fc/Fc+) was used as external standard. The corresponding HOMO and LUMO levels for porphyrin moiety were calculated using the empirical relation: $E^{HOMO/LUMO} = [- e(E_{onset(vs.Ag/AgCl)} - E_{onset(Fc/Fc+ vs Ag/AgCl)})] - 4.8$, including the ferrocene value of 4.8 eV w.r.t. the vacuum level, which is defined as zero.

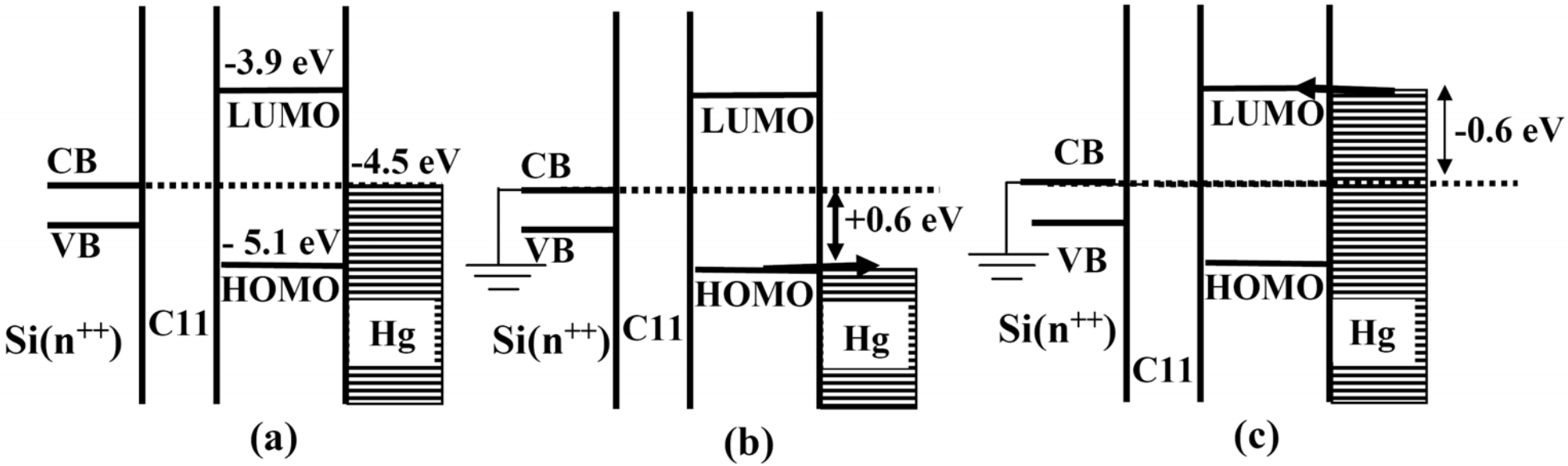

(a)Schematic energy diagram of Hg/TPP-C11 monolayer/Si(n^{++}) device.
(b) At positive Bias, for bias <0.6 V, the entire TPP-C11molecule acts as a tunnel barrier, hence, no-resonant tunneling,hence current is low. At a bias of +0.6 V, the Fermi level of Hg electrodes aligns with the HOMO of the porphyrin ring giving a sharp jump in current due to resonant tunneling though HOMO. However, during the reverse scan (+0.8 to 0 V),
as the porphyrin ring becomes conducting, and the current remain higher, due to the non-resonant tunneling through a reduced barrier height corresponding to that of C11 only.

Steps for Fabricating Molecular Diodes from tetraphenyl porphyrine (TPP)-fullerene (C60) supramolecular complex grafted on Si

1. Create H-terminated Si (n^{++}) substrates by 40% NH_4F treatment

2. Electrograft C60 on H-Si

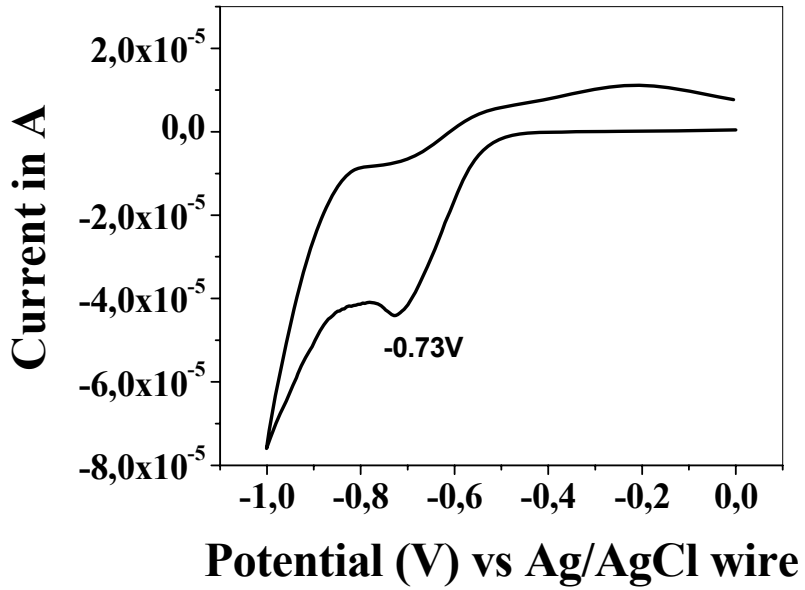

Irreversible peak at -0.73 V indicates C60 forming chemical bond with H-Si

3. Characterize C60 Layer

A. Thickness ~ 1 nm : formation of monolayer;
B. UV/Vis absorption at 328 nm indicates presence of C60

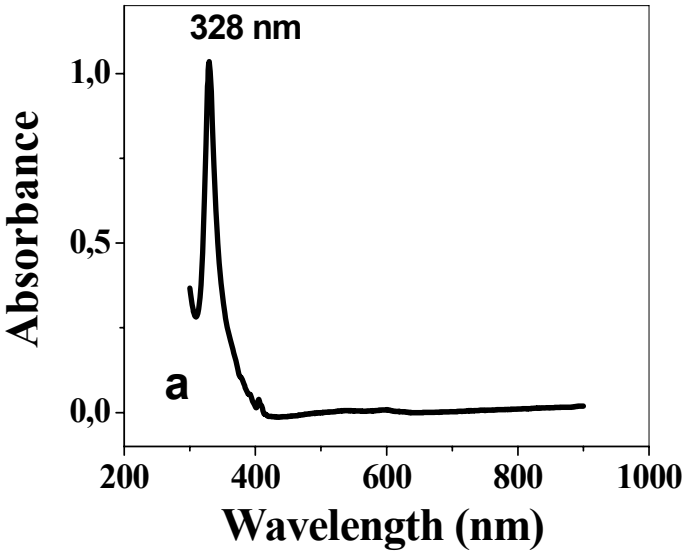

C. Reversible redox peak at -0.4 V for C60/Si indicates covalent grafting of C60 on Si.

4. Dipping C60/Si substrates in TPP solution for 24 hr forms supramolecular TPP/C60 complex

TPP/C60 molecular diodes on Si

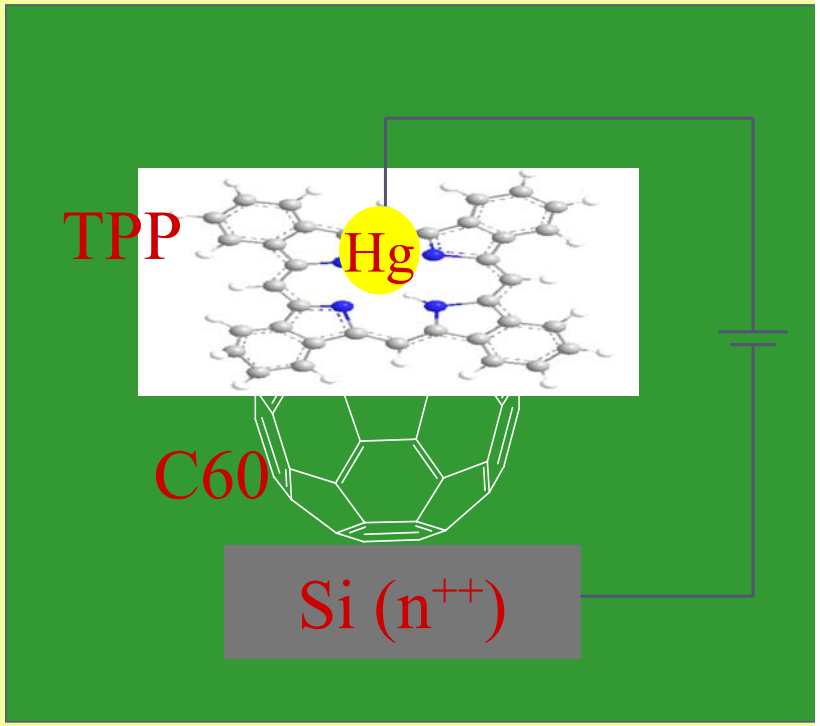

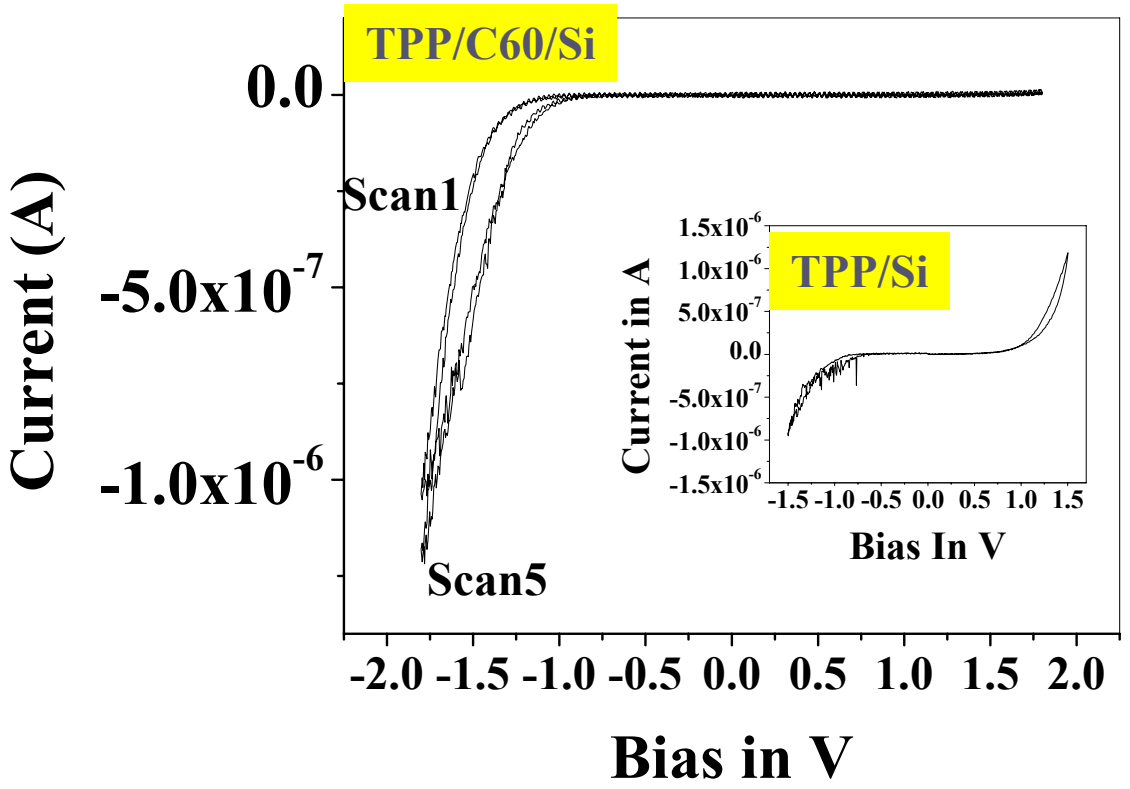

Rectification ratio $\left(\frac{|I_{-1.8V}|}{|I_{+1.8V}|}\right)$ **> 200**

(IEMN-BARC collaboration)

We successfully synthesized (using various routes) Si-SiO_2-σ-C_{60}-Hg and Si-SiO_2-σ-C_{60}-σ-Hg junctions

These junctions have been extensively characterized (contact angle, ellipsometry, FTIR, XPS, CyV...)

I-V measurements showed current rectification and resonant transport thru C_{60} molecular orbitals

Reversal of the rectification has been observed by intercalating alkyl chains between the C_{60} and the Hg electrode. This feature illustrates the strong effect of the molecule-metal coupling on the electronic structure of the junctions

Device architecture $Si/SiO_2/\sigma-\pi-\sigma/M$ for molecular diodes (IEMN-BARC collaboration)

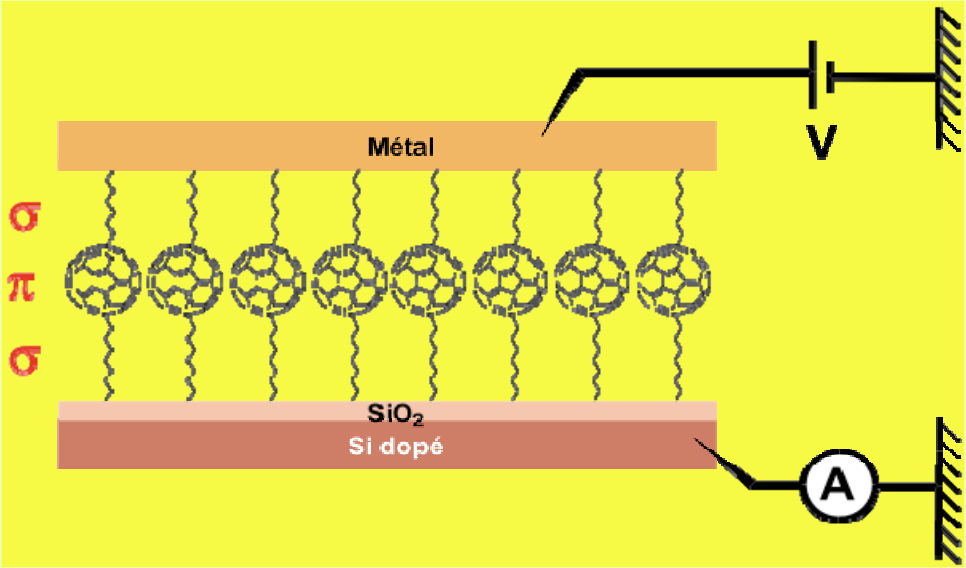

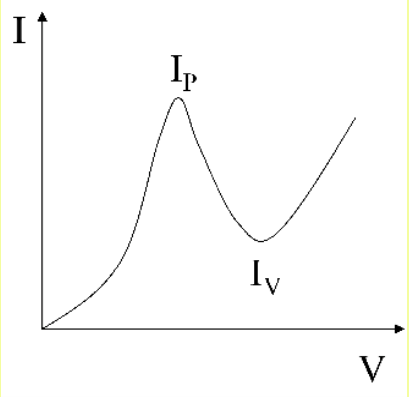

1. Synthesis of the half-structure $Si/SiO_2/\sigma-\pi$

synthesis of azidopropyltrimethoxysilane
grafting of the SAM-N_3 on Si/SiO_2
grafting of C_{60}

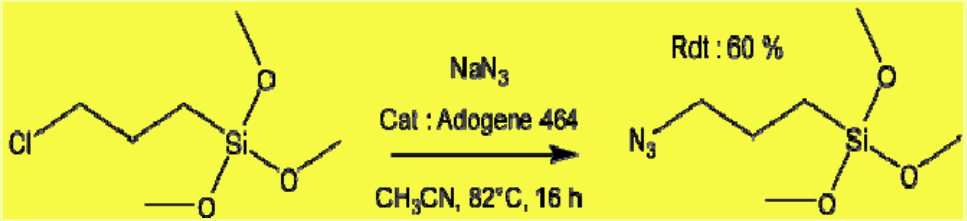

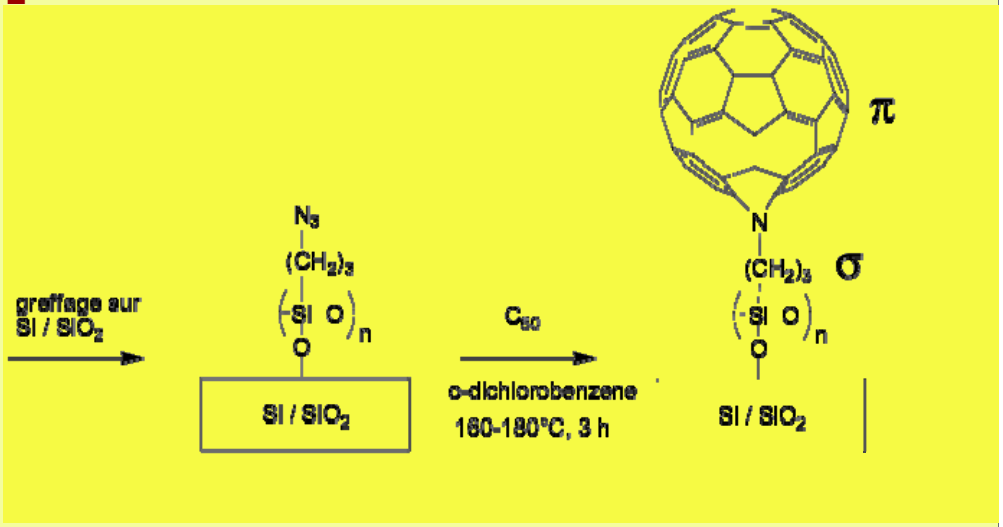

SAM characterization

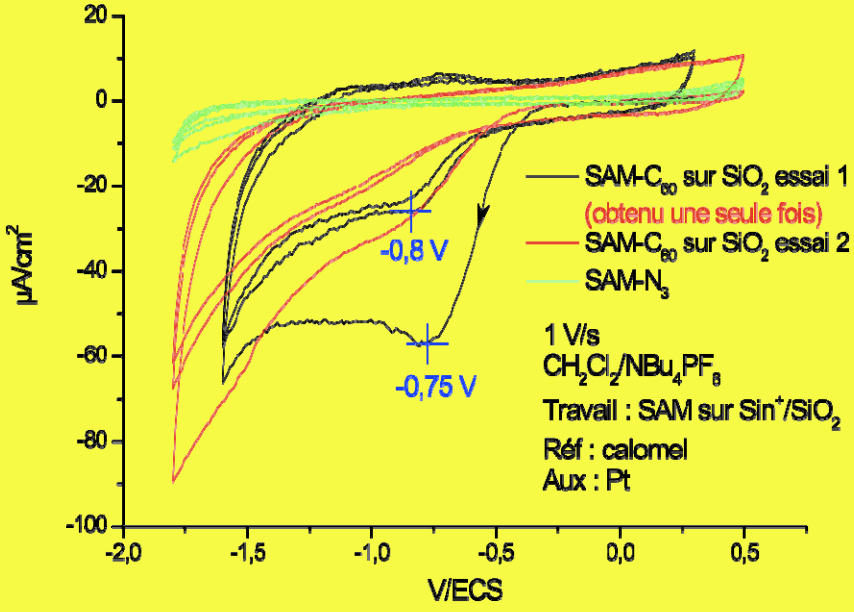

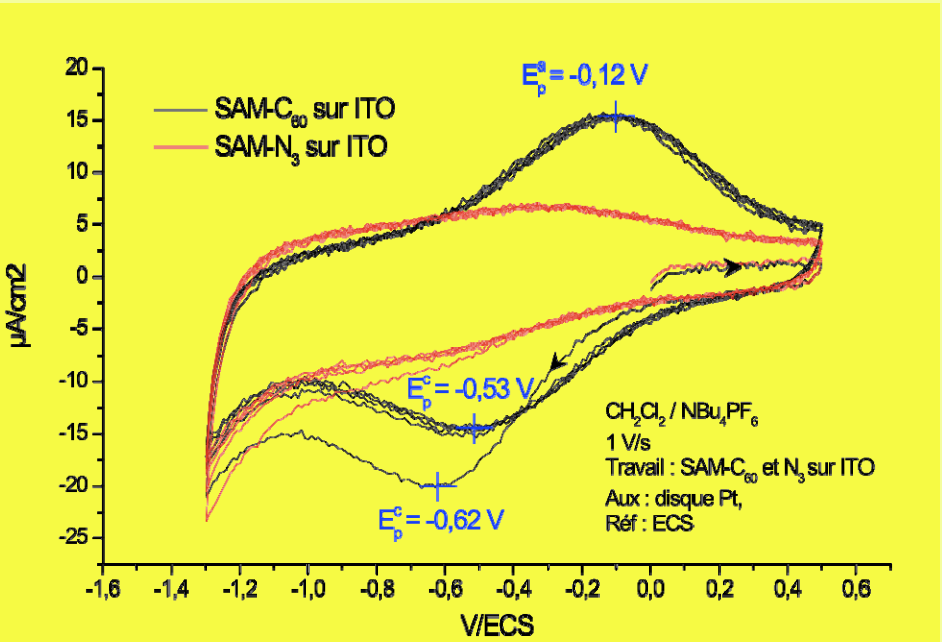

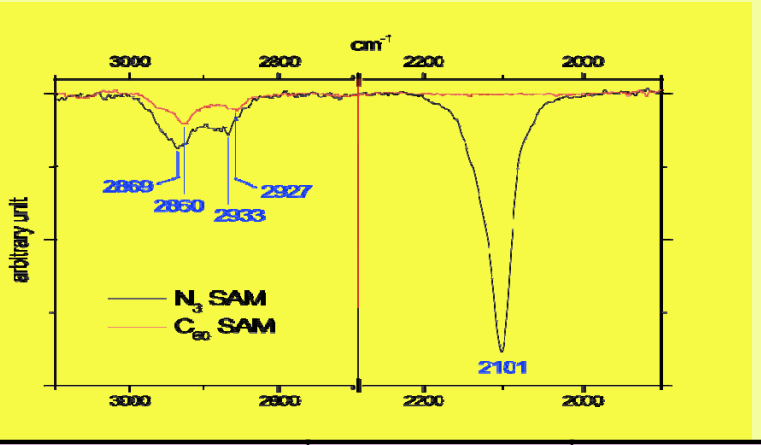

SAMs		-N_3	-C_{60}
thickness (Å)	*Theo.*	8.8 Å	14.6 Å
ellipso	*Exp.*	8±1 Å	17±1 Å
water contact angle		68±1°	70±1°
FTIR (cm^{-1})	*N_3*	2101	-
	CH_2 (s)	2933	2927
	CH_2 (as)	2869	2860
	C=C (fullerene)	-	not observed
XPS (eV)	*N1s*	405.0, 401.3	400.0
	C1s	285.4, 286,8	285.1, 286,7
	C/N theo.	1 2.5	18 (N_3 absent) 13.1
	C/N exp.		
CyV	*ITO*	-	-0.12 / -0.53
E_p^a/E_p^c (V/ECS)	*Sin+/SiO_2*	-	*E_p^c = -0.8*

Electrical measurements with Hg drop

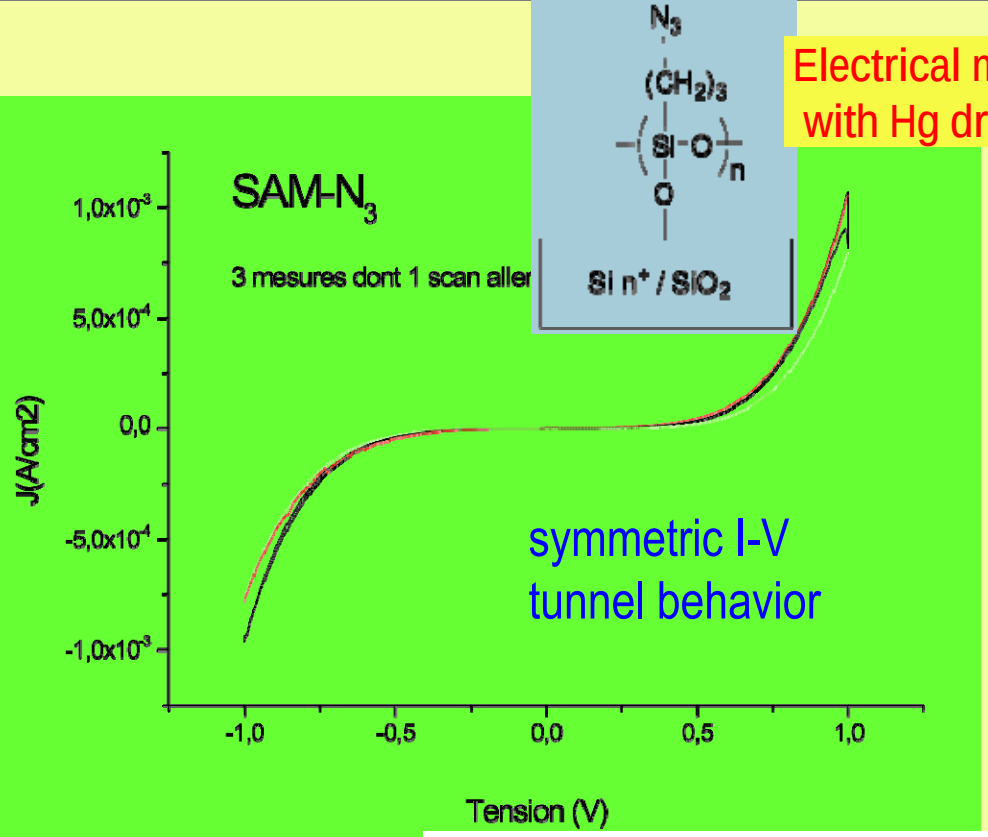

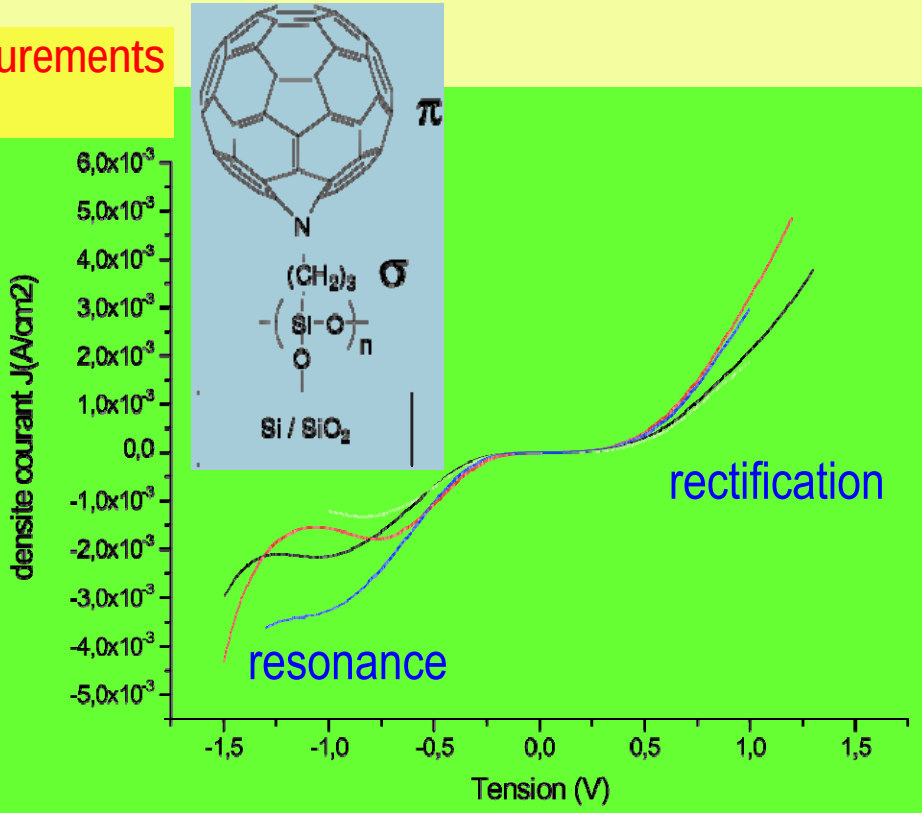

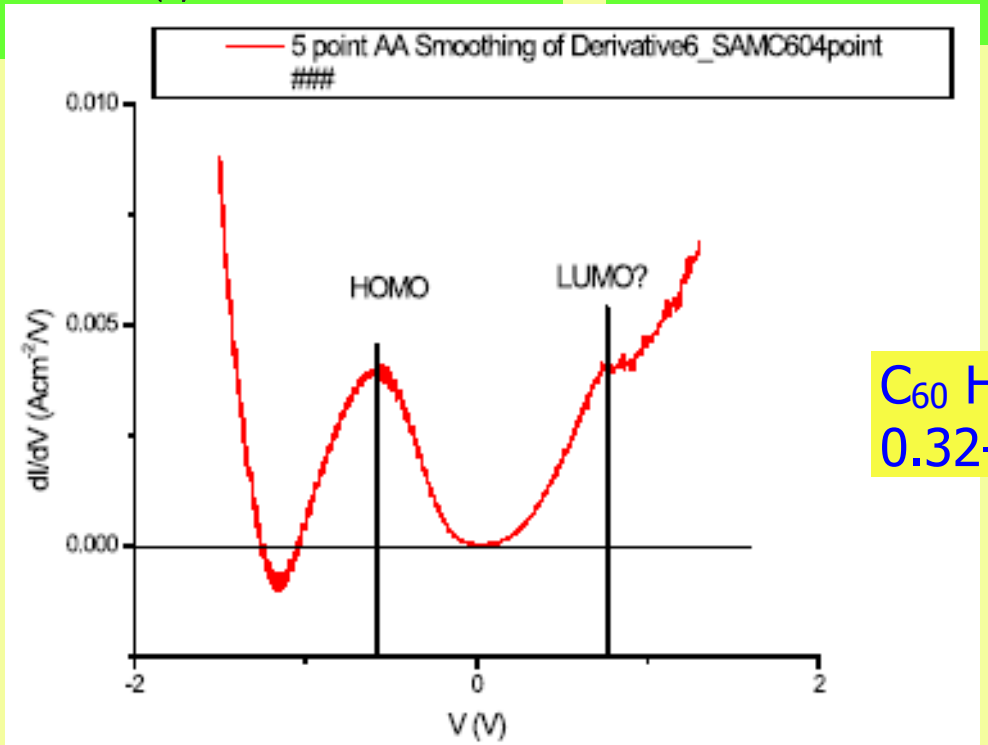

positive rectification
+ gap reduction
+ resonance thru C_{60} HOMO

C_{60} HOMO at about
0.32-0.46 eV below Si CB

We also observed positive rectification of the I-V
(sample to sample dependent)

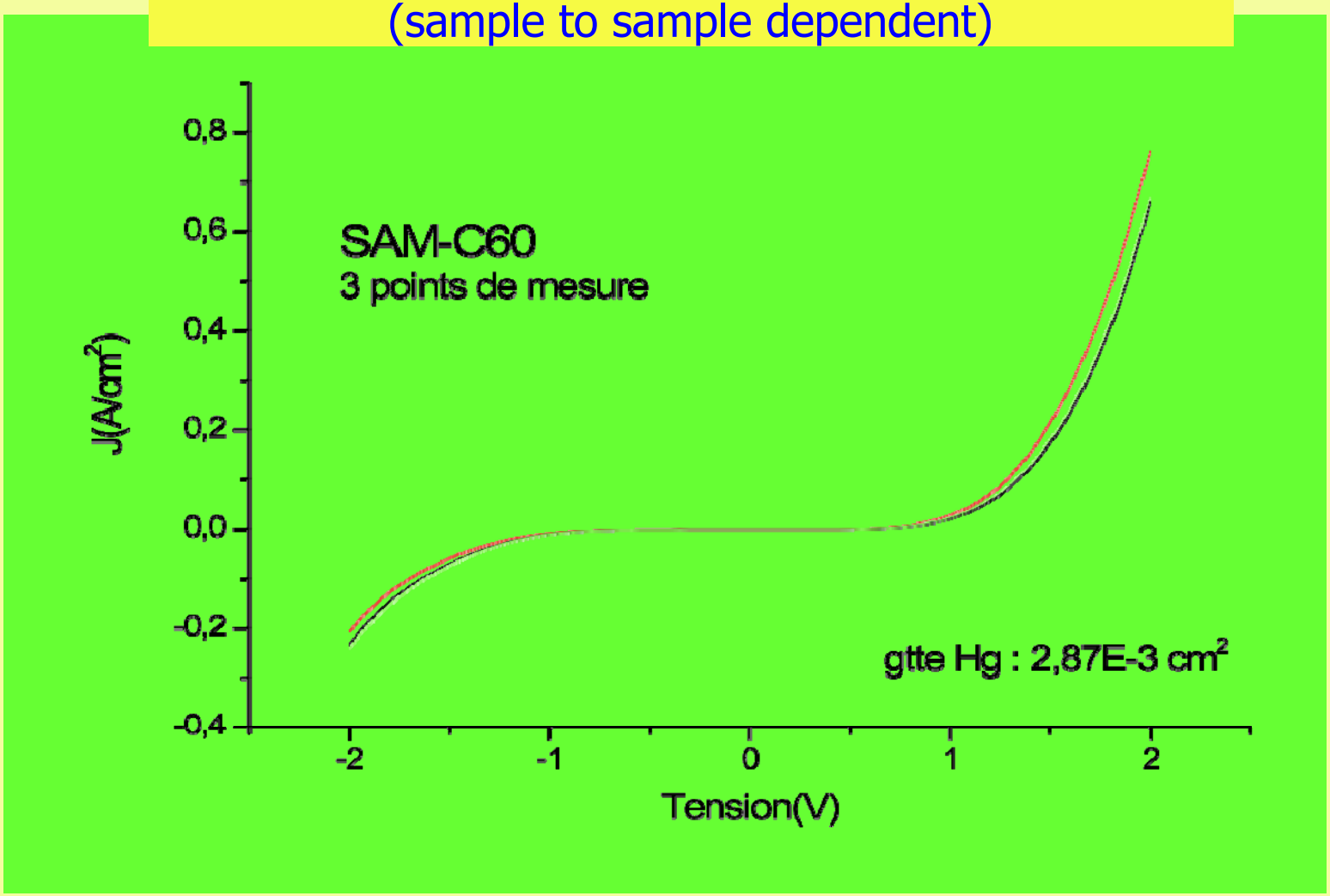

synthesis of half-structure $Si/SiO_2 - \sigma - \pi$ from SAM-aziridine

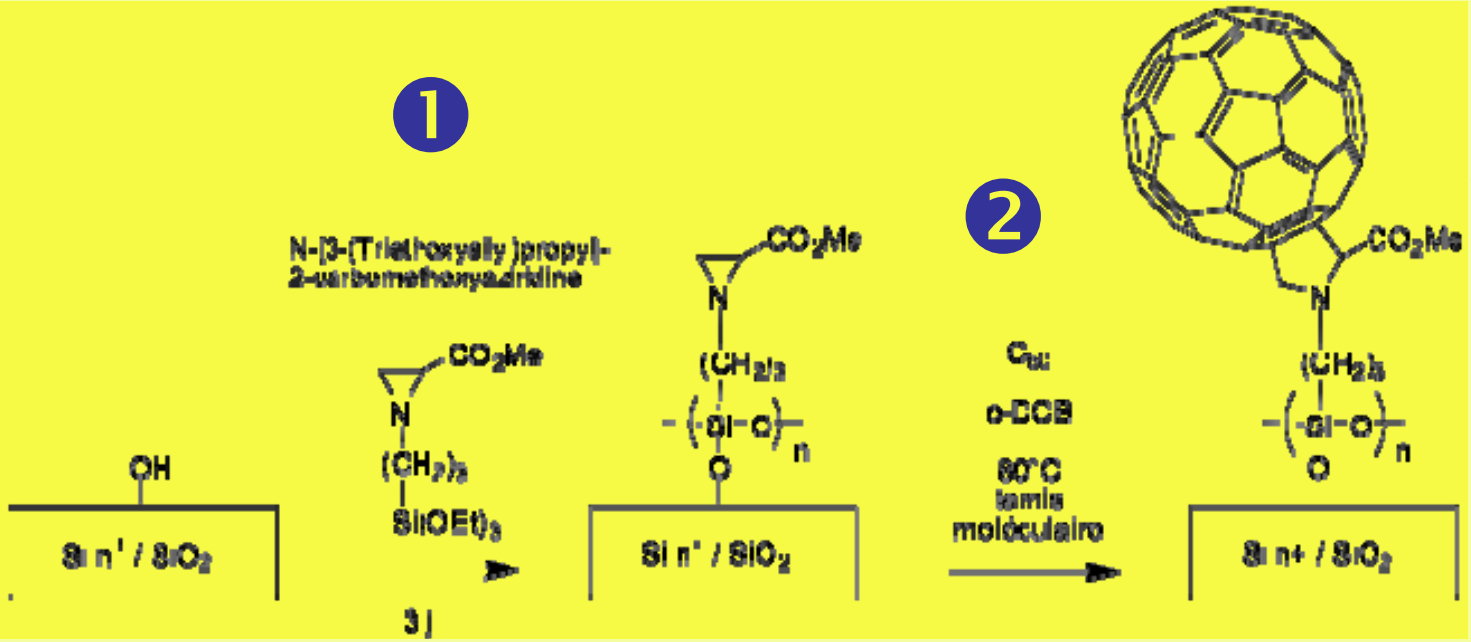

from :
JACS 1997, *119*, 7550

	contact angle	thickness (ellipsometry)
1 **SAM-aziridine**	55±1°	12 Å ☑
2 **SAM-C_{60}**		
80°C, 24 h with TM	71±1°	15.4 Å ☑
180°C, 24 h with TM	58±2°	44±2 Å (multilayer)
180°C, 24 h with TM	71±1°	20 Å (1.5 layer)

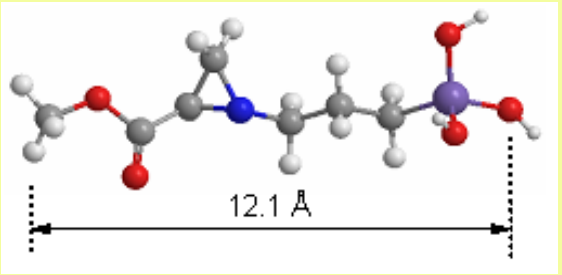

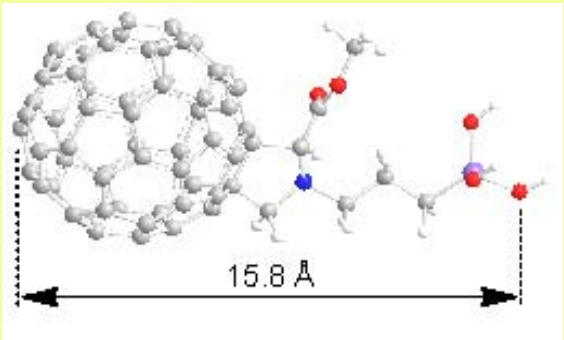

C.V. on SAM-C_{60} on Si n^+ SiO_2 Obtained using SAM-aziridine

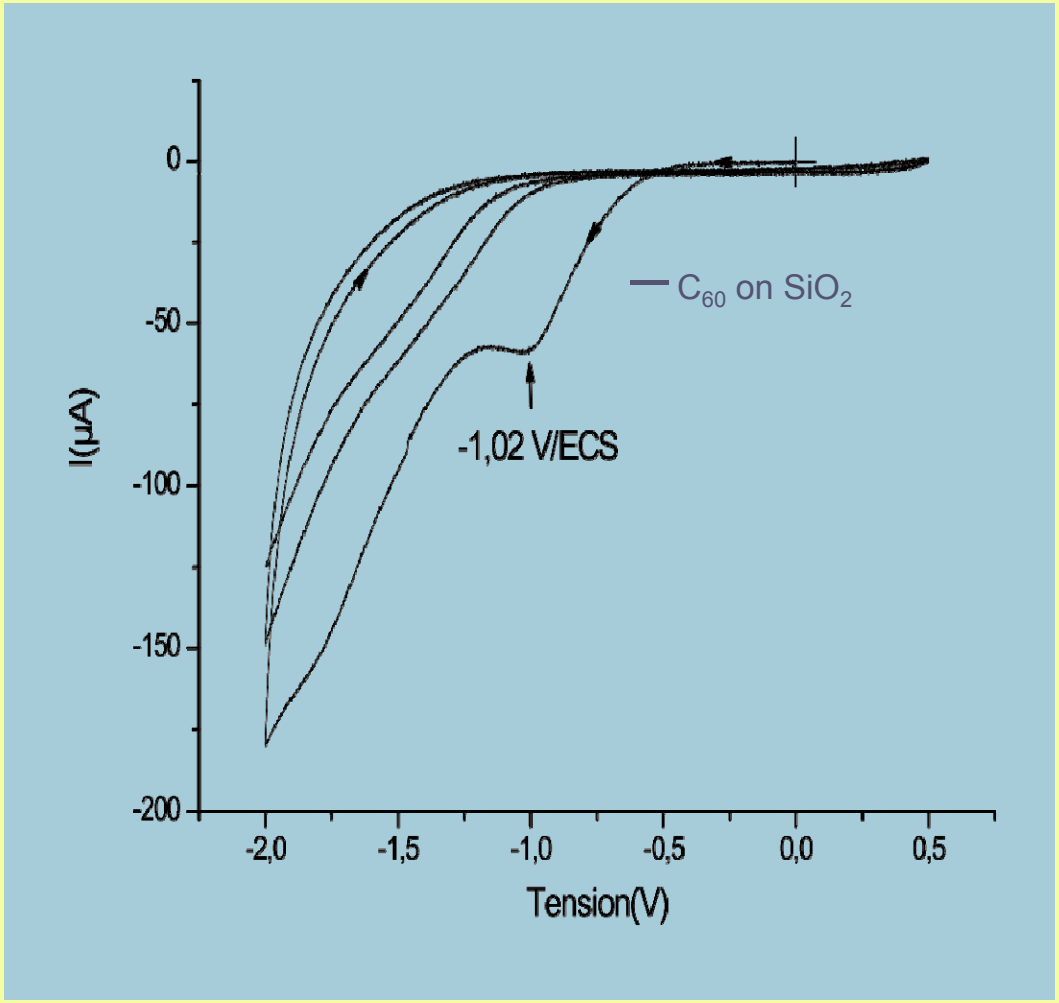

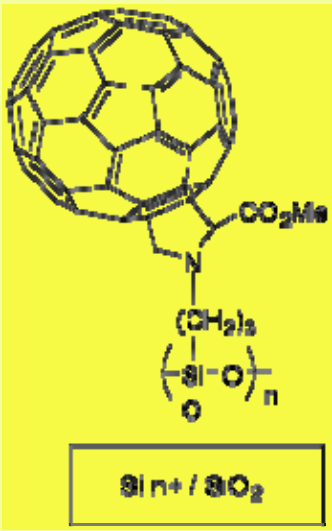

- Peak at -1.02 V (only at the fist scan)
- Almost similar to C_{60} on SAMs $-N_3$

J(V) measurements of the Si n^+ SiO_2 /SAM-C_{60} /Hg junction (naked Hg drop)

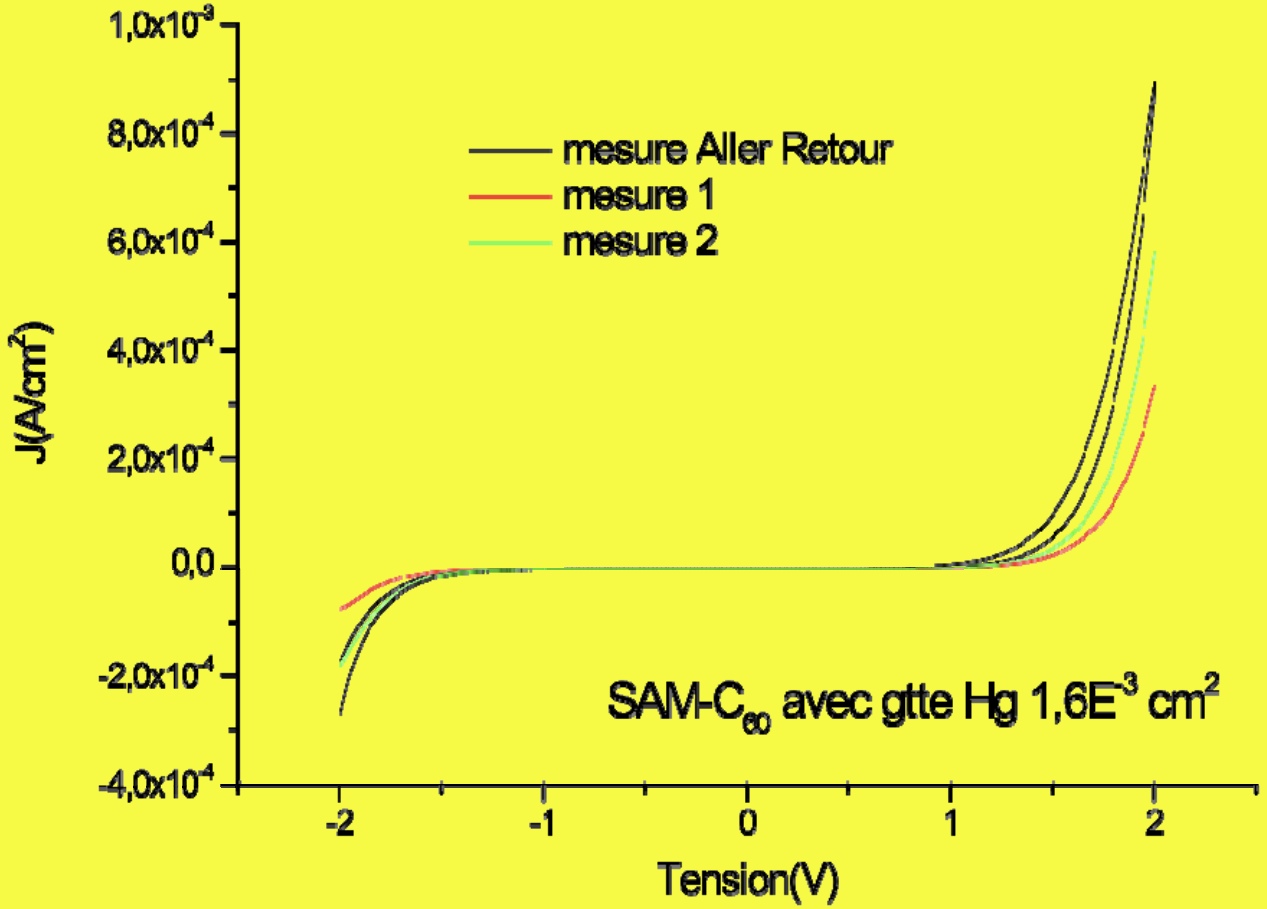

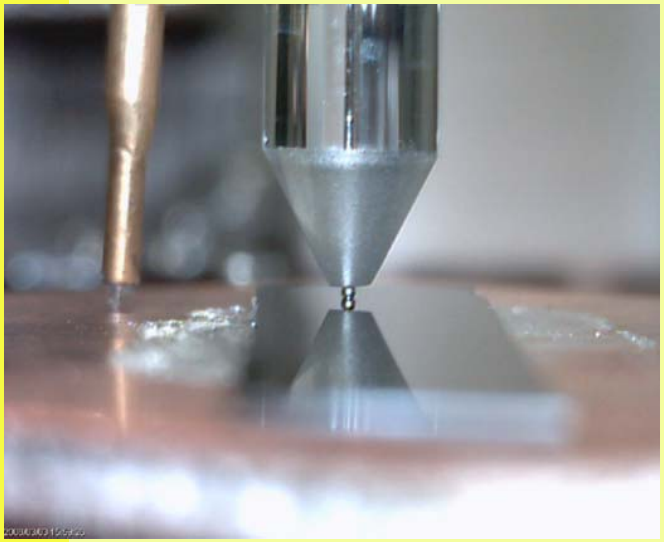

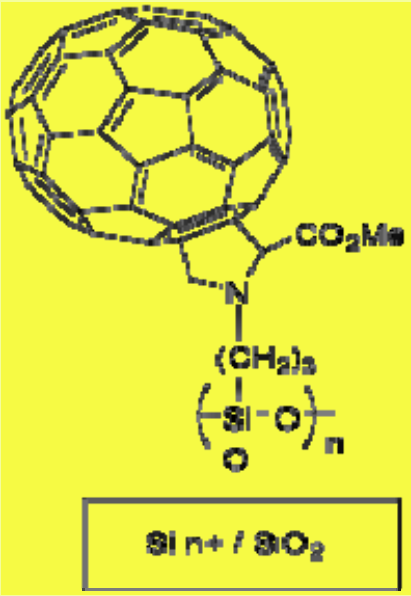

Rectification at V>0

- ► résonance thru the C_{60} LUMO?
- ► already observed for C_{60} on SAM-N_3

Electrical measurements of the Si n^+ SiO_2/SAM-C_{60}/σ-S-Hg junction

- **add a 2nd tunnel barrier (σ) on the SAM-C_{60}**
- **Hg drop capped with tetradecanethiol (10^{-3} M in tetradecane during 3 h)**

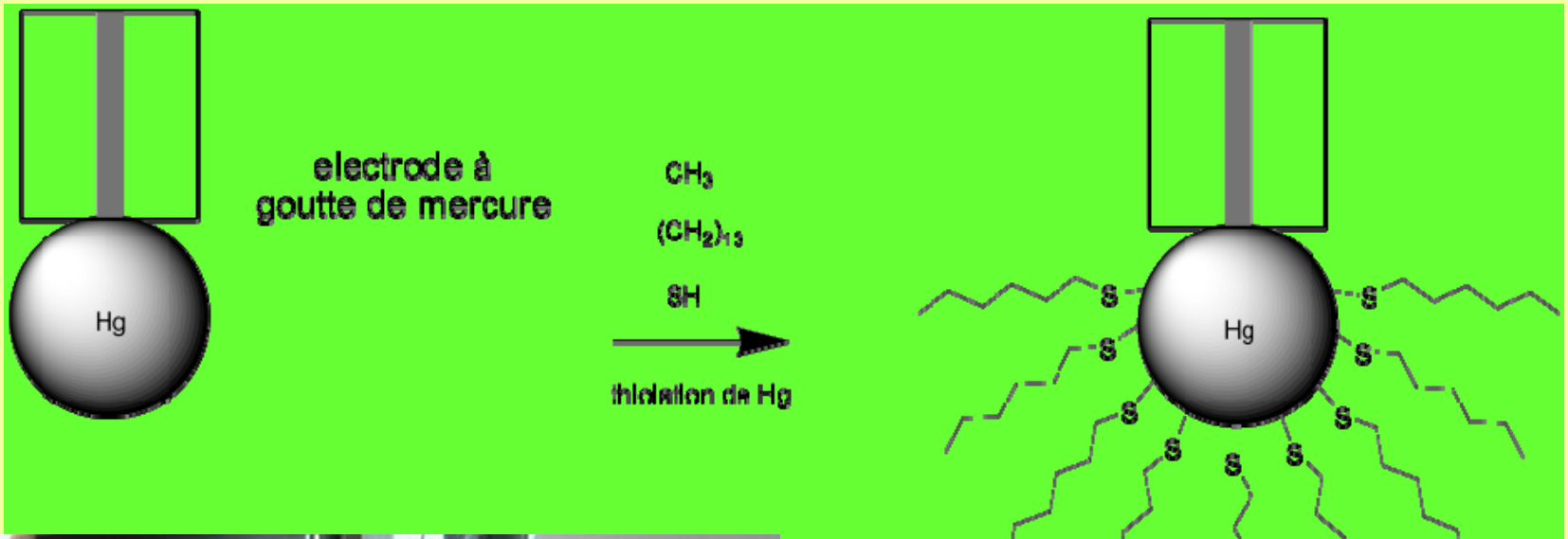

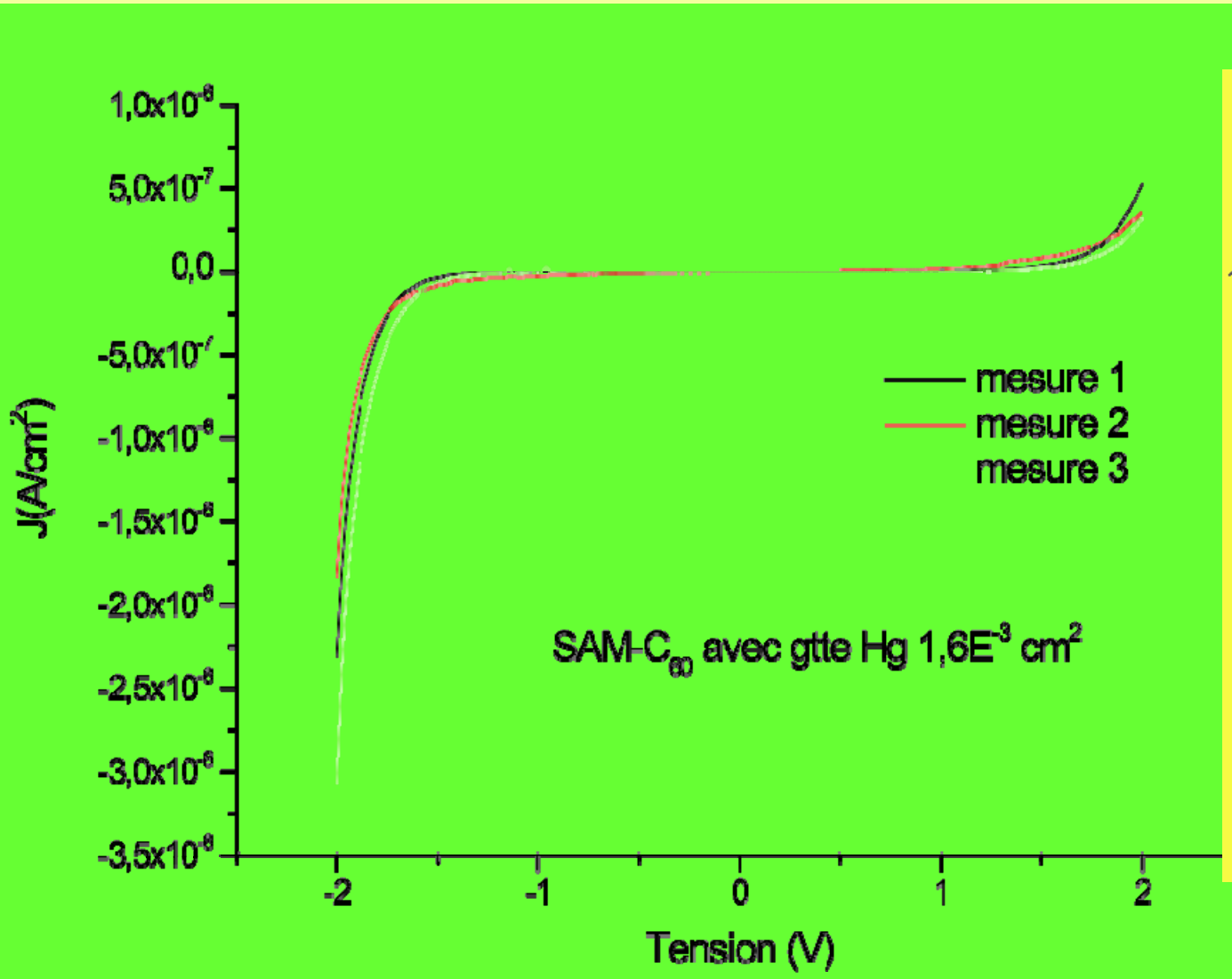

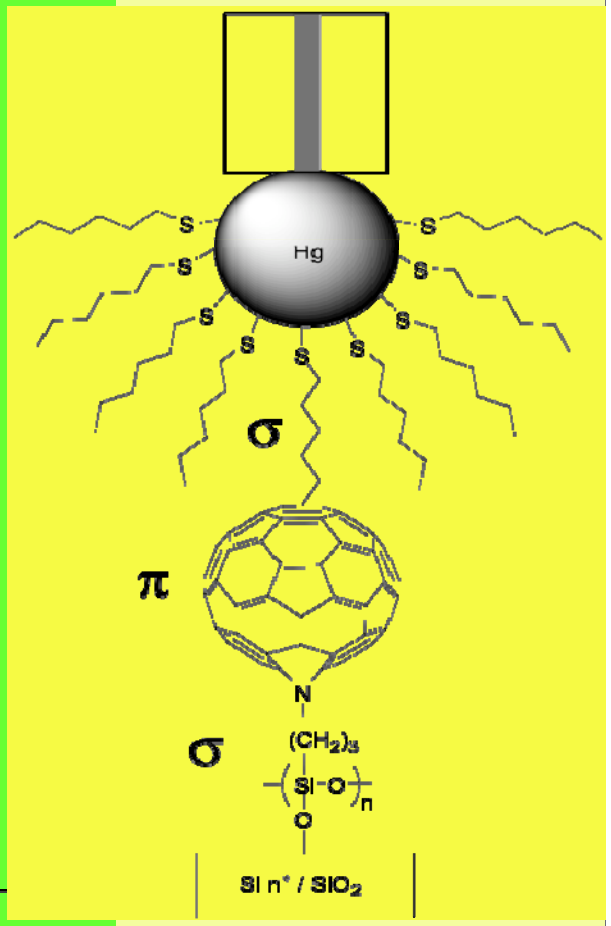

► reversal of the rectification (now at V<0)

► resonance thru the C_{60} HOMO ?

LbL deposition of multilayers of 3-aminopropyltrimethoxysilane (APTMS) on SiO*x*/Si(p++) substrates and NDR

Chauhan, Aswal, Koiry, Gupta, Yakhmi, Surgers, Guerin, Lenfant, Vuillaume, Appl. Phys. A 90, 581–589 (2008)

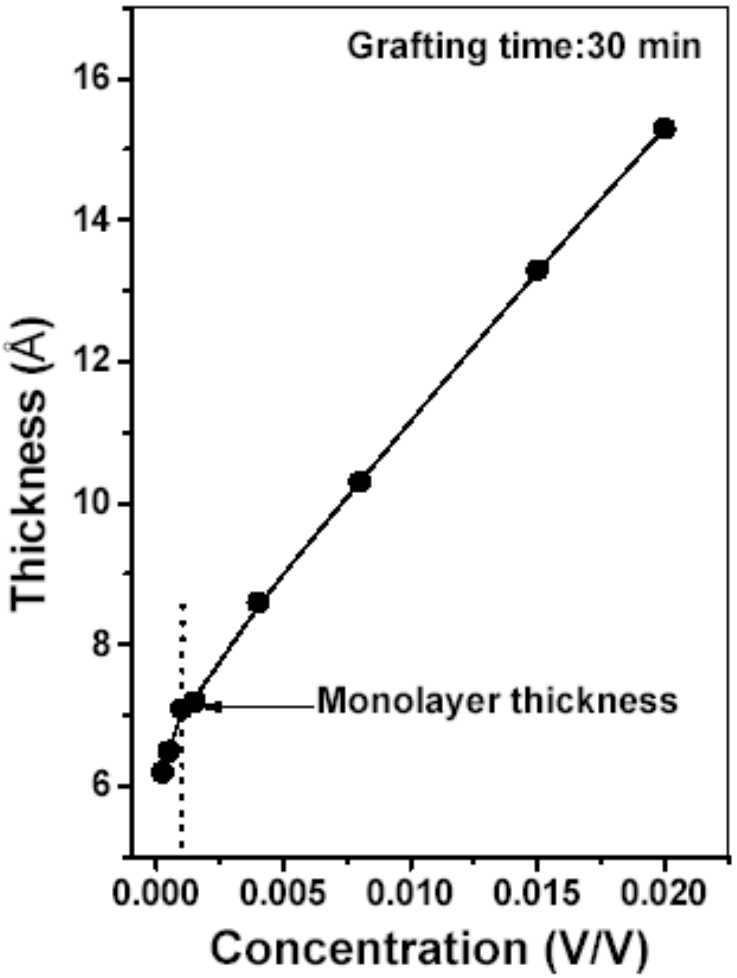

Thickness variation of the self-assembled APTMS layers grafted at R.T. on SiO2/Si as a function of solution concentration.

Done XPS and AFM For Upto 12 Mono-layers

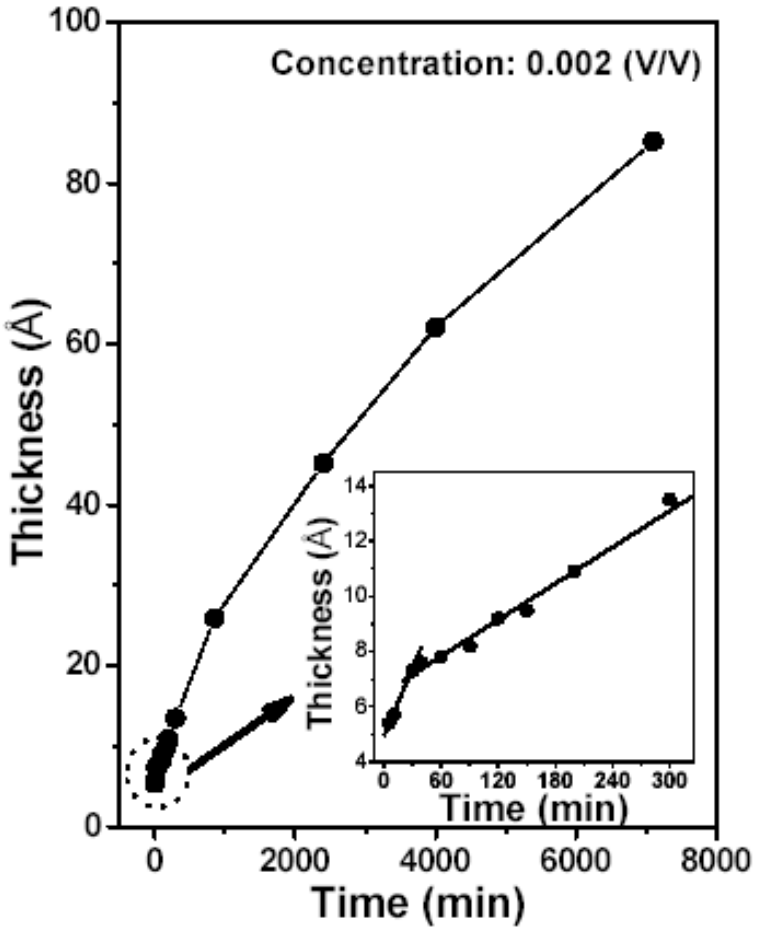

Thickness variation of the self-assembled APTMS layer on SiO_2/Si substrates as a function of grafting time, keeping solution Conc. (in toluene) fixed at 0.002 (V/V).

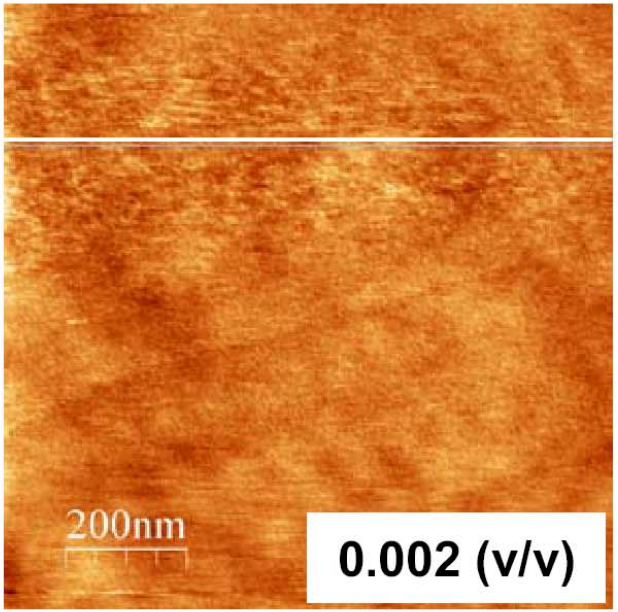

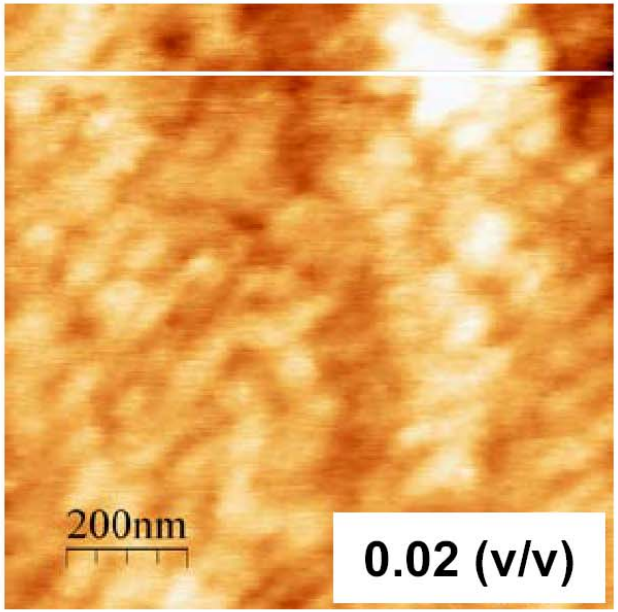

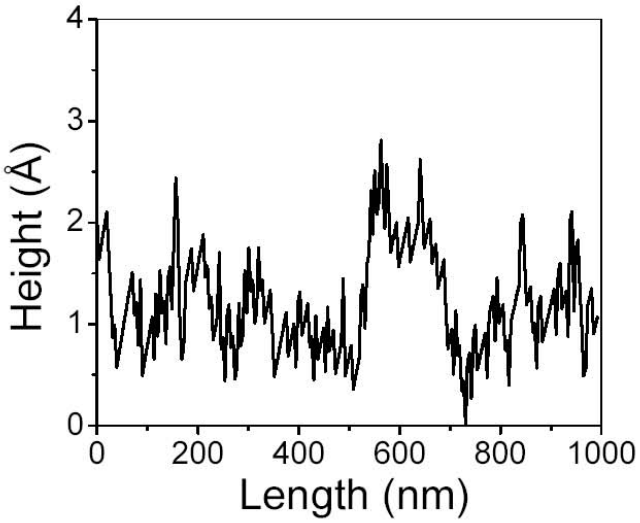

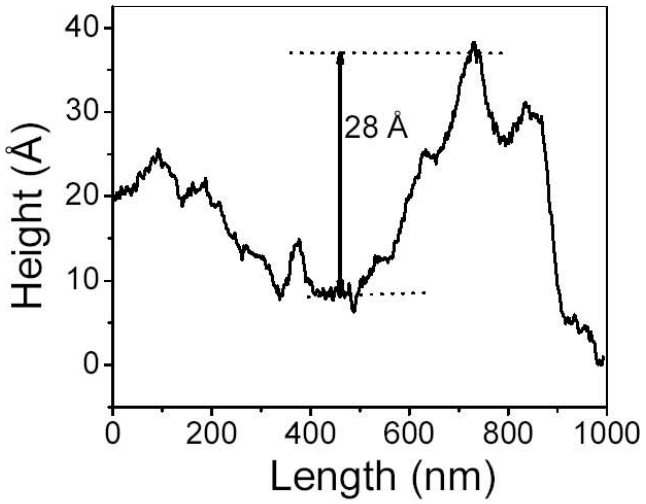

1 μm×1μm AFM images of APTMS layers deposited using solutions of different concentrations.

Height profiles are plotted across the white line drawn in the images.

uniform coverage of the substrate. DI water contact angles were < 15 and □ 40◦ on these two samples.

A low contact angle (< 15◦), and a measured thickness of 7 Å and surface roughness < 1Å, suggests that samples from 0.002 (v/v) are well organized monolayers terminated with a NH2 group.

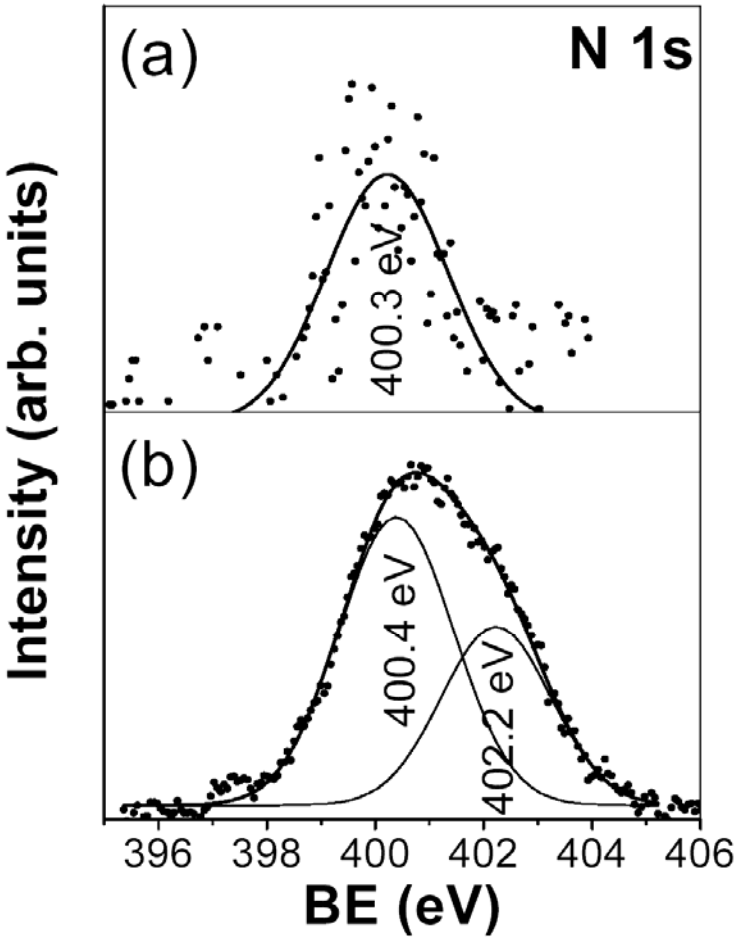

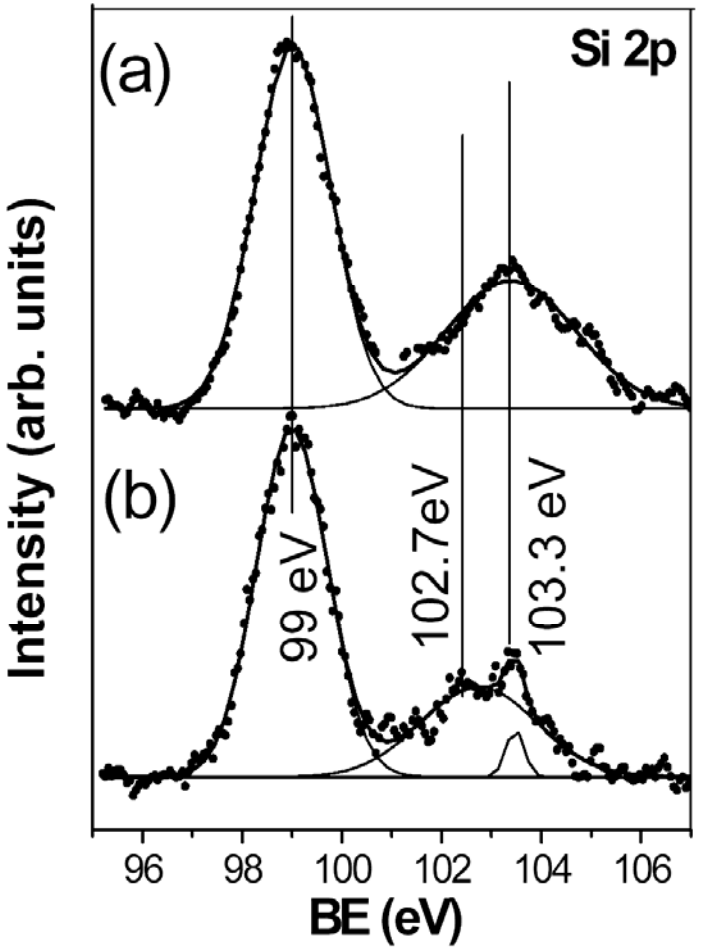

N 1s and Si 2p XPS spectra recorded for
(a) monolayer and

(b) 12-layered APTMS sample.

Peaks obtained by fitting Gaussian curve(s).

N 1*s XPS*: single peak at □ 400.3 eV for the monolayer, which corresponds to N in NH_2 group. For multilayers the N 1*s* peak is very broad, comprising two Gaussian peaks at Binding Energy of 400.4 eV (from NH_2 group) and 402.2 eV (from H-bonded amine or +vely charged quaternary nitrogen of the form $-NH^{+3}$. Intensity of 402.2 eV peak increases with no. of APTMS layers, suggesting that $-NH^{+3}$ ions is associated with the formation SAMs.

Si 2*p* XPS spectra: 2 peaks at 99 eV and 103.3 eV for the monolayer corresponding to Si and SiO2, originating from the substrate.

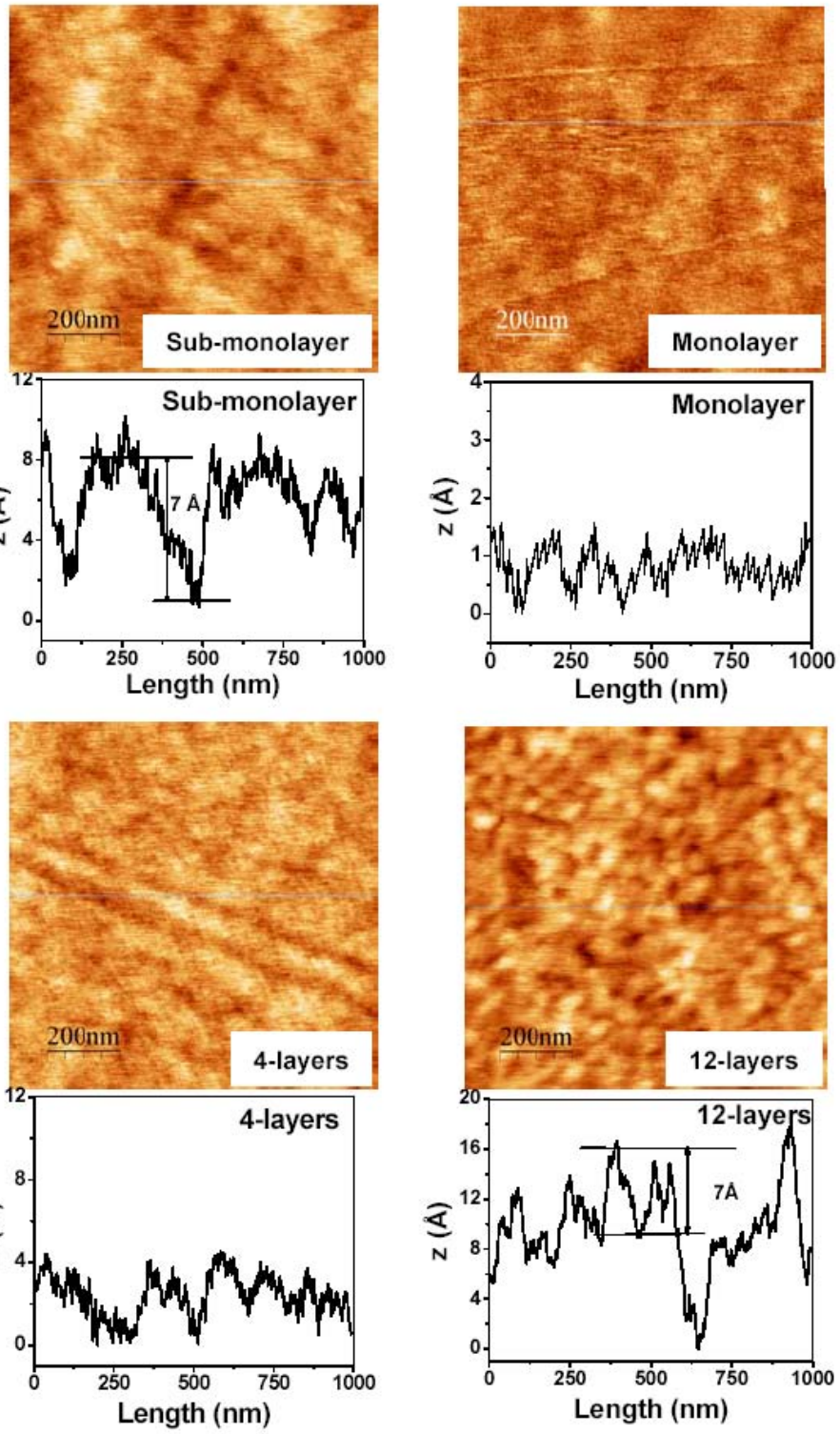

1 μm×1 μm AFM images for different APTMS layers. Height profiles are drawn across the *white line* in the respective AFM image

Partial-monolayer, formed after 20 min grafting, Shows growth via the 2D nucleation.
Height of the island is □ 7Å, which is the length of the APTMS molecule.

APTMS monolayer has surface roughness of < 1Å, Indicating its uniform coverage on the substrate.

But surface roughness increases with number of layers.
Surface morphology also changes.
12-layers sample has islands (100–200 nm, height □ 7Å).
Implies folding of alkyl-chains, as supported by contact angle data.

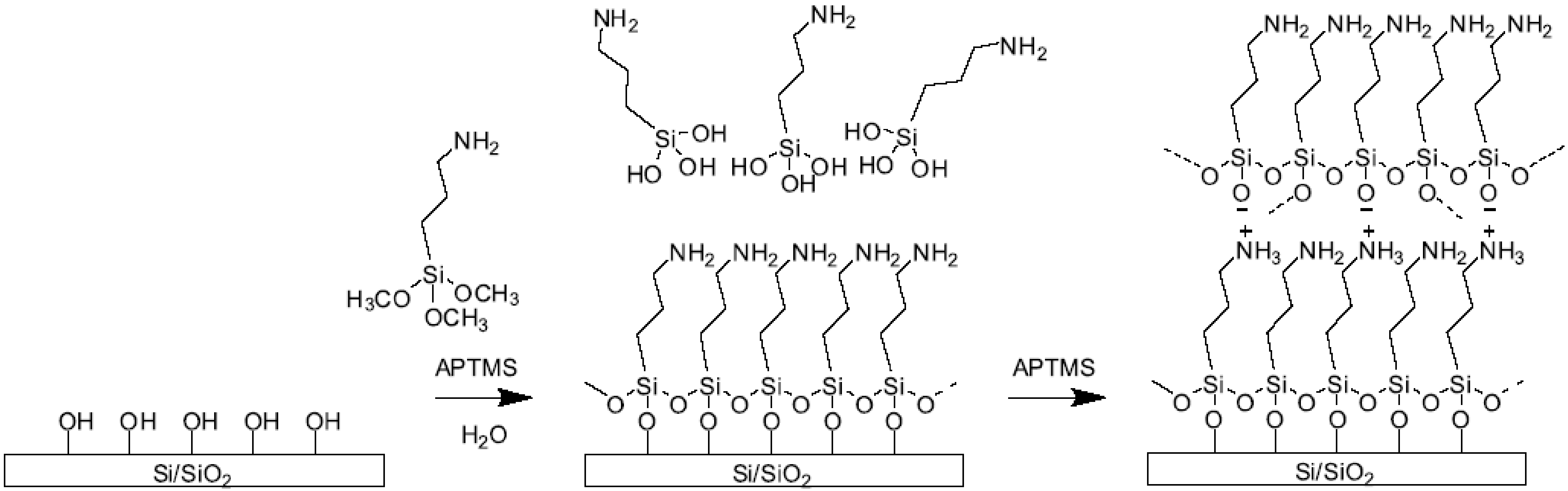

Suggested self-assembly mechanism of APTMS L-b-L formation

(i) 1st APTMS monolayer chemisorbs on hydroxylated oxide surface by silanization ,

(ii) the surface amino group of the 1st monolayer chemisorbs the hydrolyzed silane group of other APTMS molecules present in the solution, leading to the formation of a bilayer.

Thereafter, a self-replicating process results in the layer-by-layer self-assembly of the multilayers with trapped NH^{3+} ions.

I-V characteristics of the multilayers exhibit a hysteresis effect, and NDR (negative differential resistance), suggesting their potential for application in molecular memory devices.

The hysteresis effect arises from filling/de-filling of NH^{3+} acting as traps ➔

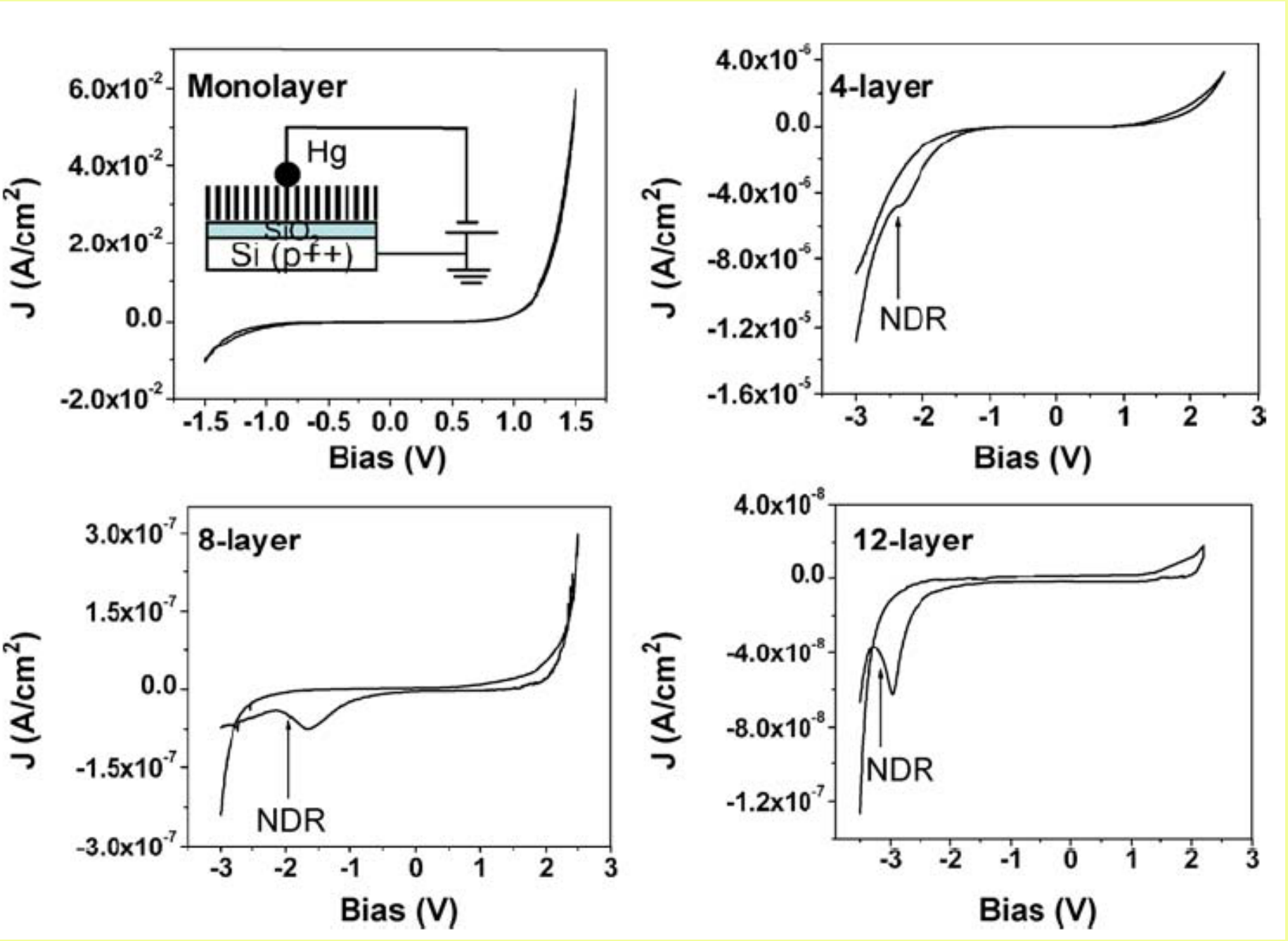

Current–voltage (*J–V*) characteristics for APTMS films by scanning the applied bias in the sequence: – *V*max→0V→+ *V*max→ 0 V→– *V*max. *Inset* shows schematic of device structure.

NH^{3+} ion-trapped 3-aminopropyltrimethoxysilane (APTMS:NH2(CH2)3Si(OCH3)3) multilayers grafted on SiO2/Si(p++) substrates by a self-assembly process exhibit electrical bistability with an on/off ratio of ~2. Chauhan, Aswal, Koiry, Padma, Saxena, Gupta, Yakhmi

phys. stat. sol. (a) **205**, (2008) 373

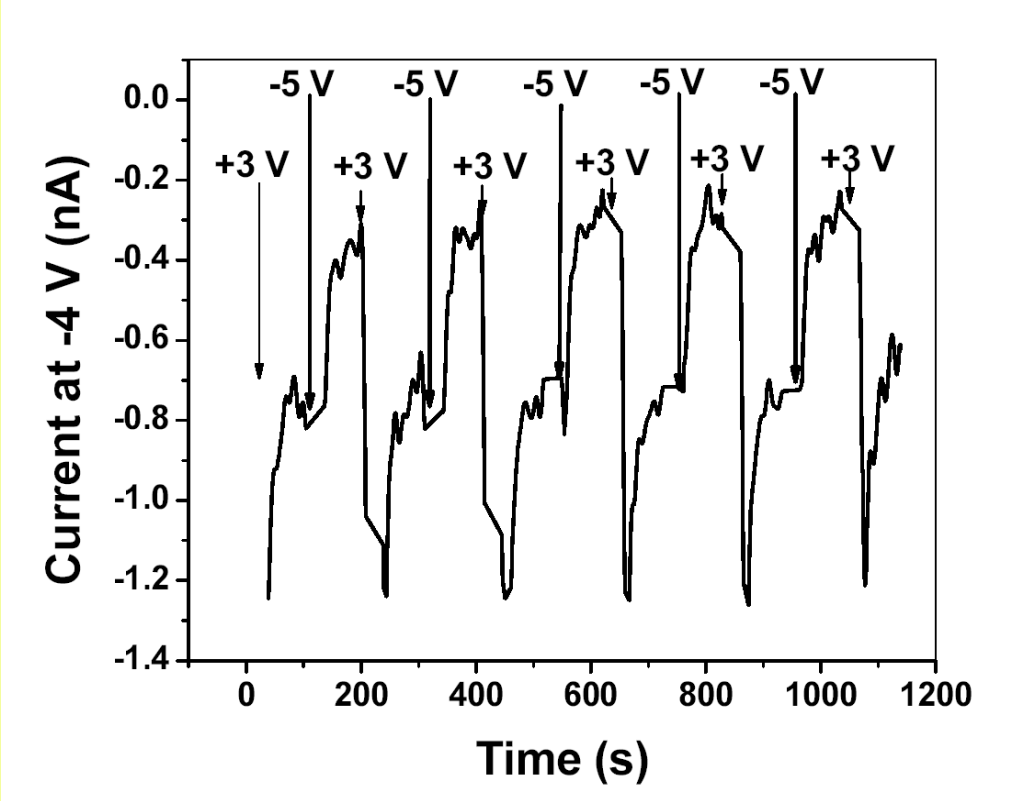

Memory effect in Hg/APTMS-multilayer/Si(p^{++}) device. The "write-read-erase-read" operations were performed by 10 s pulsing of +3V and -5V, consecutively. The device was read 50 times at -4V after each write (+3V) and erase (-5V) pulse.

Rewritable RAM. The observed on/off ratio for our device is ~2,

AMMONIA SENSOR using LB FILMS of Polycarbazol

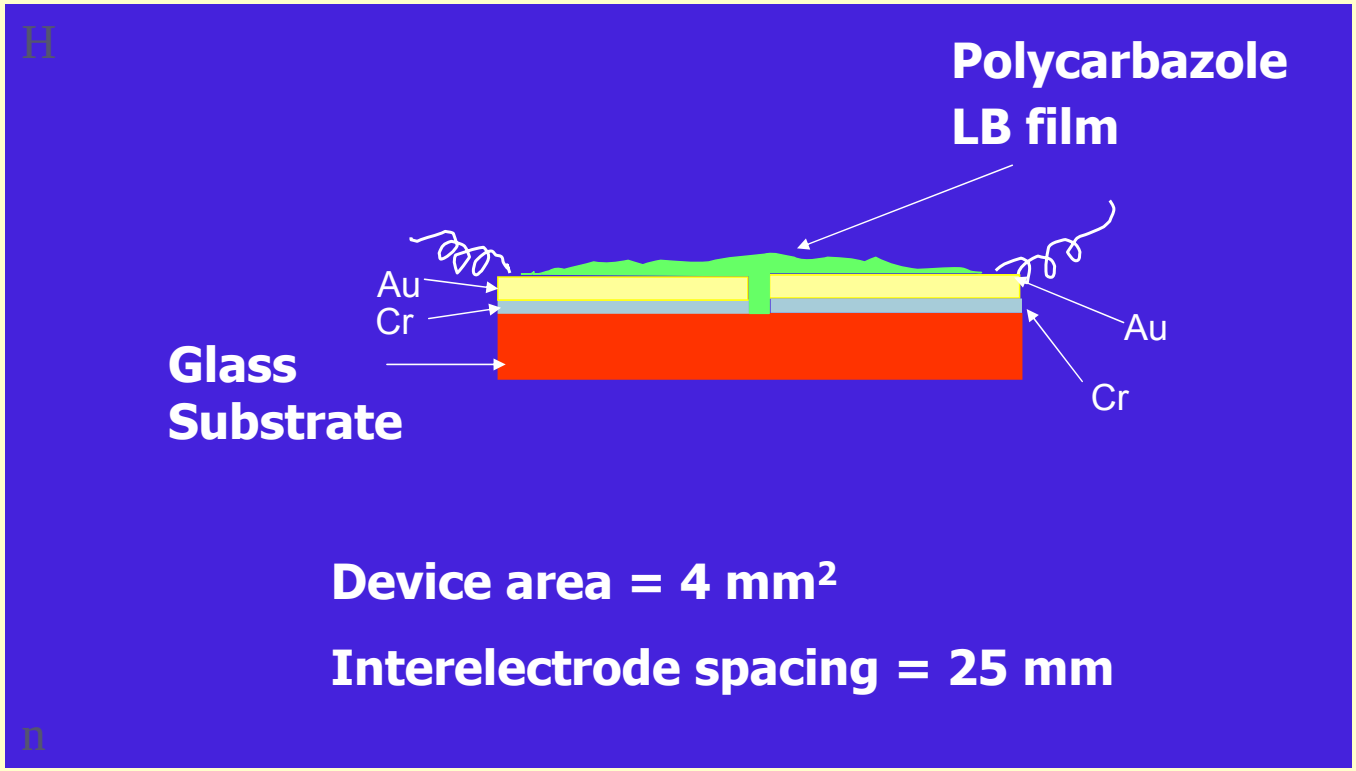

Testing done under ambient conditions in a closed 250 c.c. chamber

Saxena, Choudhury, Gadkari, Gupta and Yakhmi,
Sensors and Actuators B 107 (2005) 277

Surfactant encapsulated Nickel hexacyanoferrate nanoparticles: Synthesis and LB films

NiHCF unstable in aqueous phase

HMP (hexametaphosphate) cyclic anion stabilizes nano particles by covering their surface,

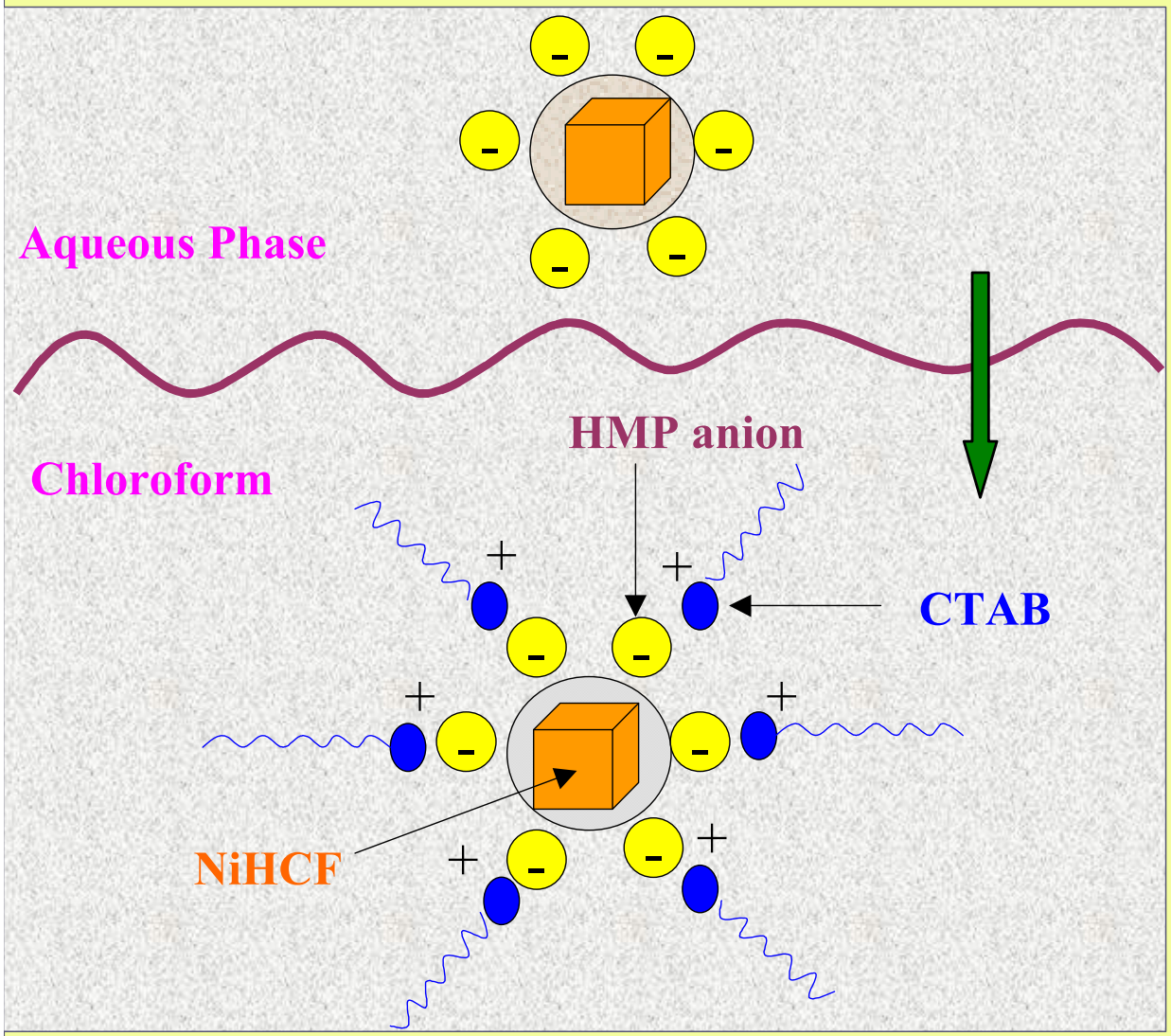

Electrostatic interaction between negatively charged HMP ions and positively charged CTAB helps in extraction of NiHCF nanoparticles from aqueous to organic phase -facilitating deposition of stable Langmuir monolayers

TEM images indicate cubic nanocrystals of NiHCF of size 22 nm. Av. size confirmed with DLS study

Bagkar, Ganguly, Choudhury, Hassan and Yakhmi, *J. of Mater. Chem.* 14 (2004) 1430

K^+ ions on DODA-NiHCF nanoparticles deposited as LB films

Peak potential shifts with increase in K^+ concentration.

During reduction, the film takes cations from the solution.
During oxidation (on the hcf centers) the cations are released from the film.

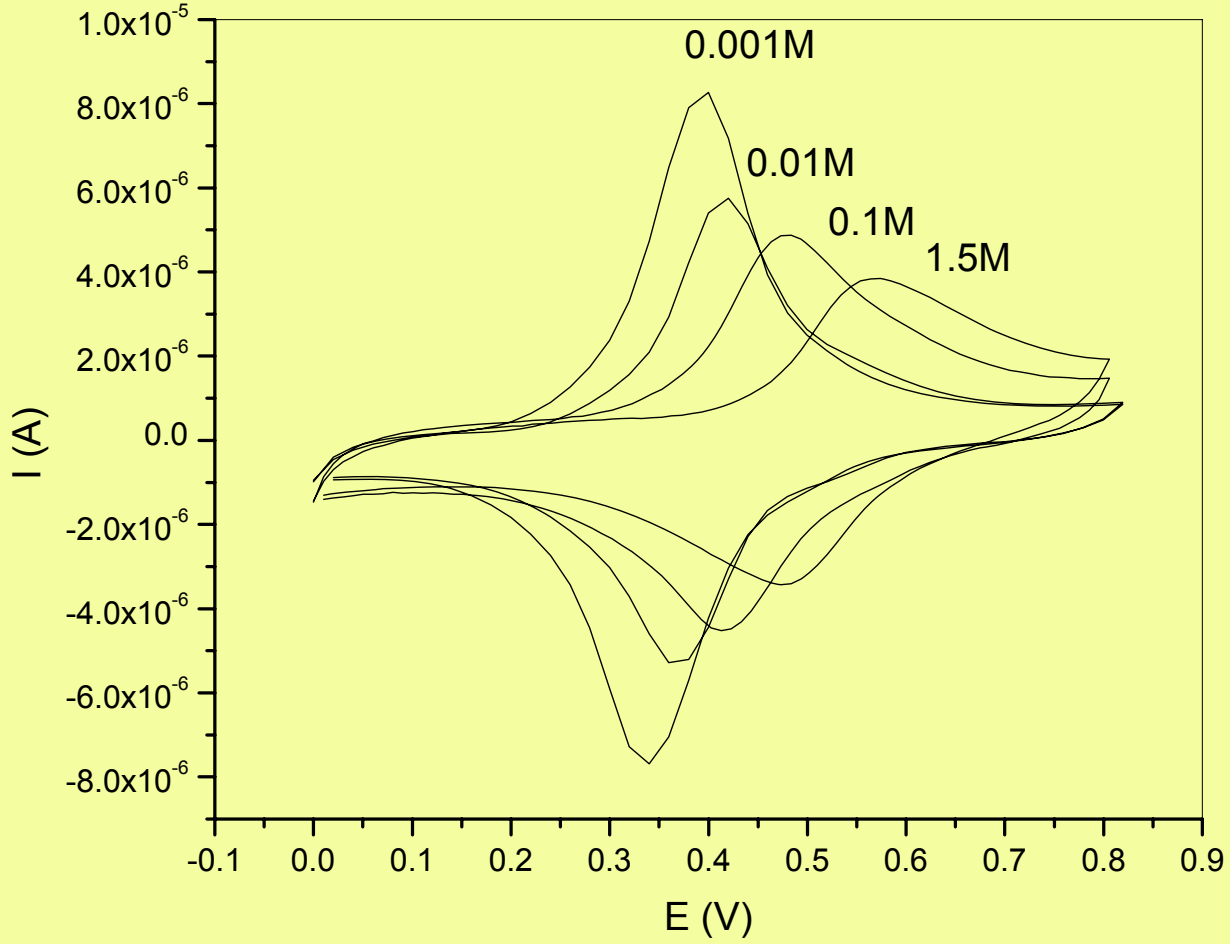

During oxidation/reduction reactions e's are exchanged between the electrode and particle, whereas K^+- ions are exchanged between the particles and adjacent electrolyte.

K^+ ions neutralize negative charge and make the film maintain charge balance.

Bagkar, Betty, Hassan, Kahali, Bellare and Yakhmi,
Thin Solid Films, 497 (2006) 259

CVs of 19 layers of DODA-NiHCF multilayers to different K^+-ion concentrations using 0.001, 0.01, 0.1 and 1.5M KCl solutions.

MBE grown Metal Phthalocyanines, MPc ($MC_{32}H_{16}N_8$) films: M (Cu, Fe, Ni) square-planar coordinated to 4 pyrrolic N's.

2 monoclinic polymorphs, α and β, differ mainly in tilt angle of the molecular stack from the *b*-axis, which is 26.1° for α-phase and 44.8° for β-phase.

Highly anisotropic molecular structure. Crystals: high aspect ratio needles. α-FePc nanobrush and nanowebs grow on glass substrate *via* VdW epitaxy.

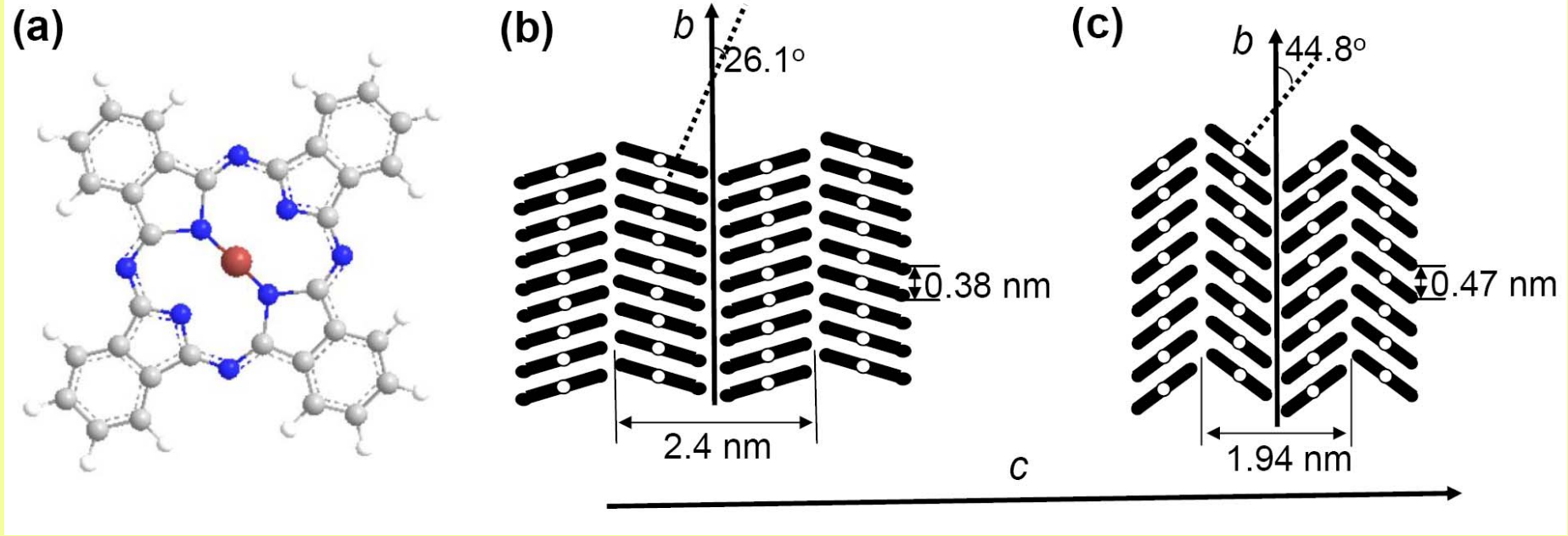

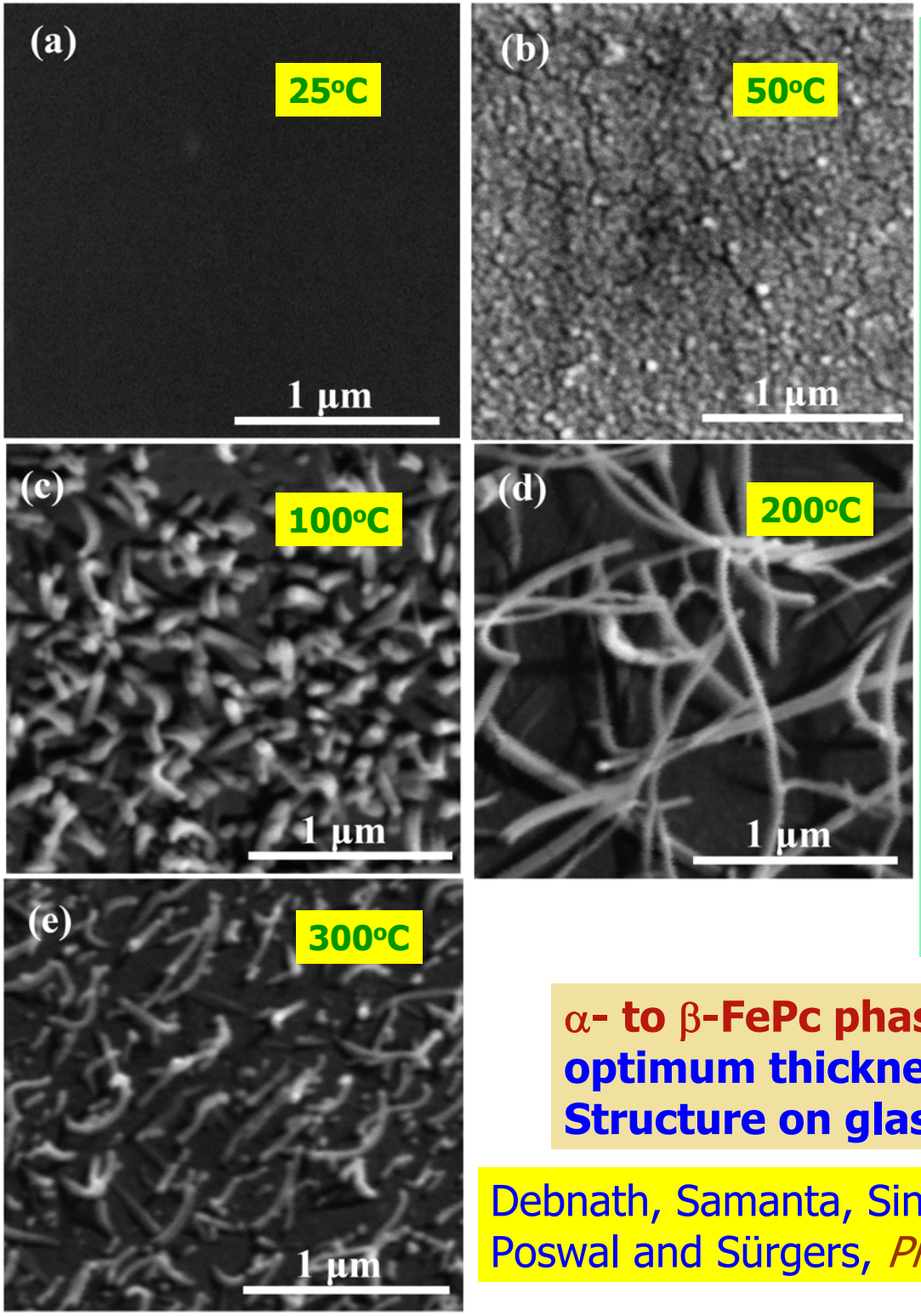

SEM of MBE grown FePc thin films (thickness 60 nm, *obtained from GI X-ray reflectivity*) at deposition rate of 0.07 nm/s, and substrate temperatures (a) 25°C, (b) 50°C, (c) 100°C, (d) 200°C and (e) 300°C.

At 25°C: amorphous film.
At 50°C: dense-packed grains ~70 nm.
At 100°C: FePc grains get *elongated in the plane of the substrate.*

At 200°C, long FePc nanowires (~100 nm dia, ~ 2 μm length), *lying in the plane of the substrate* -- **a nanoweb**.

At 300°C, the length of nanowires decreases to <500 nm.

α- to β-FePc phase transition occurs above 200°C.
optimum thickness for growing nanoweb Structure on glass substrates: 50-60 nm

Debnath, Samanta, Singh, Aswal, Gupta, Yakhmi, Deshpande, Poswal and Sürgers, *Physica E (2008) accepted*

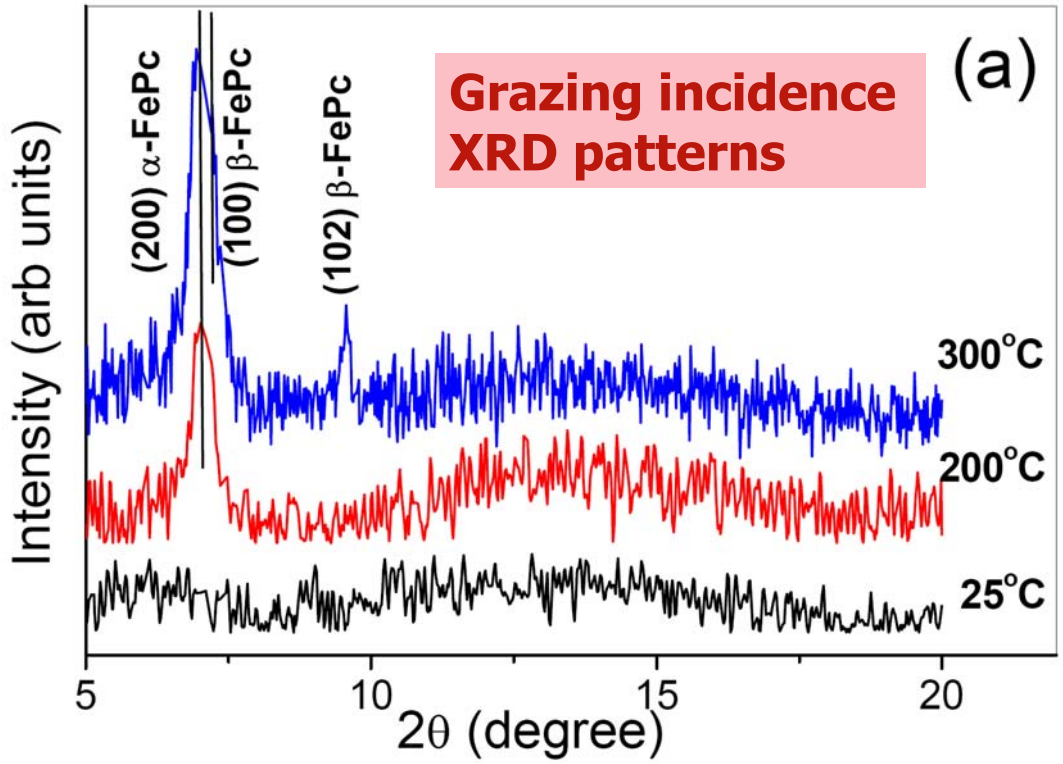

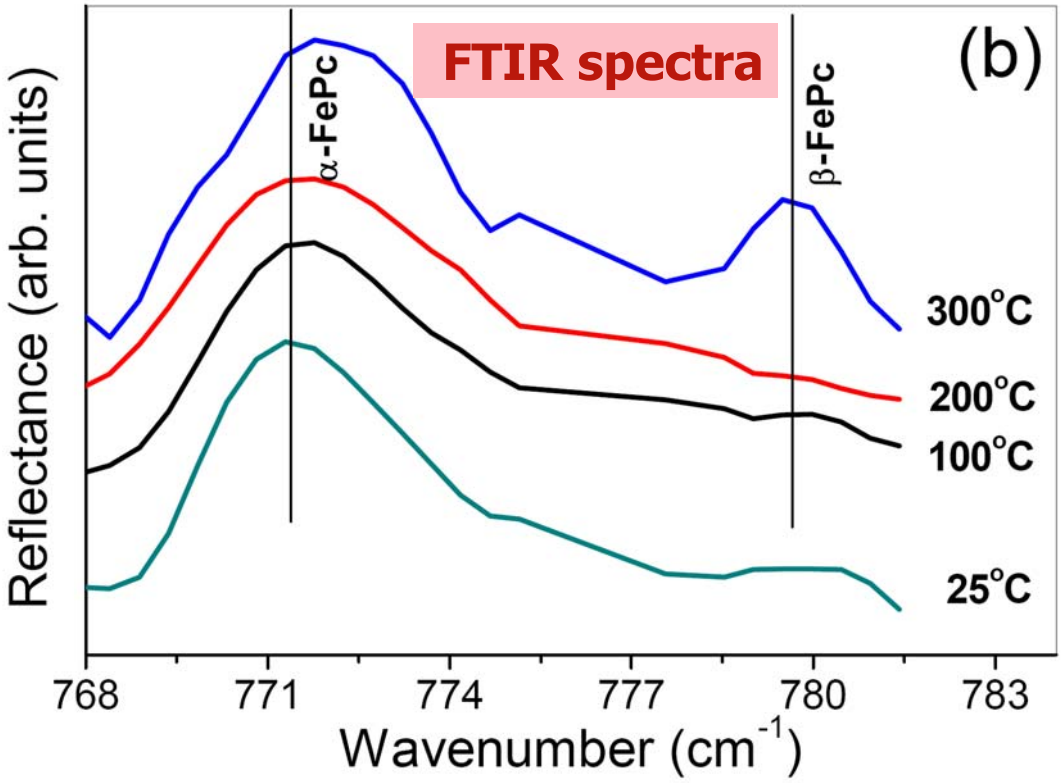

60 nm thick FePc films deposited at Different substrate temperatures.

25°C: film is amorphous.

Upto 200°C: only one peak (2θ = 6.96°), the (200) peak of the **α-FePc** phase, indicating edge-on stacking

At 300°C: two more peaks at 2θ = 7.01° and 9.6°, which are (100) and (102) peaks of the **β-phase** FePc.

ν(C-N) stretching vibration for α–, β-phase at 773 and 780 cm^{-1}, resp.

Upto 200°C: pure α-phase films

At 300°C: aditional peak at 780 cm^{-1} due to partial transformation from α- to β-phase.

A nanoweb structure of pure α-FePc EVOLVES for films (60nm) deposited at 200°C.

SEM of 60 nm FePc thin films grown in-situ at a rate of 0.2 Å/sec at substrate temperatures (a) 50°C, (b) 100°C, (c) 200°C and (d) 300°C

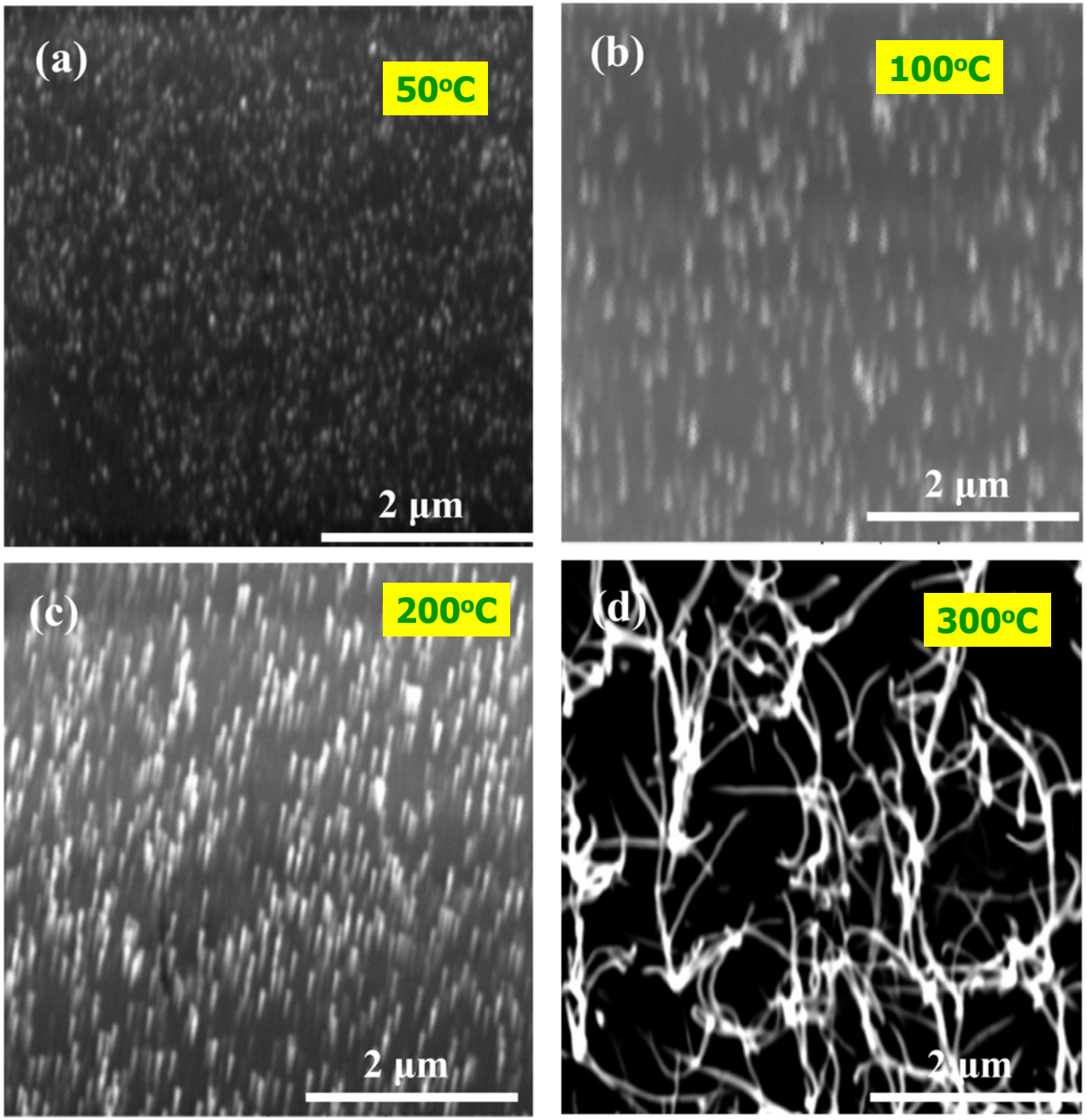

Effect of slow deposition rate 0.02nm/s, vis-à-vis 0.07 nm/s Keeping thickness at 60 nm

50°C: needle tip like structure, pointed perpendicular to the plane of the substrate.

100°C: vertical growth of needle-like tips.

200°C: needles grow to form vertical nanorods (a nanobrush).

300°C: No nanobrush. Nanoweb grows (it has mixed α-and β-FePc phases.

at 200°C, the 60 nm thick α-FePc phase gets transformed from nanoweb to nanobrush if growth rate is lowered from 0.07 to 0.02 nm/s.

growth mechanism

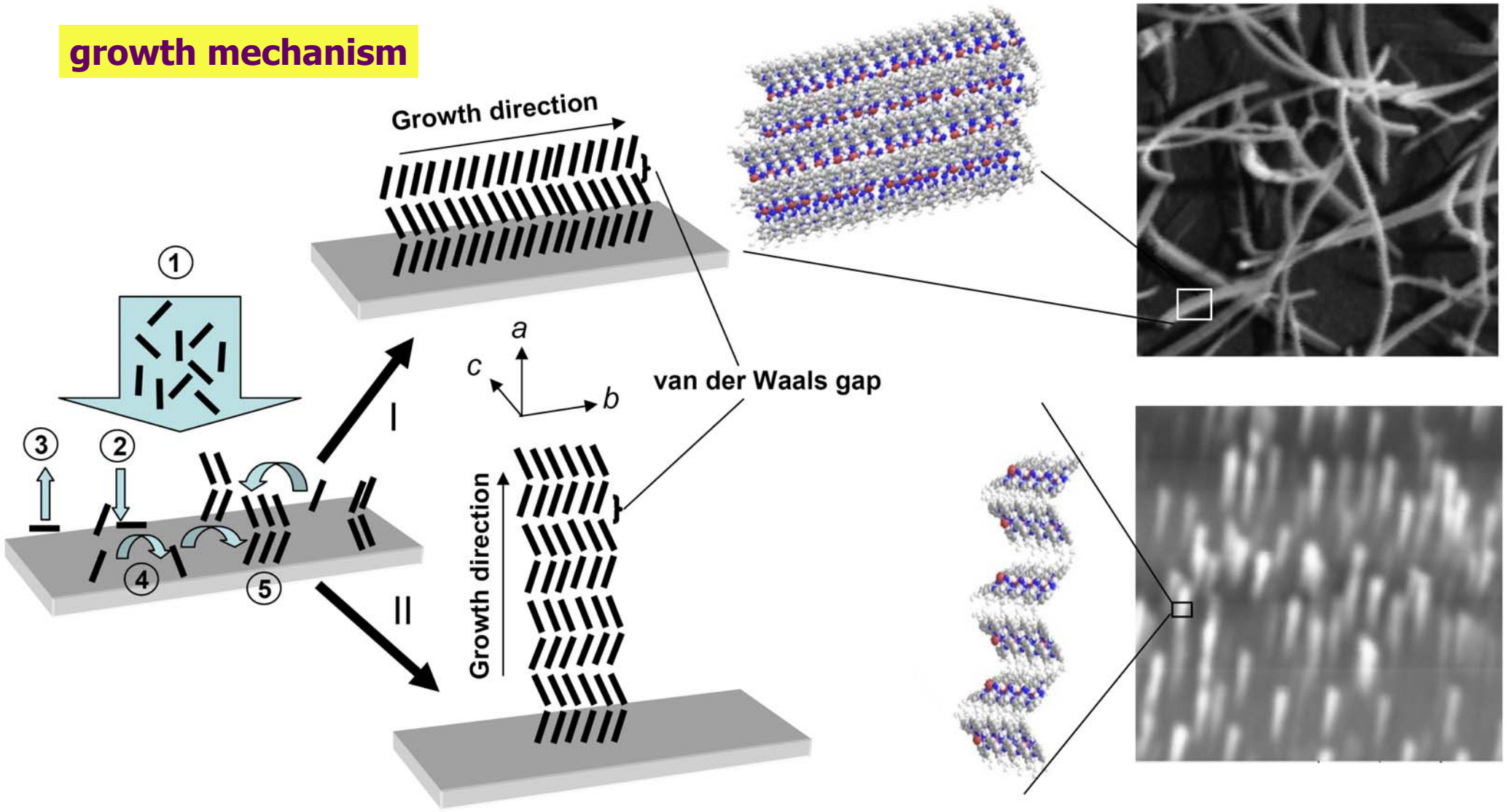

planar molecules adsorb on substrate in: (1) "lying-down" or (2) "standing-up" configurations. (3), (4) and (5) show desorption, diffusion & formation of nucleus

Nucleus grows: (I) along b-axis at 0.07 nm/s, with molecules face-on; giving nanoweb, in the plane of the substrates; (II) along *a*-axis at 0.02 nm/s, due to VdW epitaxy, forming nanrods aligned vertical to the substrate plane (nanobrush)

FePc film grows epitaxially for Nominal Thickness : >100 nm; Growth at : 200C

SEM, GIXRD confirm densely packed FePc crystallites. Single (200) peak of the α-FePc phase . Indicates *a*-axis preferentially oriented normal to the substrate plane, i.e.

edge-on stacking of FePc molecules. a = 2.54 nm, from XRD data

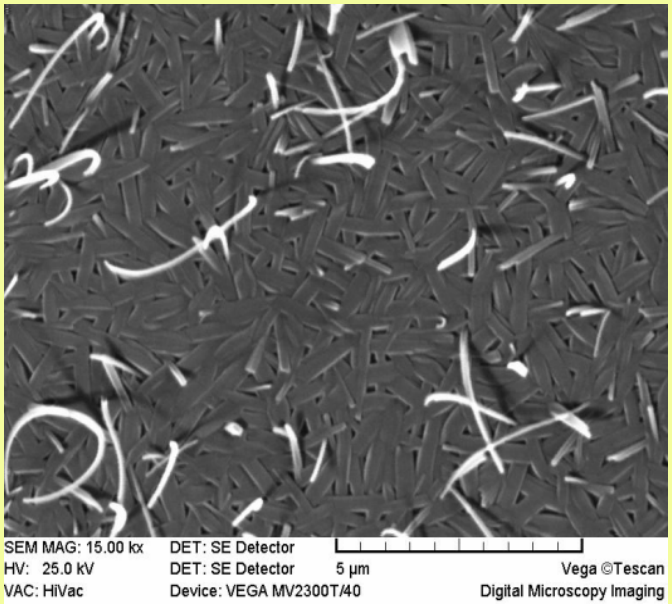

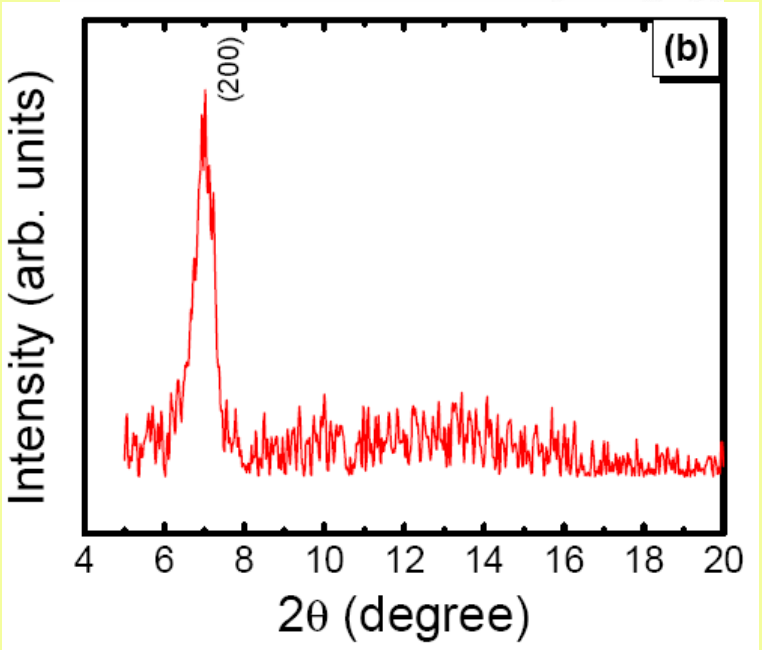

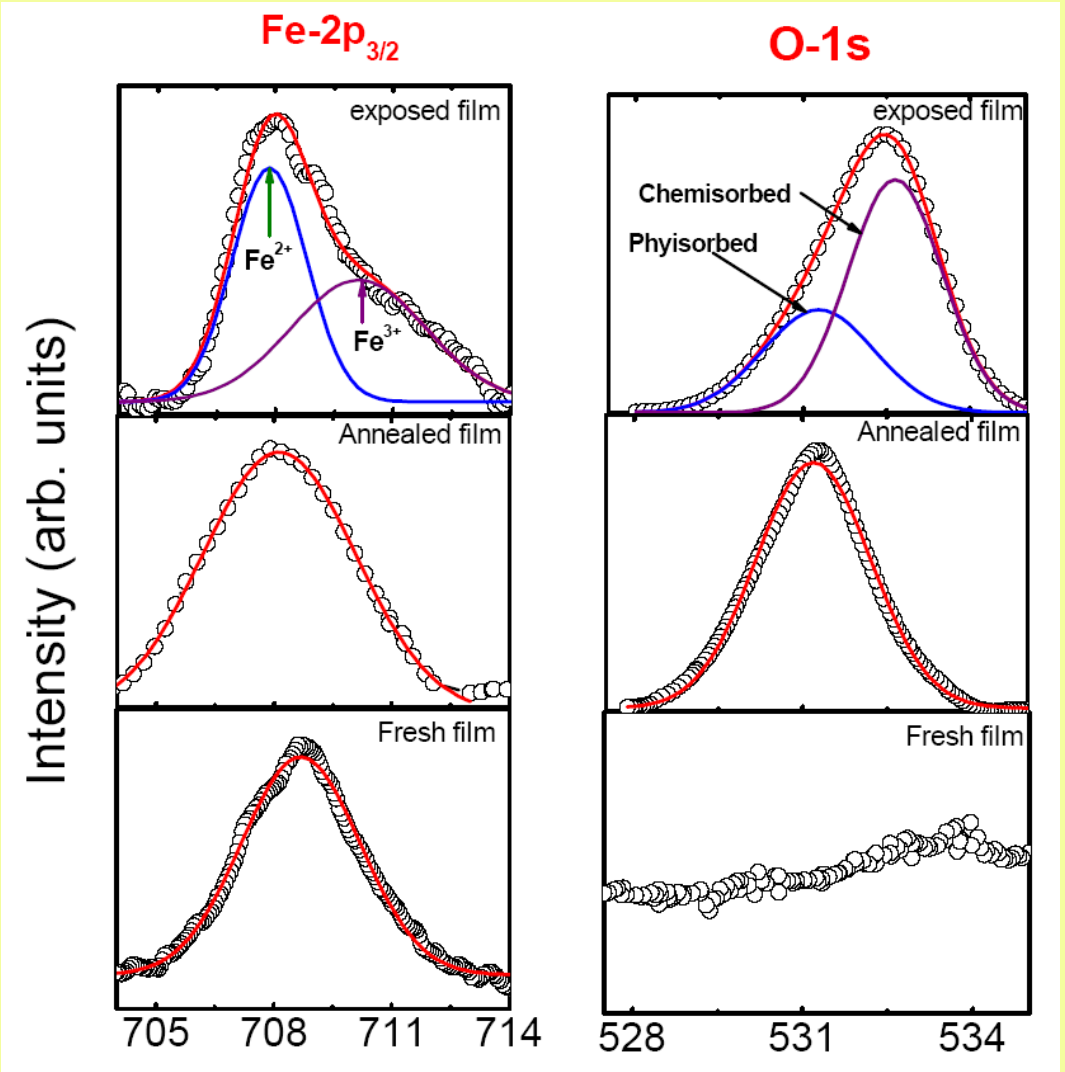

Core level Fe-2p $_{3/2}$ and O-1s XPS spectra of fresh, vacuum annealed, and air exposed FePc films.

Strong reactivity to the oxygen from atmosphere

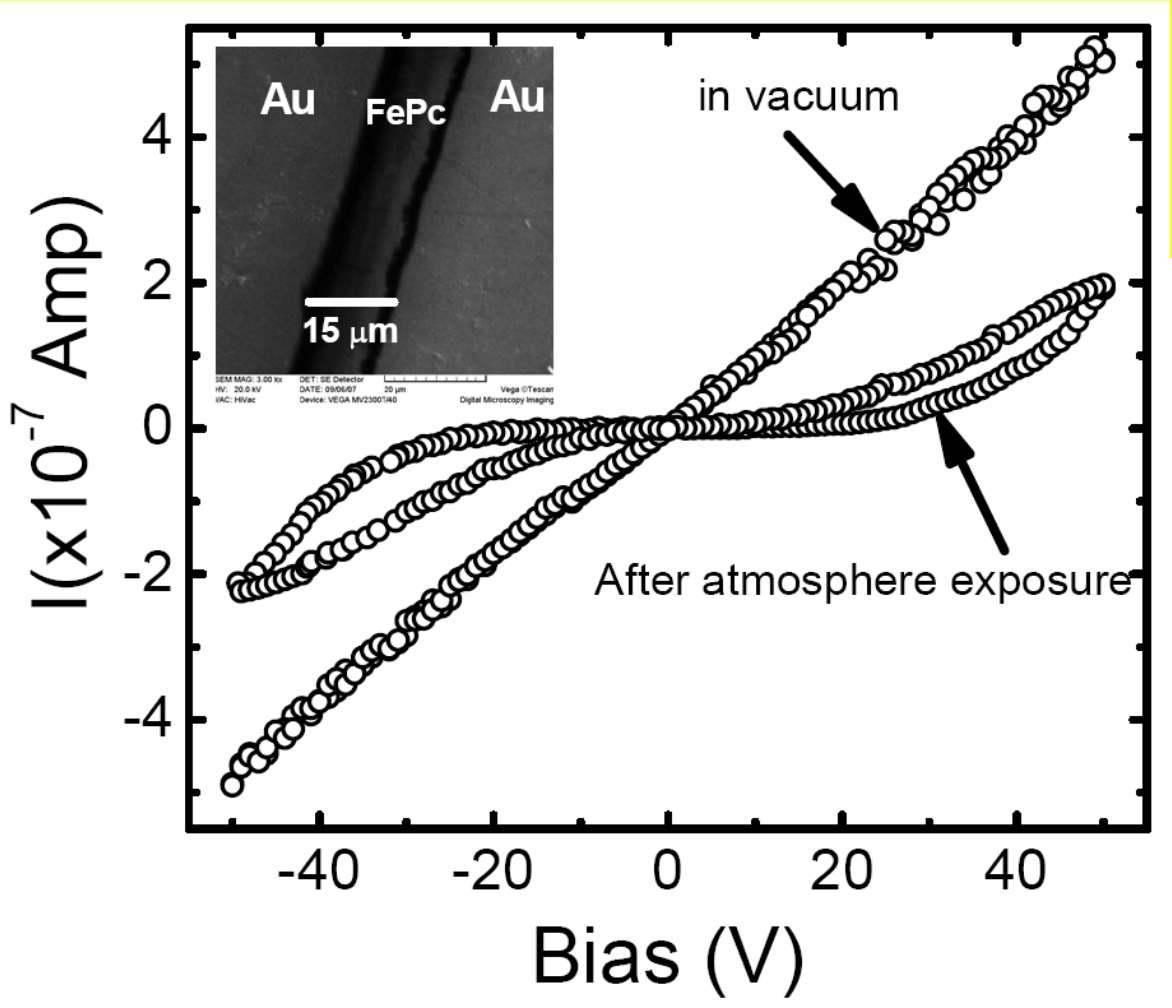

Oxygen induced Hysteretic I-V characteristics of OMBE grown FePc thin films under ~ 2 x 10^{-8} mbar vacuum.

I-V* characteristics at 300 K for vacuum annealed (at 200°C) FePc film: *under vacuum and after exposing to the atmosphere.

Inset shows SEM of the planar Au/FePc/Au structure used

vacuum annealed film exhibits ohmic behavior and no hysteresis;

hysteresis appears on atmospheric exposure of the films.

The chemisorbed oxygen desorbs on vacuum annealing.
Hysteresis in FePc films is directly related to the chemisorbed oxygen.

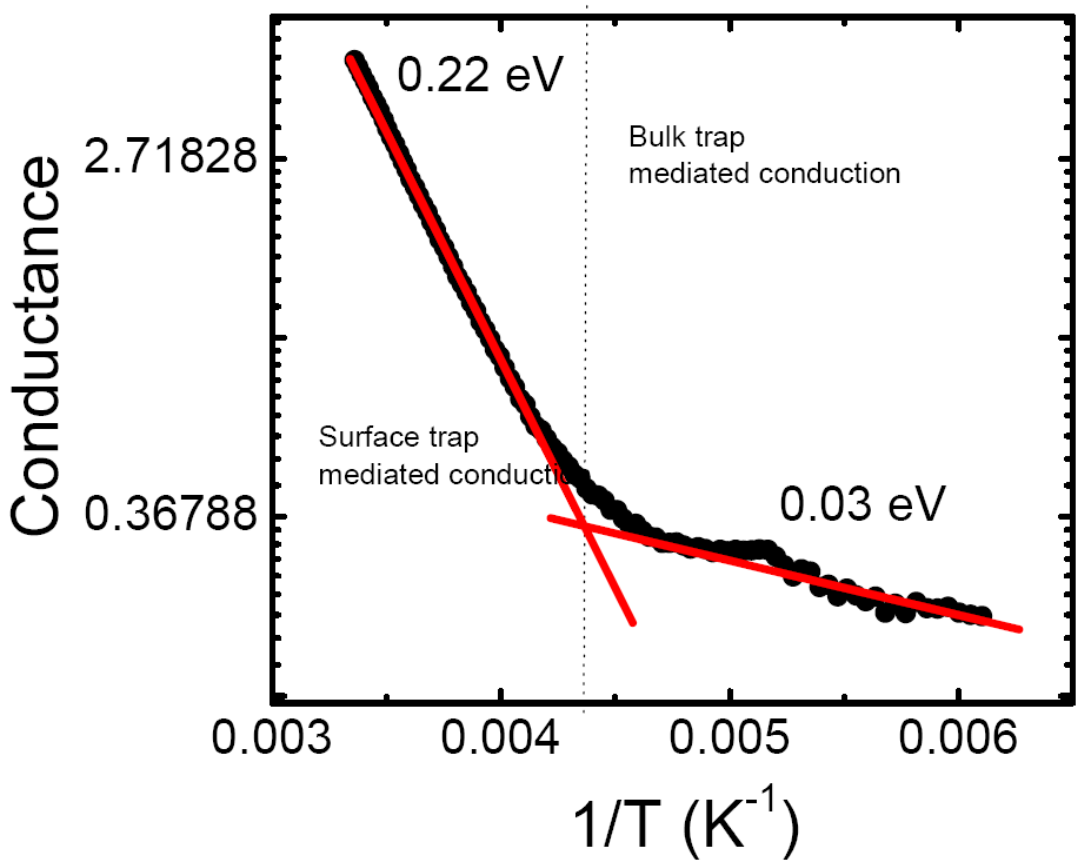

A change in conduction mechanism at ~ 250 K. Two activation energies, above and below 250 K.

>250 K, the chemisorbed oxygen induced surface traps in FePc which govern the charge transport.
<250K, bulk traps determine the charge transport.

Samanta, Singh, Debnath, Aswal, Gupta, Yakhmi, Singh, Basu, and Deshpande, *J. Appl. Phys.* 104 (2008) 073717:1-6

non linearity and hysteresis vanish below 250 K, indicating that oxygen induced surface traps becomes in-effective below 250 K

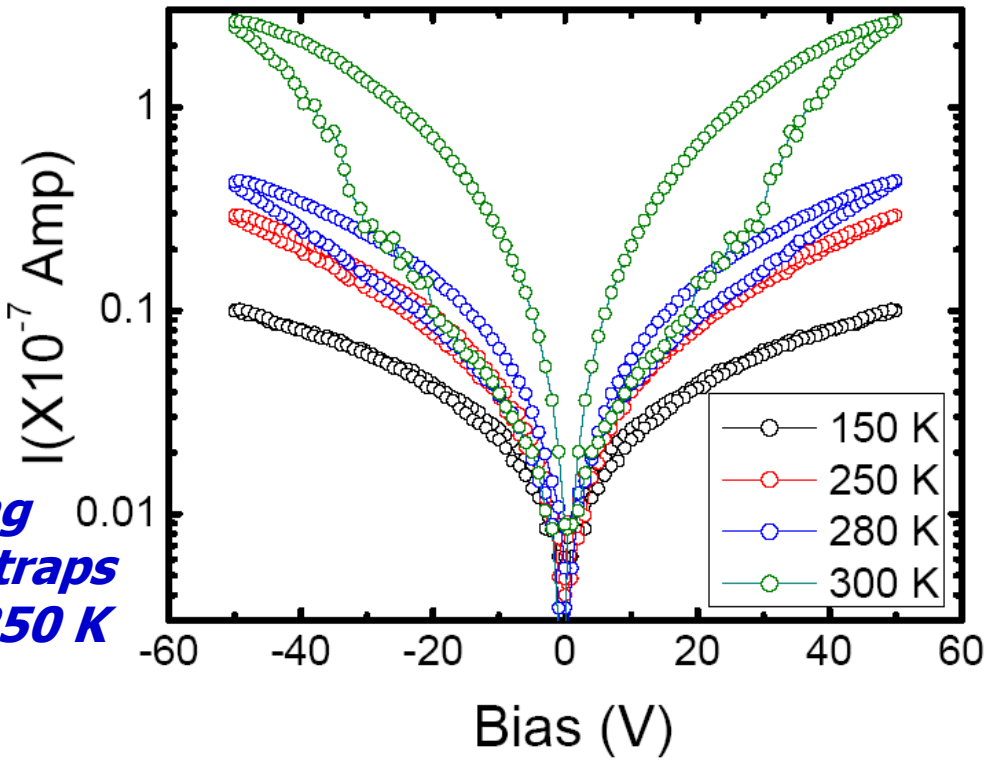

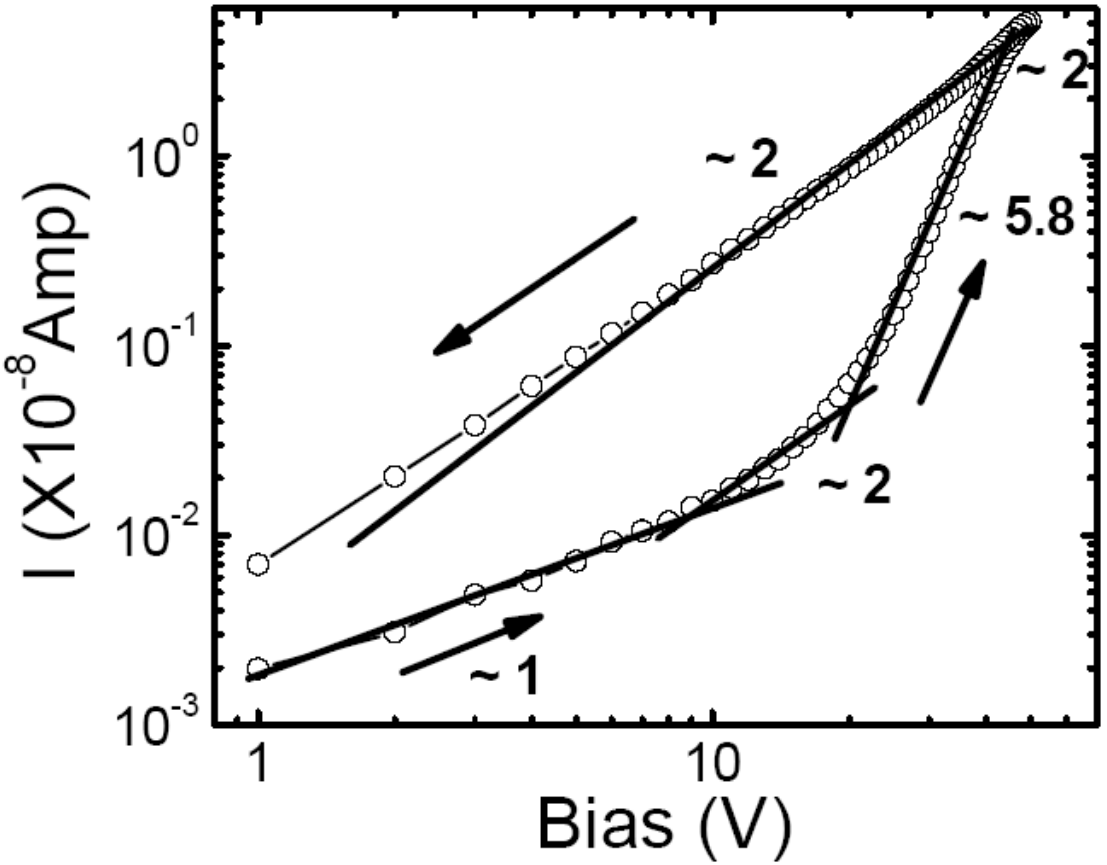

***I-V* characteristics of FePc films (at 300 K in log-log scale).**

obtained by sweeping voltage between 0 → + 50 volt → 0 volt,

Hysterisis indicates different resistance states during the voltage sweep.

slope (> 2) suggests SCLC mechanism in the presence of deep Traps.

Using the slope value of 5.8, the calculated total surface trap density was 3×10^{19}cm-3 and the surface trap concentration per unit energy range at valence band edge was 1.5×10^{39} J/cm3. ***(agrees with reported values for FePc)***

Above 40 volts, the current rises slowly and then slope reduces to ~ 2 again. It can be understood as complete filling of all shallow and deep traps.

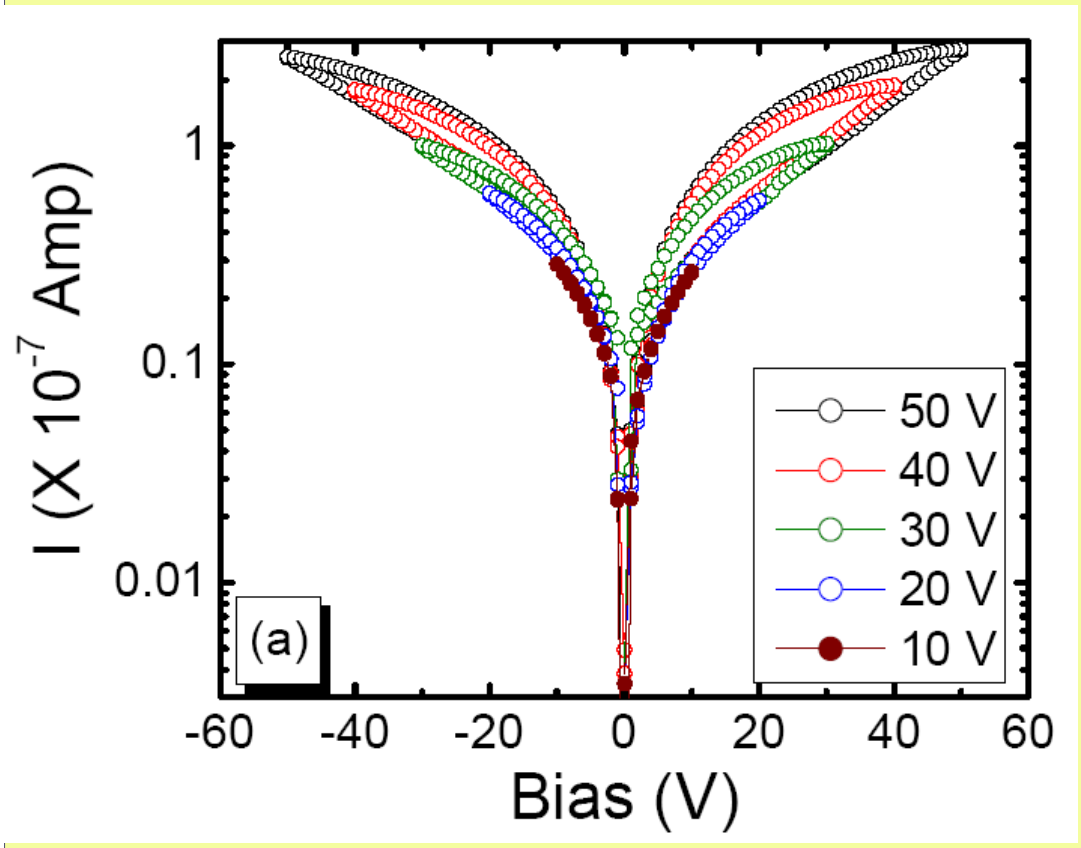

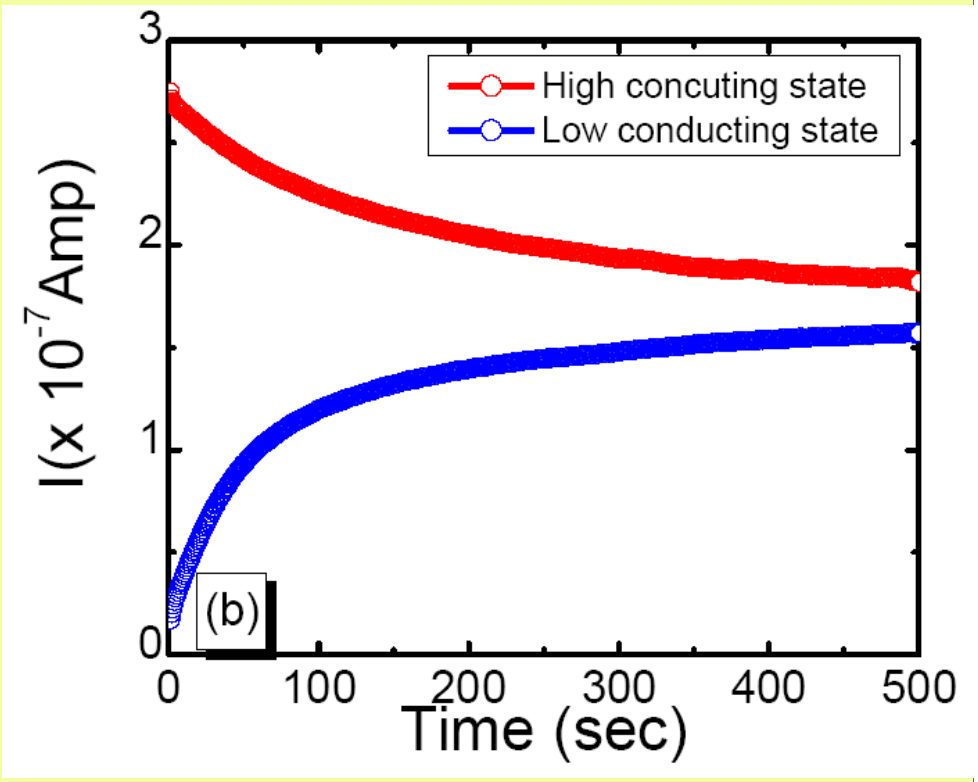

FePc films data at 300 K:

(a) under different bias. Hysteresis depends on applied bias. Is NIL for ≤ ±10V

(b) Time dependence of the current recorded for high and low conducting states at a "read" voltage of 30 V. Applied 0 V for 100s and then +30 is applied to read the low conducting ("write") state. After that applied + 50 volt for 100s (to "erase" low conducting state) and then +30 volt is applied to "read" the high conducting state.

Current during "read" pulse is higher for "high conducting state" than for "low".

Switching useful for R-RAM applications. Initial on/off ratio is ~16 and after 500 seconds the on/off ratio remains 1.2.

NO_2 Gas sensing behaviour of OMBE-deposited FePc thin films, on 10 mm x 10 mm glass substrates under a base vacuum of ~ 2 x 10^{-8} mbar

All FePc films showed change in conductance upon introduction of NO_2 gas.

Higher sensitivity observed for R.T. deposited films, since the amorphous nature (loose stacking of FePc molecules) of film, provides more adsorption sites for NO_2 molecules.
Improved crystallinity at higher temperature reduces the no. of such sites.

Sensitivity S = Conductance in gas (C_{gas})/Conductance in air (C_{air})

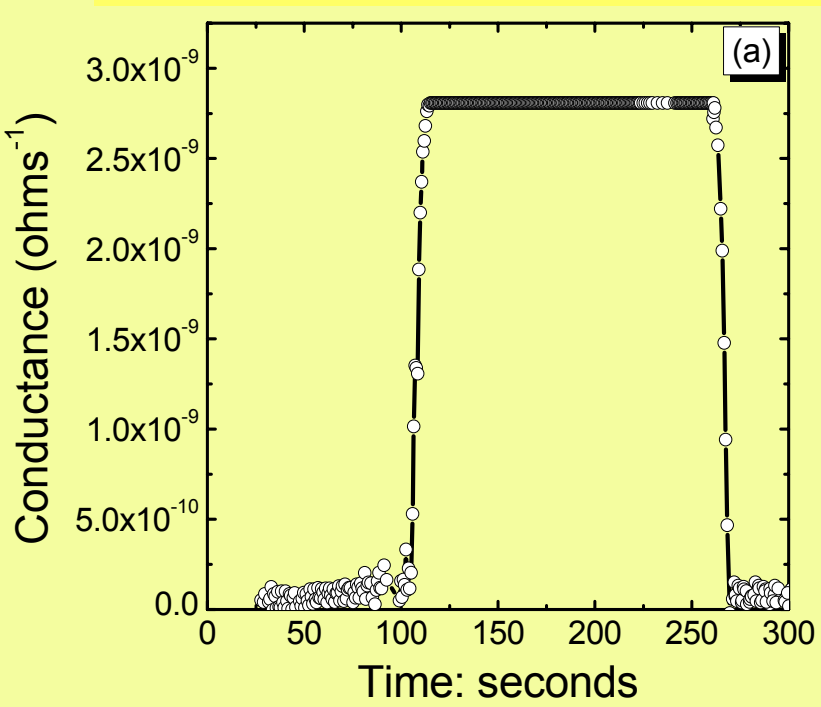

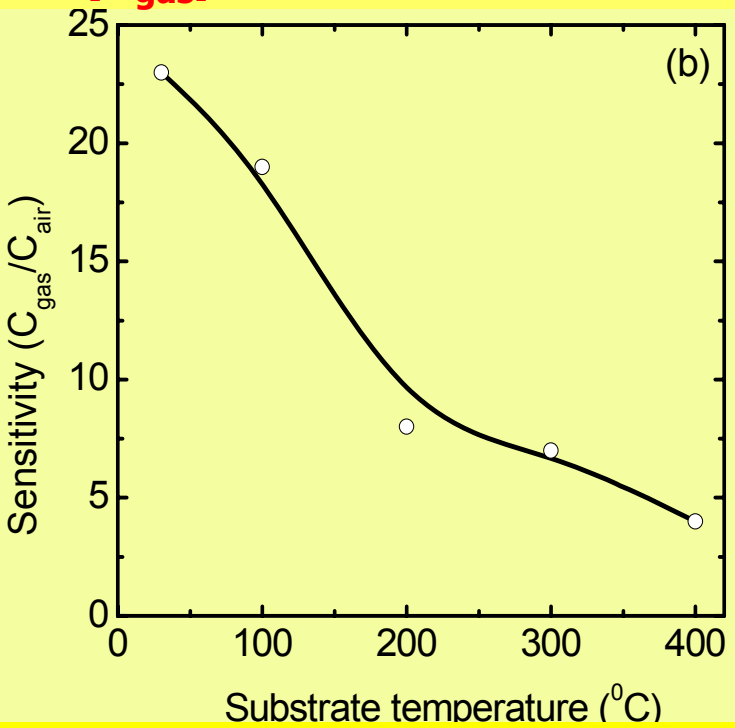

(a)Variation of conductance of FePc film deposited at R.T. under 40 ppm of NO_2 exposure and return to air.
(b) Sensitivity (for 40 ppm of NO_2**) for films grown at different substrate temp's**

Microscopic Understanding of Negative Magnetization in a Cu, Mn and Fe based Prussian Blue Analogue

Amit Kumar, Yusuf, Keller, and Yakhmi

P.R.L (2008) to appear

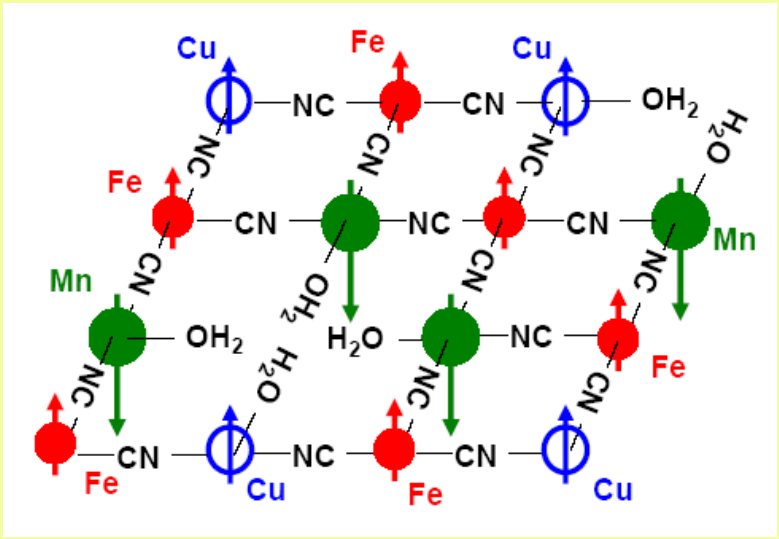

magnetic structure at 1.7 K for $Cu_{0.73}Mn_{0.77}[Fe(CN)_6].zH_2O$

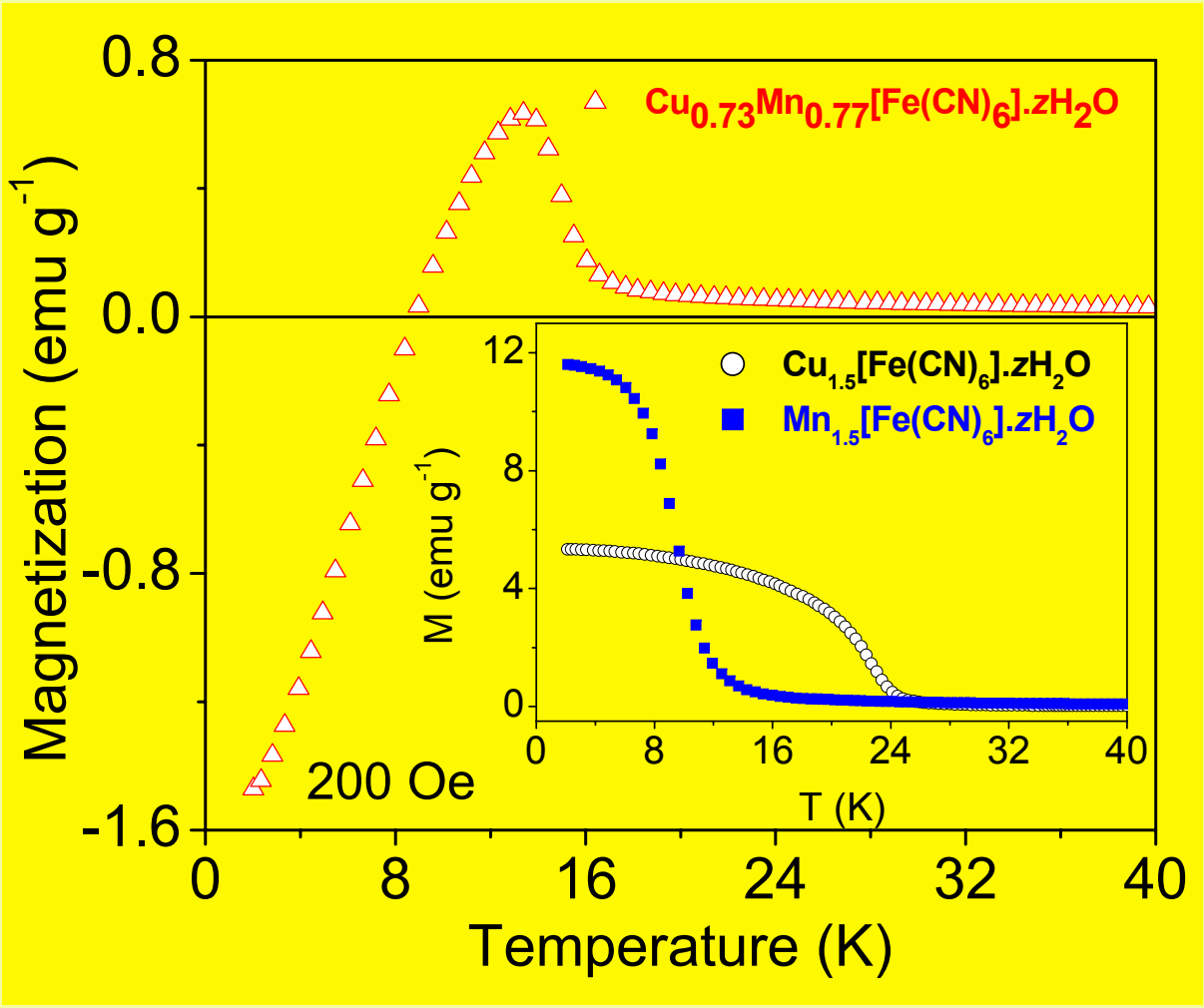

FC magnetization curves at 200 Oe for the two end compounds (inset) and the $x = 0.486$ compound of the $\{Cu_xMn_{1-x}\}_{1.5}[Fe(CN)_6].zH_2O$ series.

Large Magnetocaloric Effect in $Ru_{0.2}Ni_{2.7}[Cr(CN)_6]_2.zH_2O$

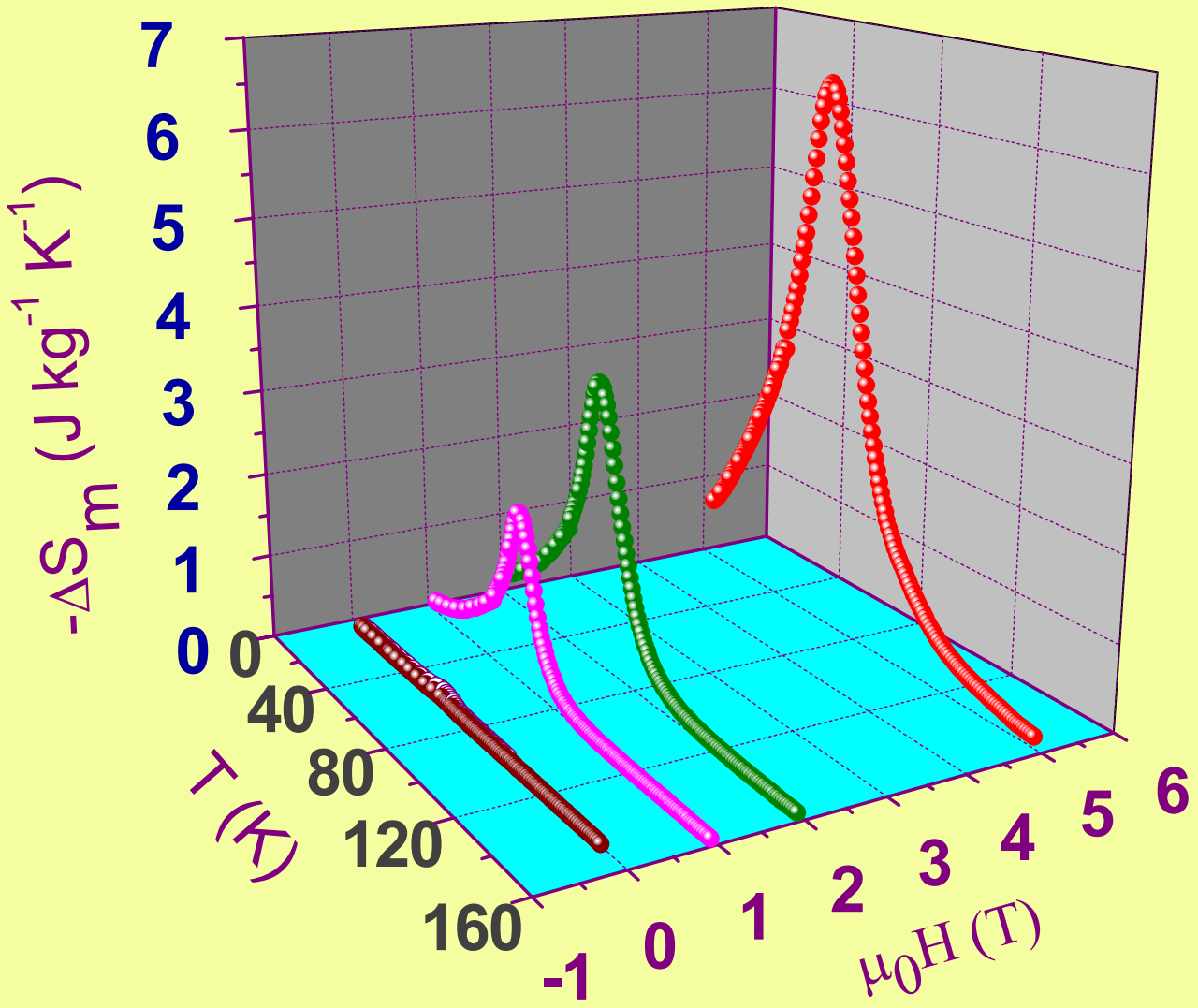

Isothermal magnetic entropy change is defined as.

$$\Delta S_m(T) = \int_{H_i}^{H_f} \frac{\partial M(T,H)}{\partial T} dH$$

$-\Delta S_m$ = 6.94 J Kg^{-1} K^{-1} for ΔH = 50 kOe; For Gd_7Pd_3:6.55J Kg^{-1} K^{-1}

Nidhi Sharma, S.M. Yusuf, Amit Kumar and J.V. Yakhmi

Proc. of ICCM-2007, Kolkata (India), Dec. 11-16, 2007 published as AIP Proc. (2008)